

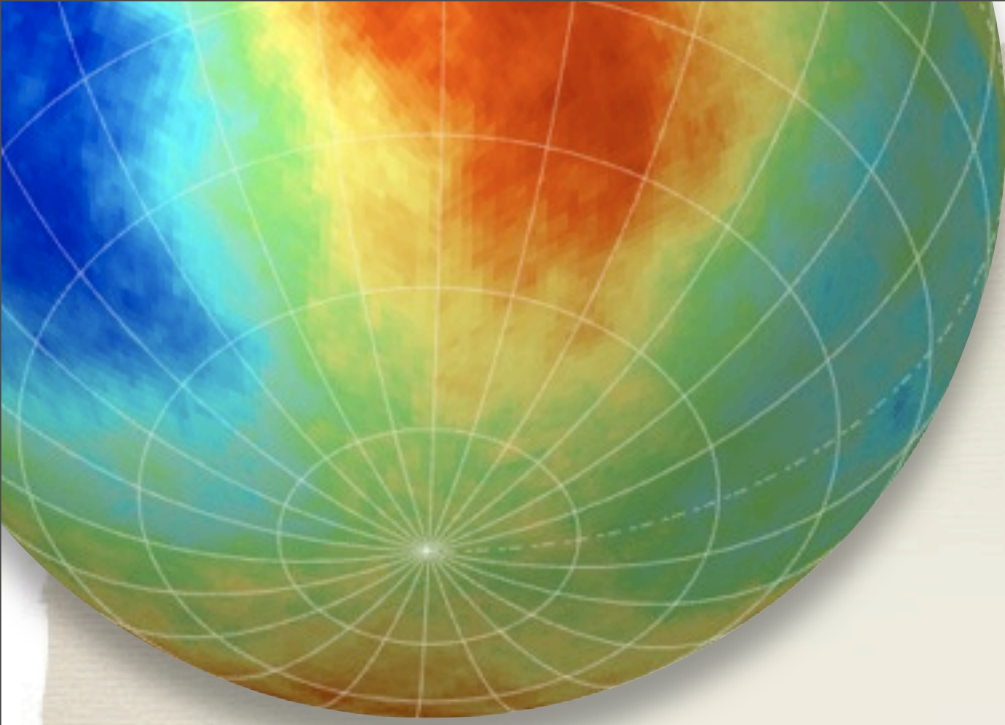
# OBSERVATION OF COSMIC RAY ANISOTROPY ABOVE TEV ENERGIES IN ICECUBE

*Simona Toscano on behalf of the* **IceCube** collaboration



**3rd Roma International Conference  
on Astro-particle Physics**

**25-27 May 2011  
Roma Italy**



# Outline

- \* The **IceCube** detector
- \* Energy dependence of the **large scale anisotropy** (*paper in preparation*):
  - ▶ preliminary results at 20 and 400 TeV.
  - ▶ solar dipole
- \* **Medium and small scale** structures (submitted to ApJ, **arXiv:1105.2326**):
  - ▶ analysis
  - ▶ results
- \* Conclusions

Bartol Research Inst, Univ of Delaware, USA  
 University of Alaska Anchorage, USA  
 Pennsylvania State University, USA  
**University of Wisconsin-Madison, USA**  
 University of Wisconsin-River Falls, USA  
 LBNL, Berkeley, USA  
 UC Berkeley, USA  
 UC Irvine, USA

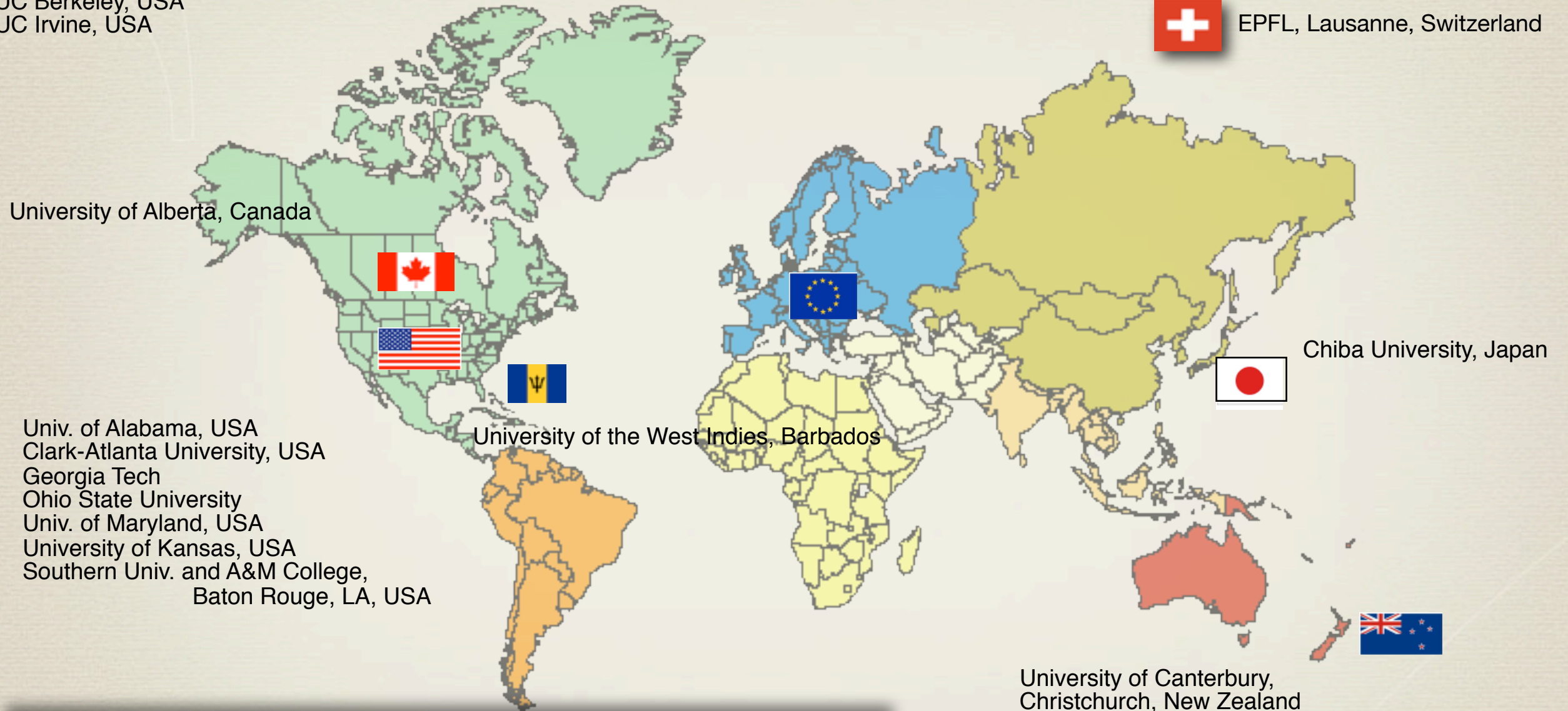
 Universität Mainz, Germany  
 DESY Zeuthen, Germany  
 Universität Wuppertal, Germany  
 Universität Dortmund, Germany  
 Humboldt Universität, Germany  
 TWTH Aachen, Germany  
 Universität Bonn, Germany  
 Ruhr-Universität, Bochum, Germany  
 MPI, Heidelberg, Germany

 Uppsala Universitet, Sweden  
 Stockholm Universitet, Sweden

 Imperial College, London, UK  
 University of Oxford, UK

 Université Libre de Bruxelles, Belgium  
 Vrije Universiteit Brussel, Belgium  
 Université de Mons, Belgium  
 Universiteit Gent, Belgium

 EPFL, Lausanne, Switzerland



# IceCube Collaboration

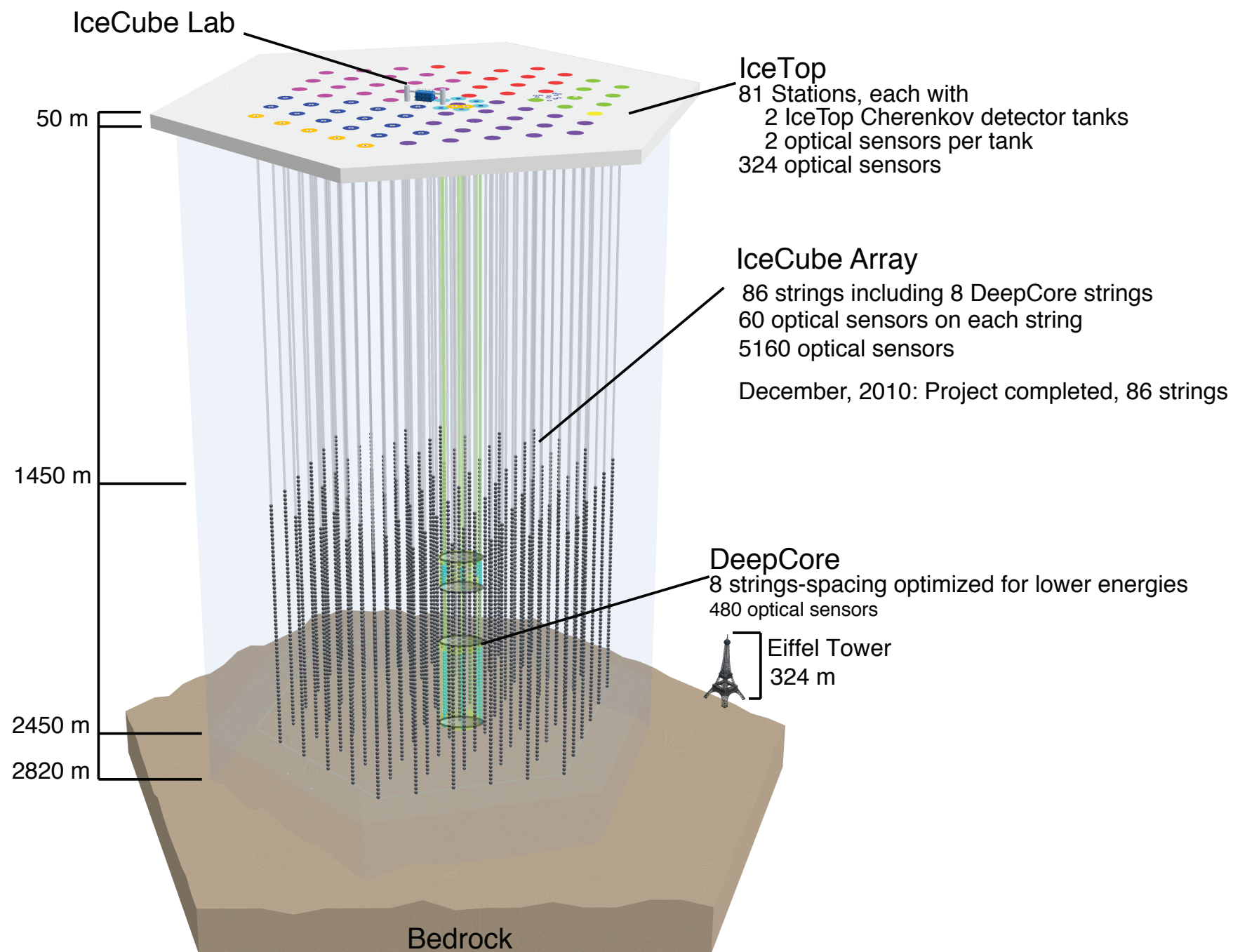
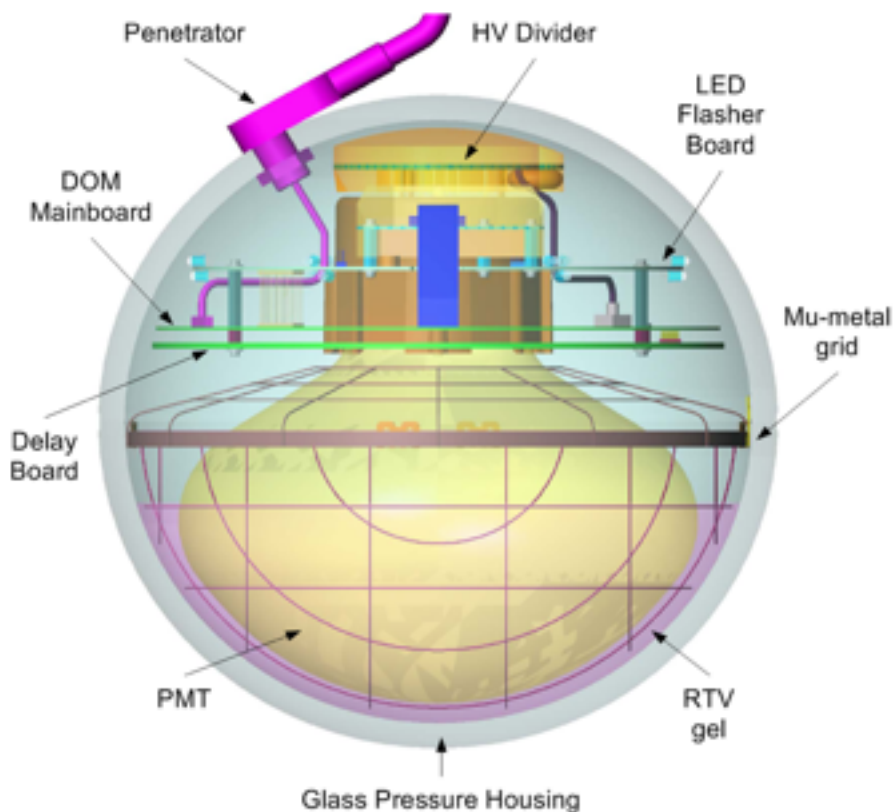
**10 countries**  
**36 institutions**  
**~260 collaborators**

# The IceCube detector

- ➔ **G. Sullivan** - *Status and Recent Results from the IceCube km<sup>3</sup> Neutrino Detector* (tomorrow Plenary)
- ➔ **T. DeYoung** - *Particle physics in ice with IceCube DeepCore* (today next Parallel session)

- **86 strings**
- **5160 DOMs**
- **17 m vertical spacing**
- **125 m between strings**

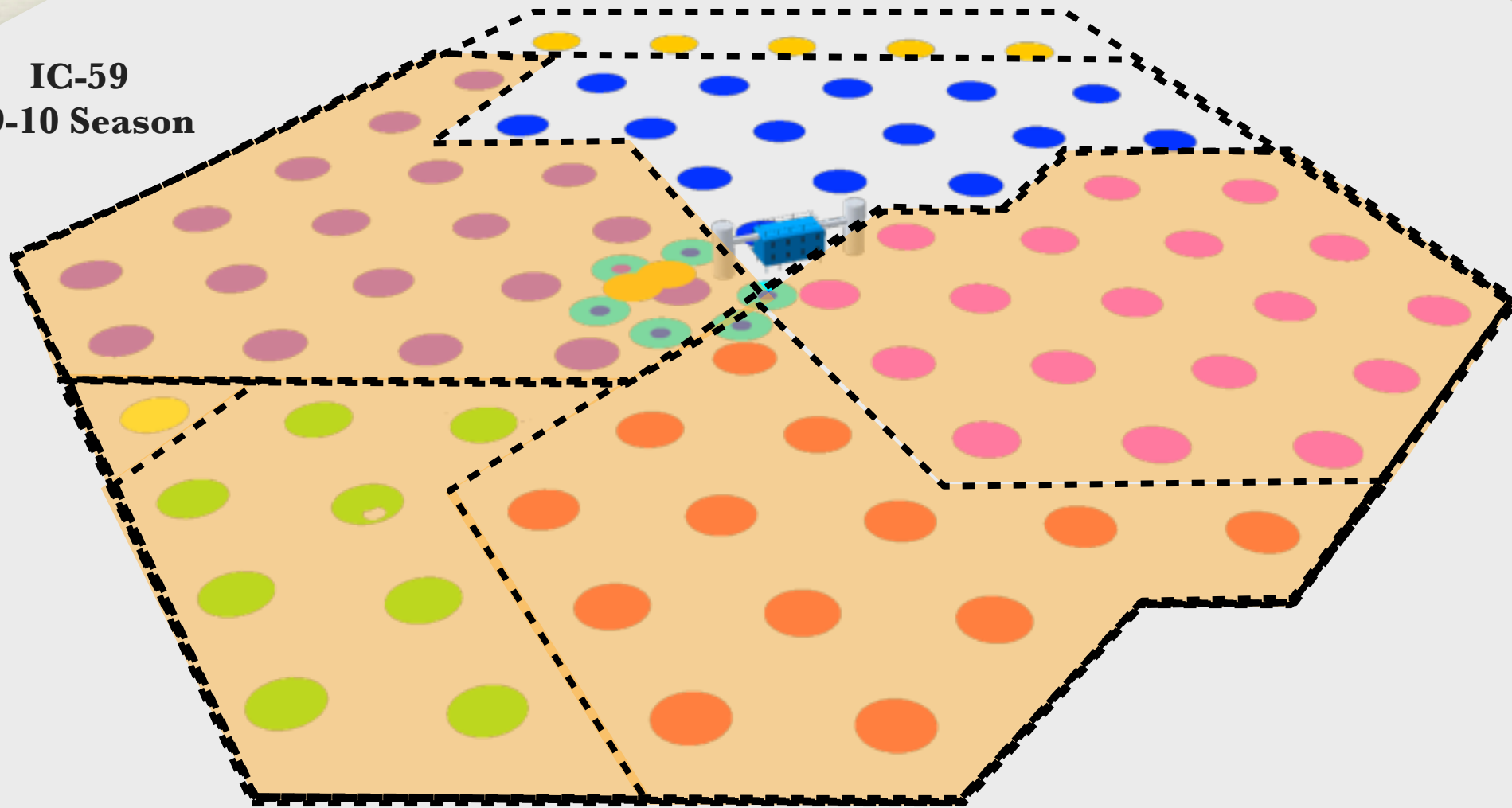
## Digital Optical Module



# IC59 configuration

Season 2009-2010

IC-59  
09-10 Season

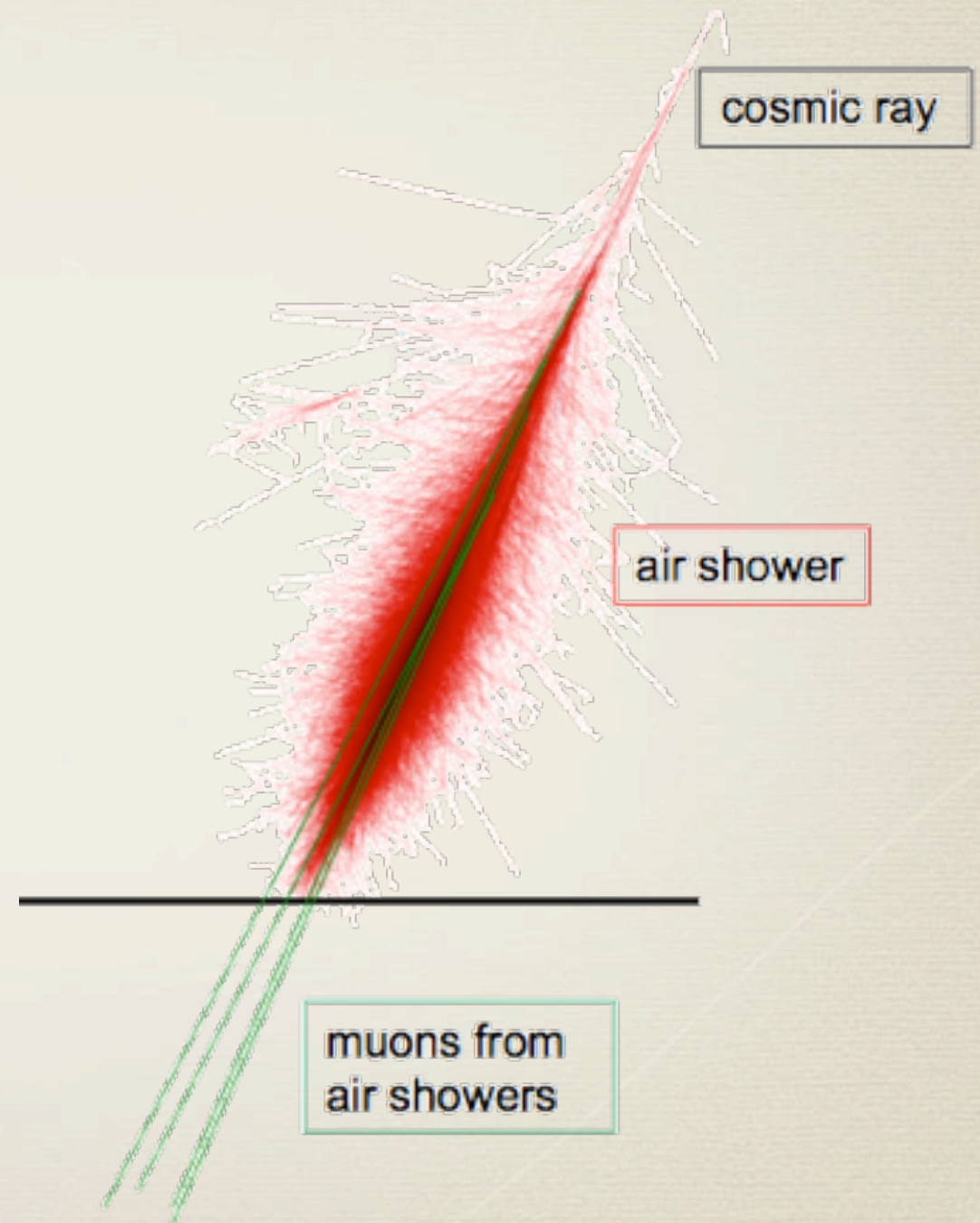


**Construction finished on December 2010**

# Cosmic rays in IceCube

IceCube tries to identify cosmic ray sources by their neutrino signal, but it also allows for a study of the *cosmic ray flux* itself, as the detector is sensitive to *downward going muons* produced in cosmic ray air showers in the southern hemisphere.

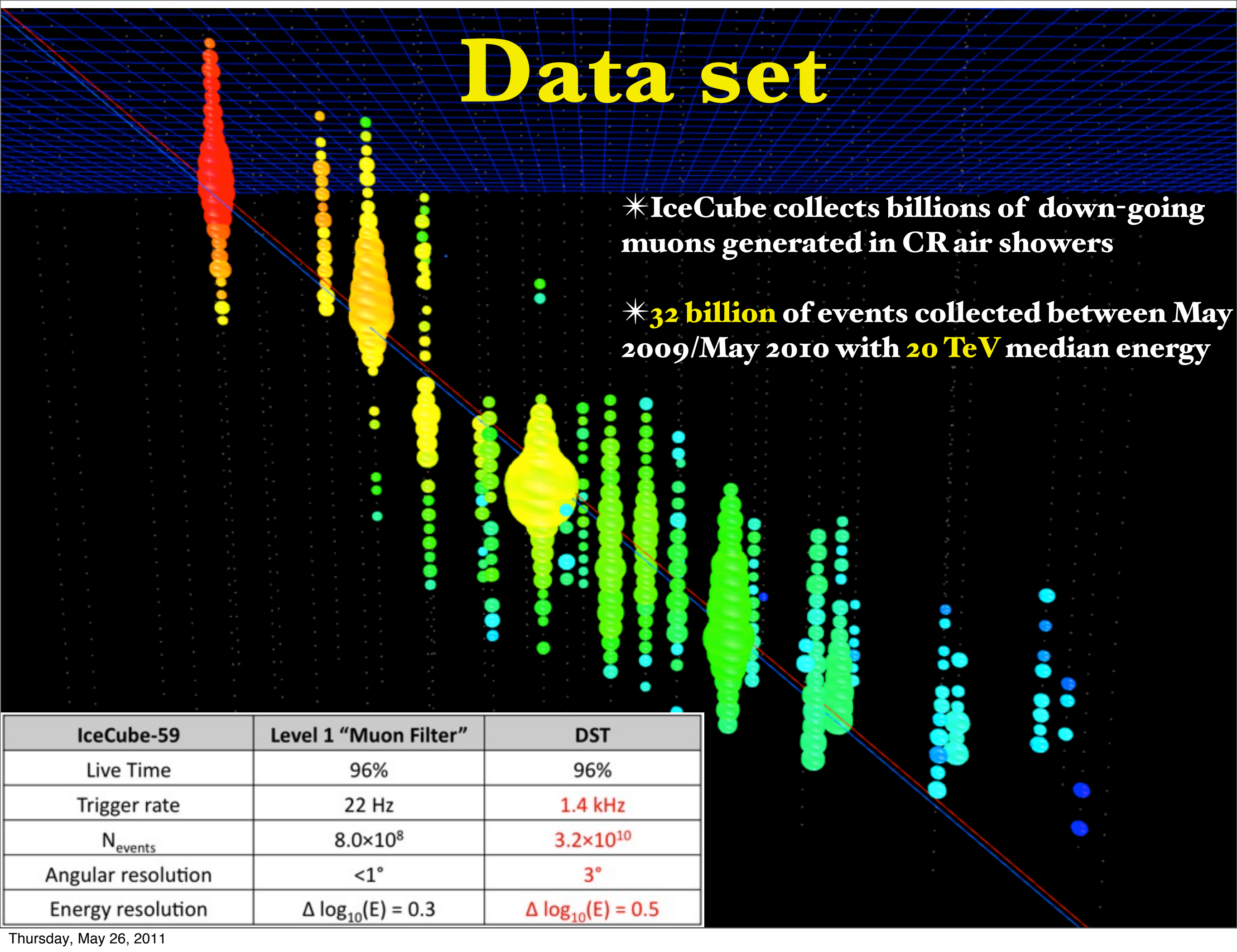
By detecting downgoing muons, IceCube can study the *arrival direction distribution of cosmic rays* in the energy range  $\sim 10$  TeV to several 100 TeV and produce a cosmic ray sky map of the southern sky.



# Data set

\* IceCube collects billions of down-going muons generated in CR air showers

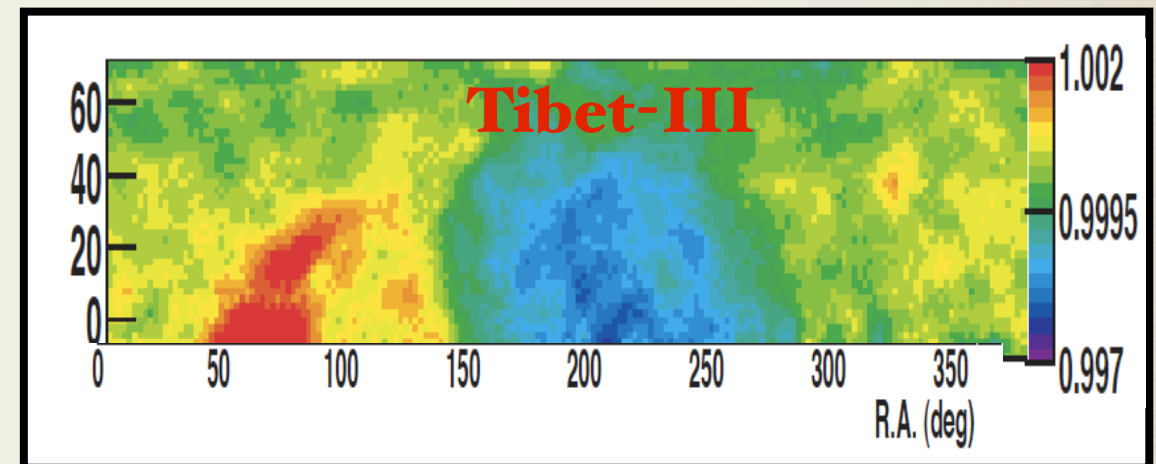
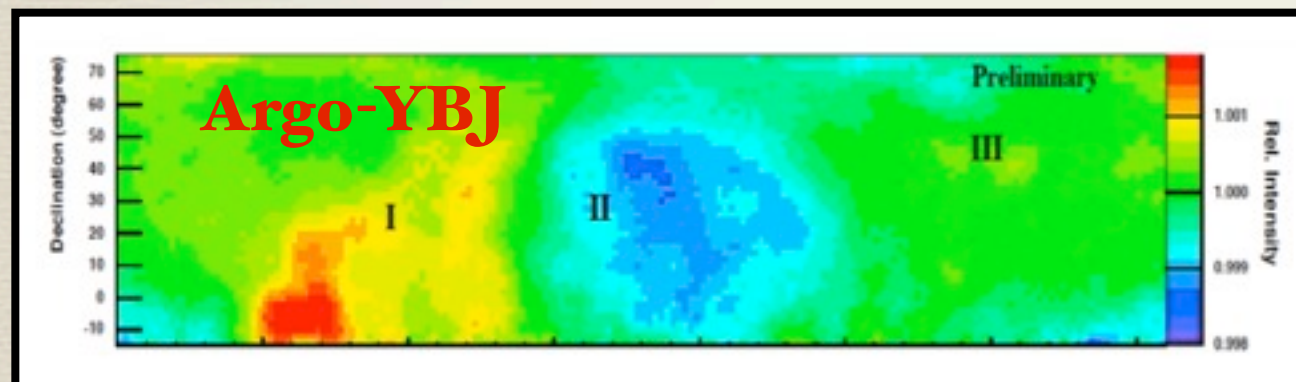
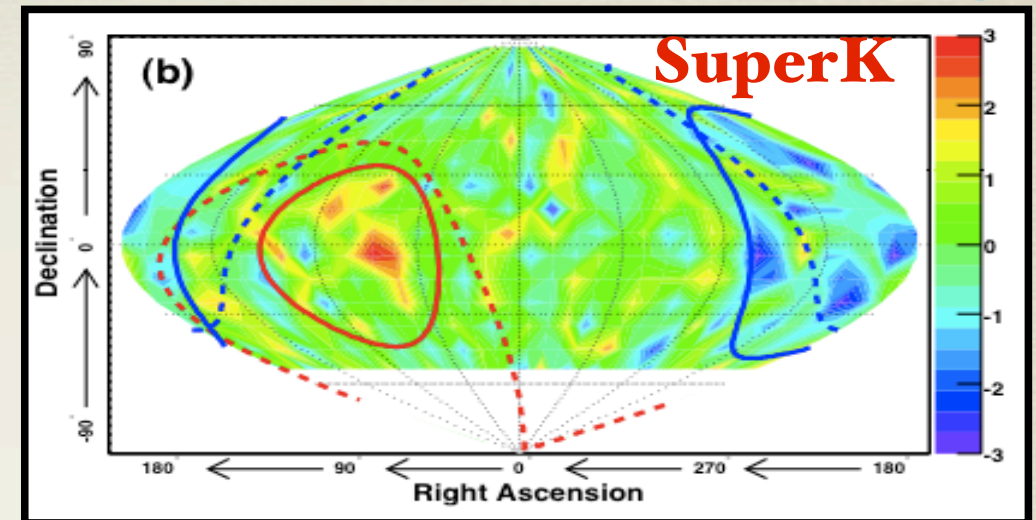
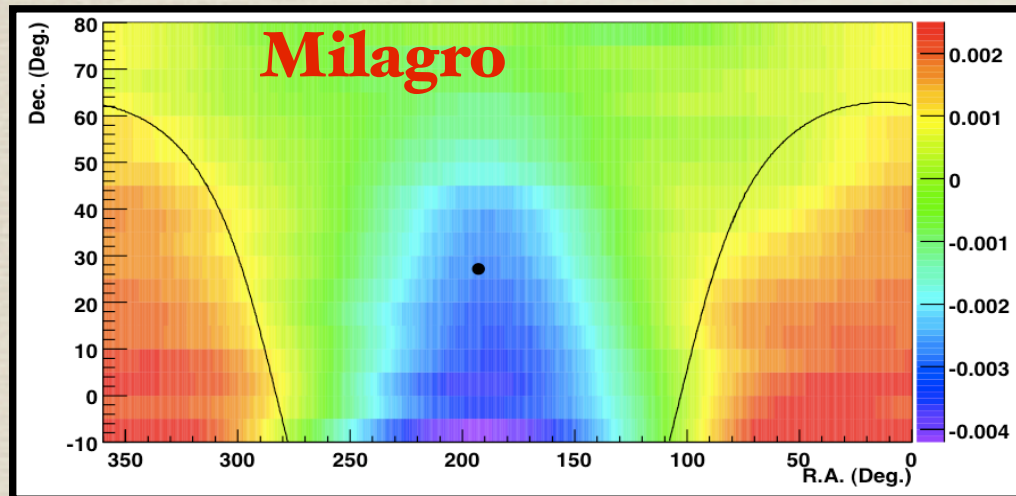
\* **32 billion** of events collected between May 2009/May 2010 with **20 TeV** median energy



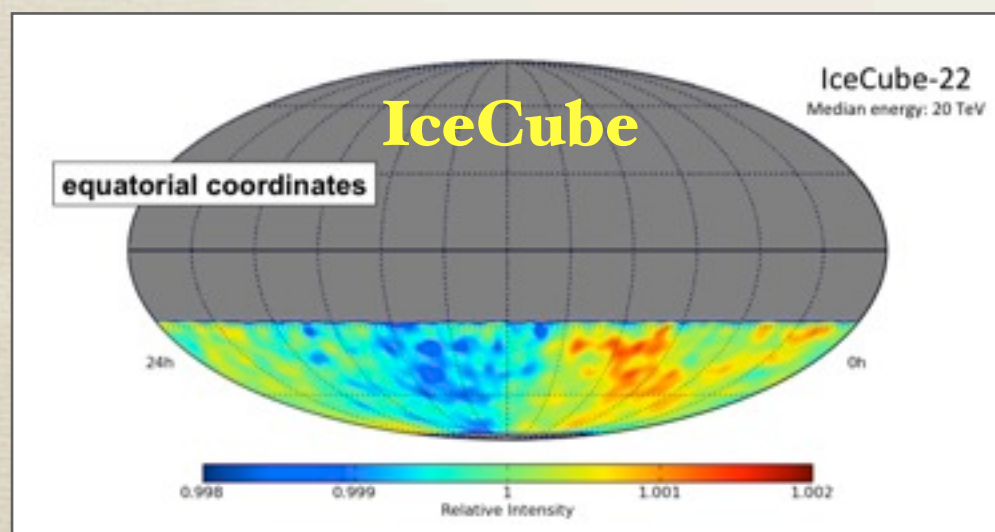
IceCube-59	Level 1 "Muon Filter"	DST
Live Time	96%	96%
Trigger rate	22 Hz	1.4 kHz
$N_{\text{events}}$	$8.0 \times 10^8$	$3.2 \times 10^{10}$
Angular resolution	$< 1^\circ$	$3^\circ$
Energy resolution	$\Delta \log_{10}(E) = 0.3$	$\Delta \log_{10}(E) = 0.5$

# Observation of the CRs large scale anisotropy

There have been several observations of *large-scale, part-per-mille anisotropy* in cosmic ray arrival directions between 0.1 and 100 TeV.



## Northern Sky

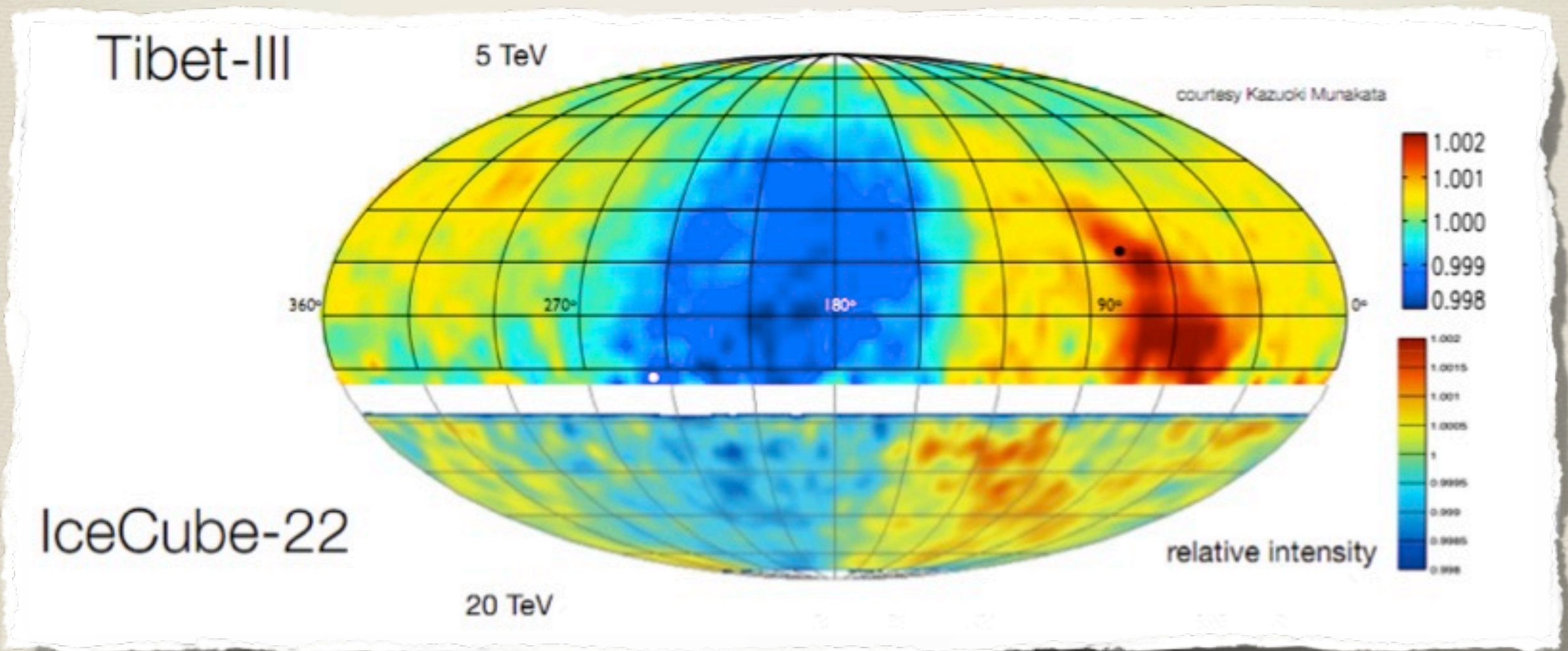


## Southern Sky

Tibet ASy	M. Amenomori et al., <i>Astrophys. J.</i> 626 (2005) L29
SuperK	G. Guillian et al., <i>Phys. Rev. D</i> 75 (2007) 062003
Milagro	A. Abdo et al., <i>Astrophys. J.</i> 698 (2009) 2121
ARGO-YBJ	S. Vernetto, Proc. 31st ICRC, 2009
EAS-Top	M. Aglietta, <i>Astrophys. J.</i> 692 (2009) L130
IceCube	R. Abbasi <i>et al</i> , <i>Astrophys. J.</i> 718 (2010) L194

# Large scale anisotropy

- \* IceCube observed a large scale anisotropy at  $10^{-3}$  level for the first time in the Southern Sky.
- \* The anisotropy appears to be a continuation of large scale structures observed in the Northern Hemisphere.



*Relative intensity* of the cosmic ray event rate in equatorial coordinates: for each declination belt of width  $3^\circ$ , the plot shows the number of events relative to the average number of events in the belt.

# Energy dependence of the anisotropy

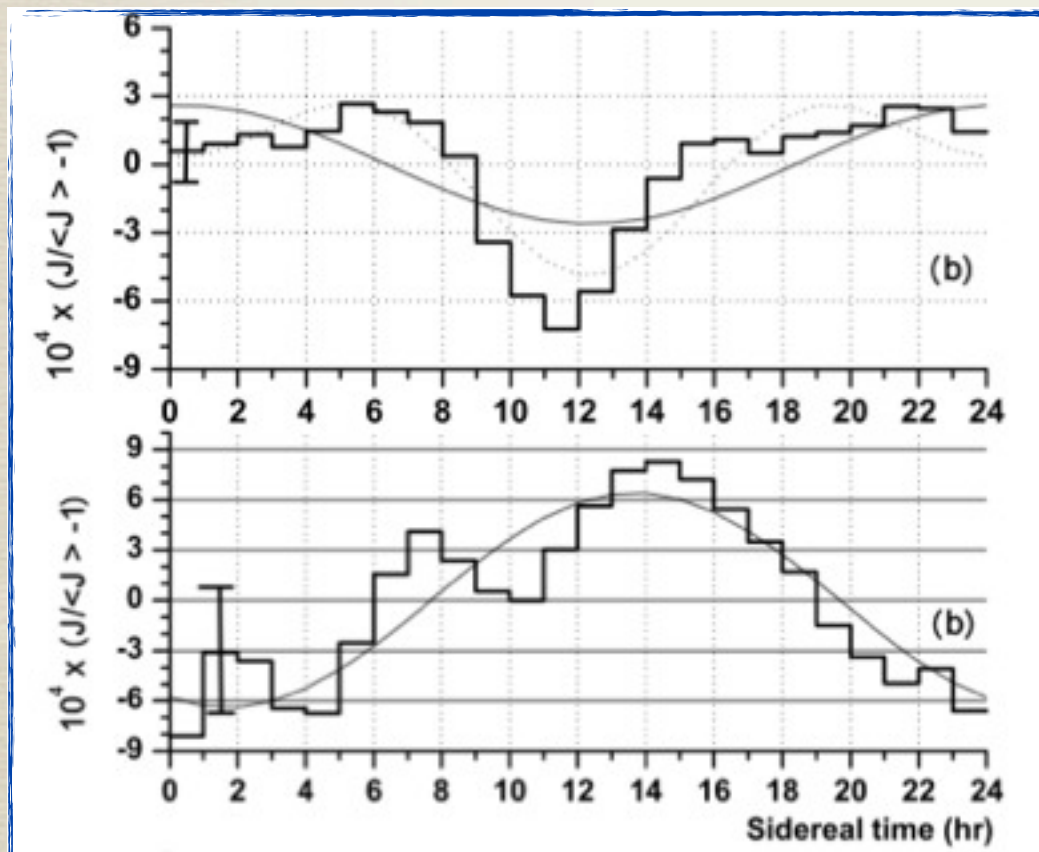
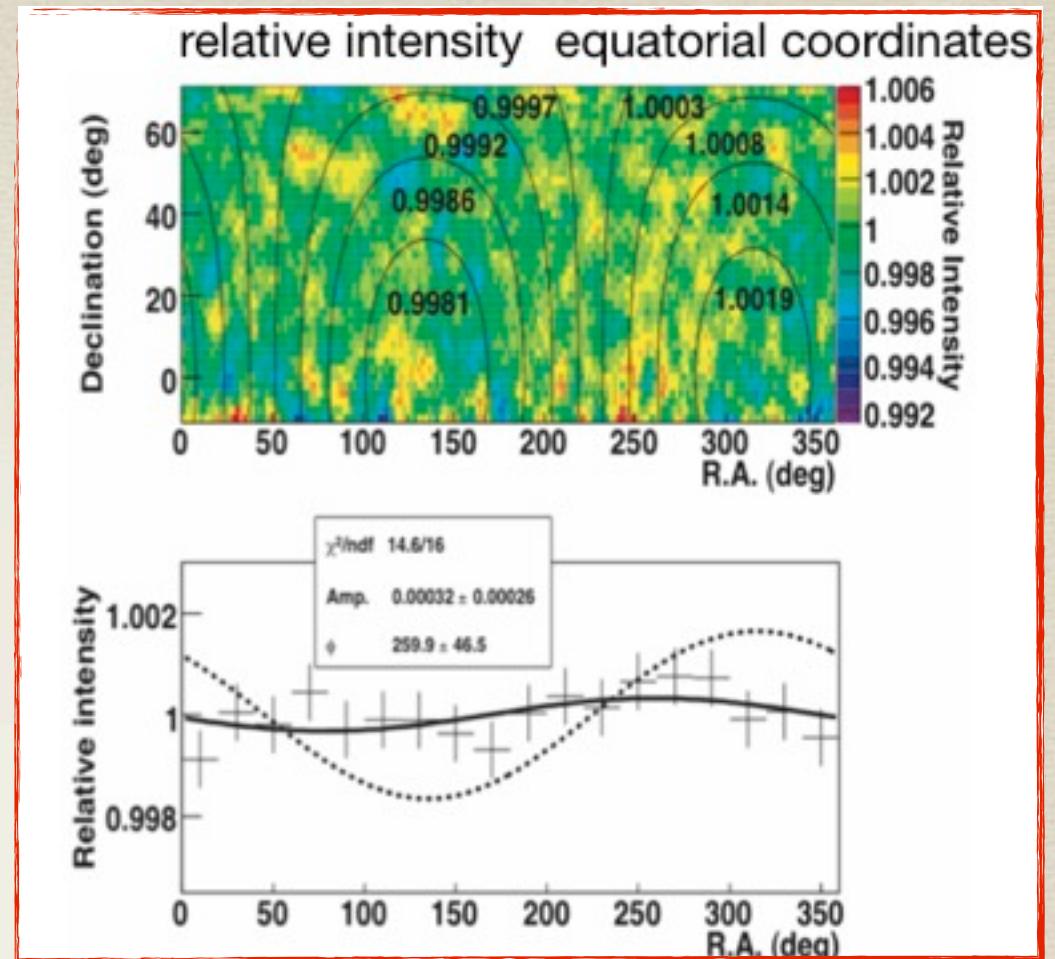
300 TeV

## Tibet - III

Amenomori et al., Science Vol. 314, pp. 439, 2006

**Amplitude:  $(3.2 \pm 2.6) \times 10^{-4}$**

consistent with **no anisotropy**



110 TeV

370 TeV

## EAS-Top

Aglietta et al., ApJ 692, L130, 2009

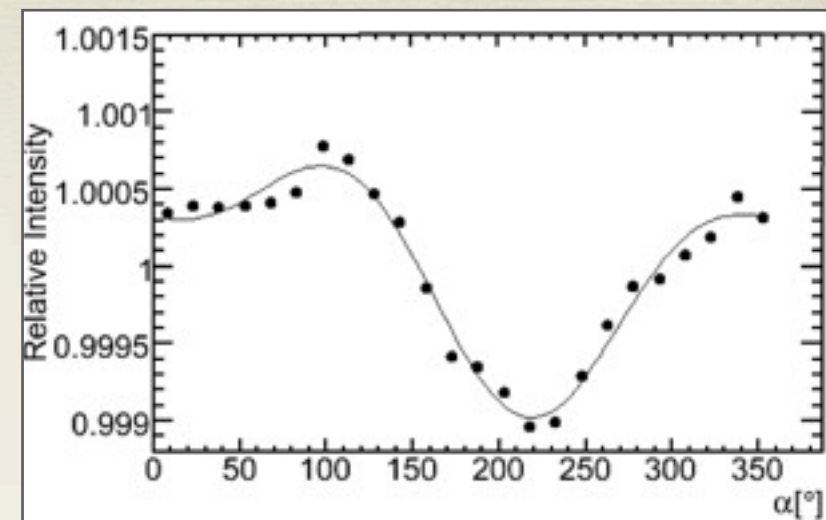
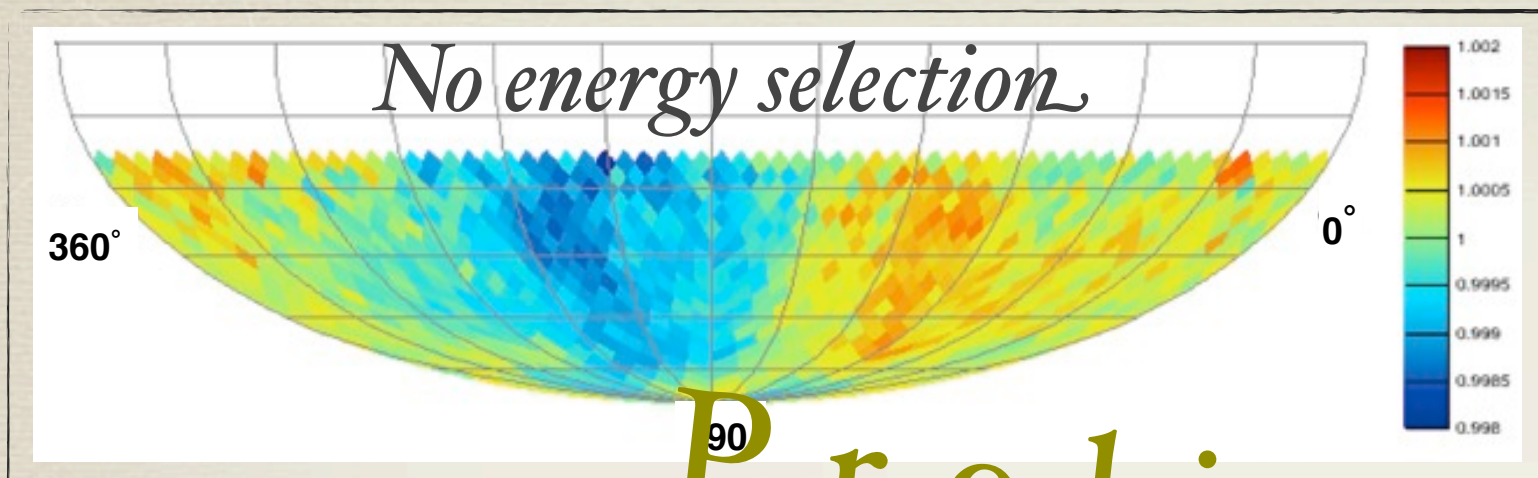
**Amplitude (370 TeV):  $(6.4 \pm 2.5) \times 10^{-4}$**

low significance, still not conclusive.

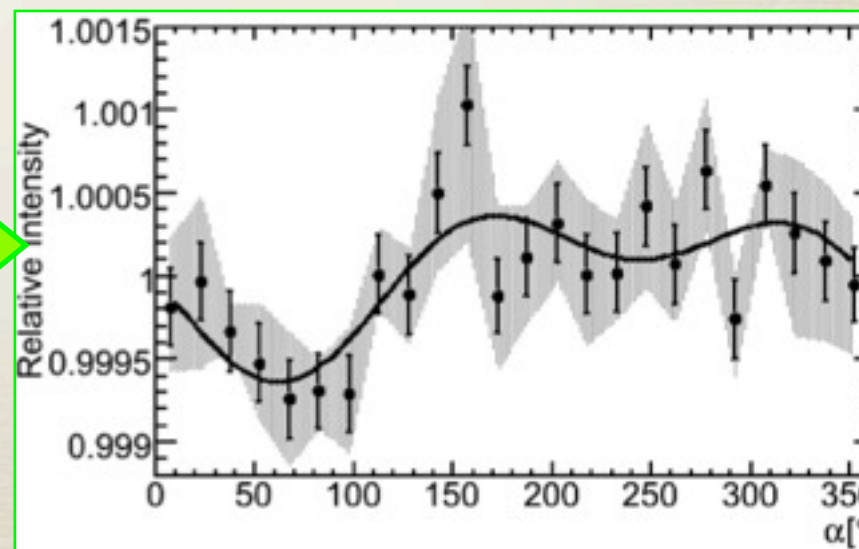
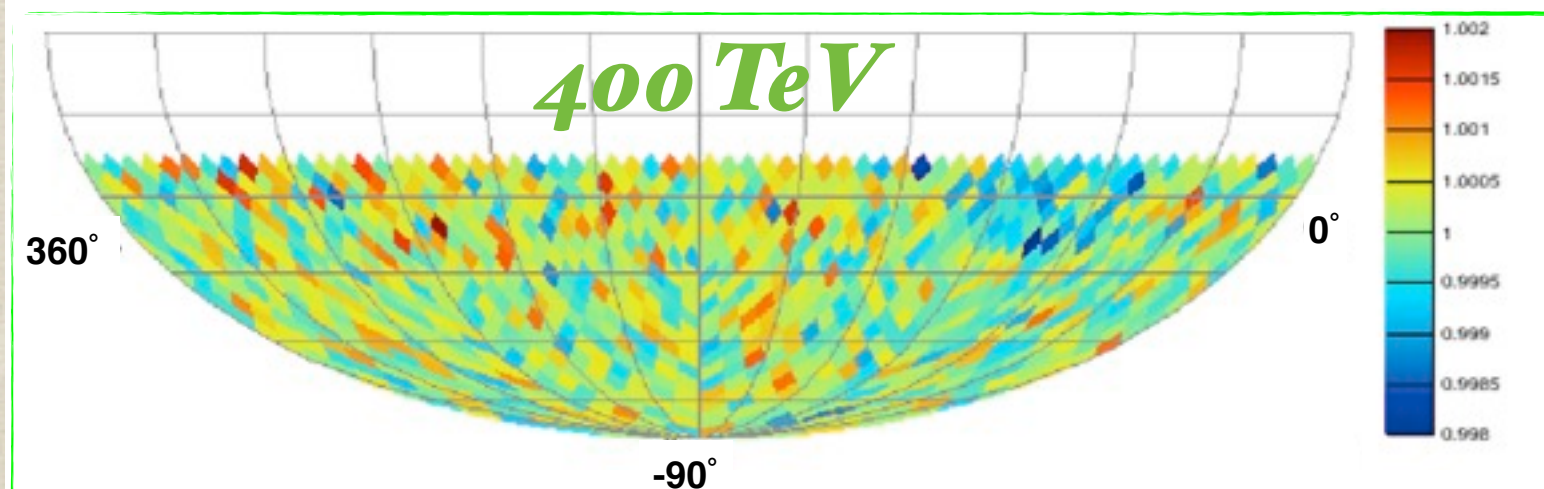
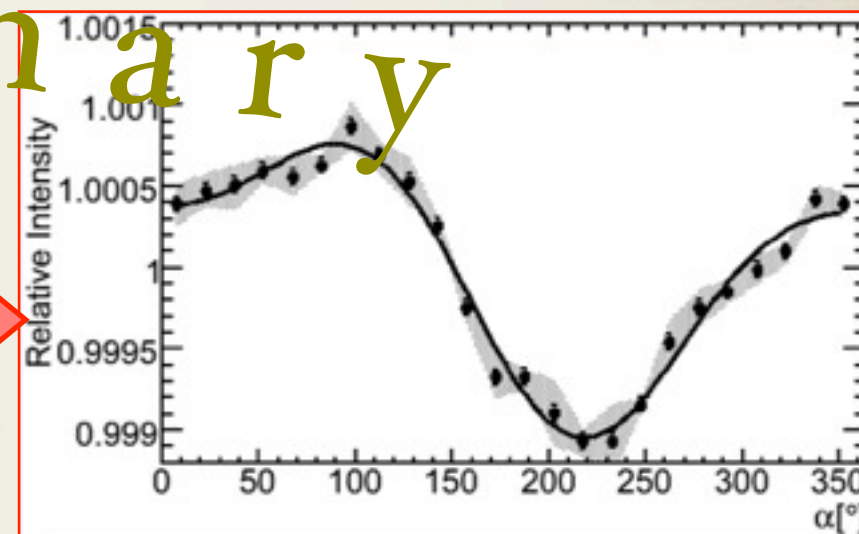
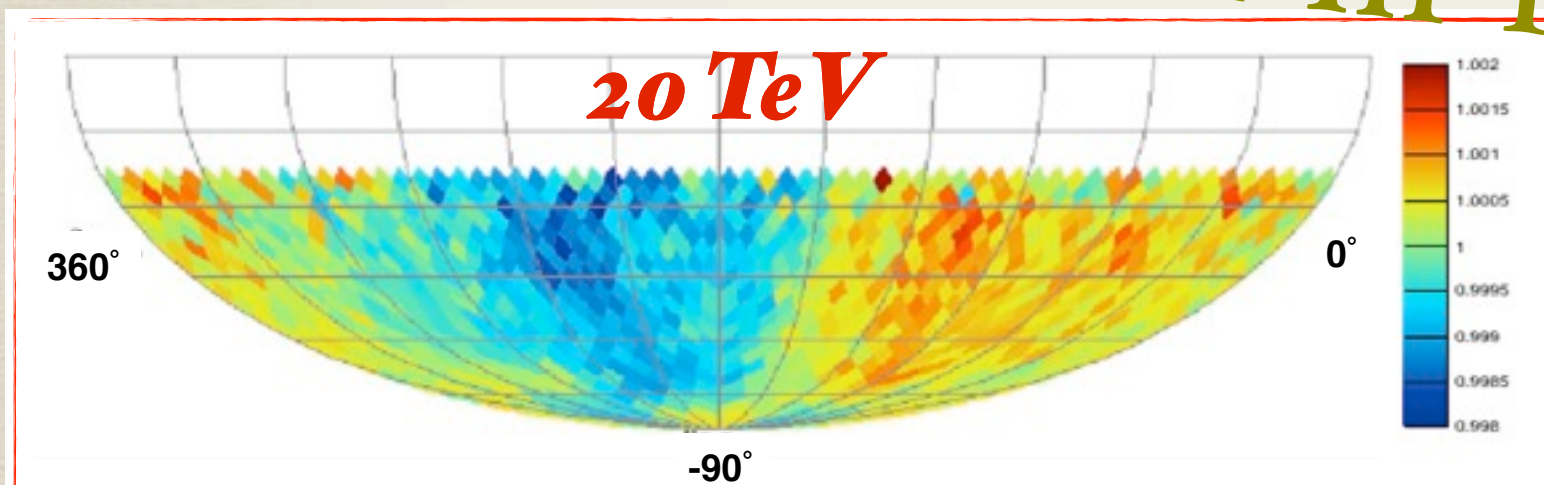
IO

# Relative Intensity

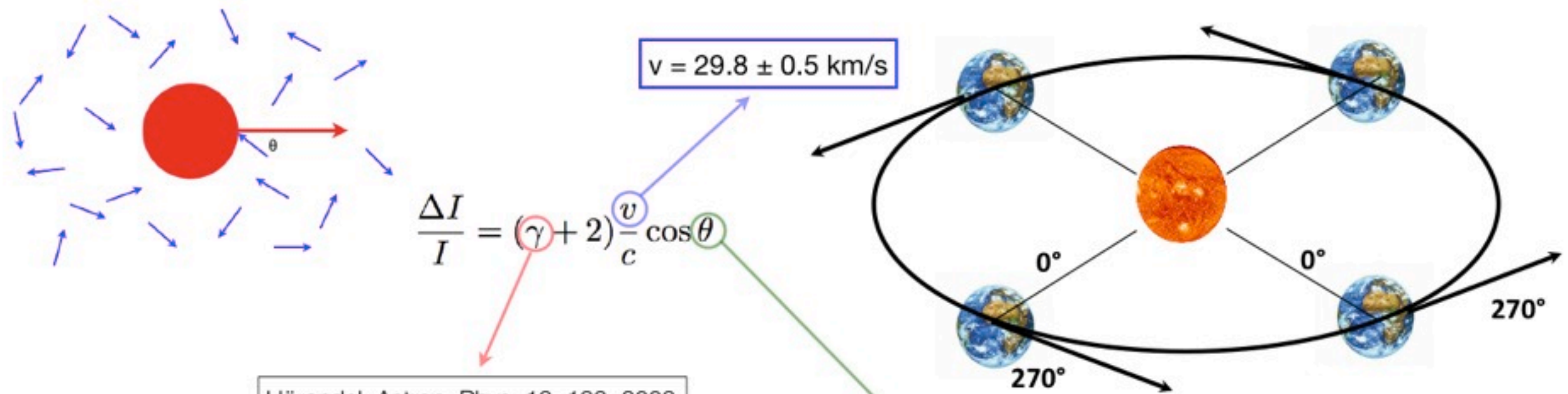
Equatorial sky maps in HEALPix with  $N_{\text{Side}} = 16$ ,  $\text{pix resol} \sim 3^\circ$



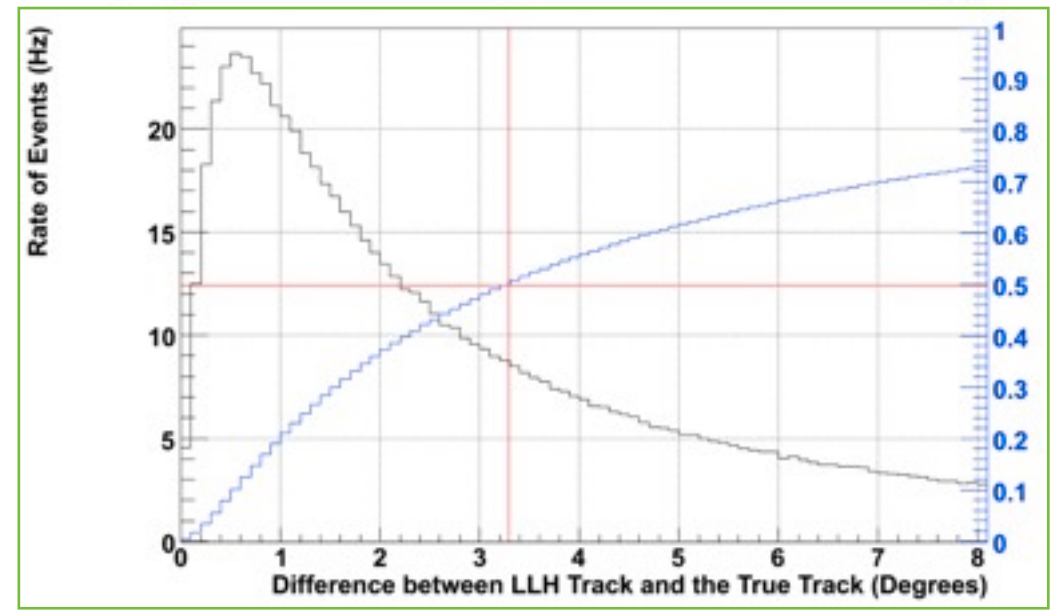
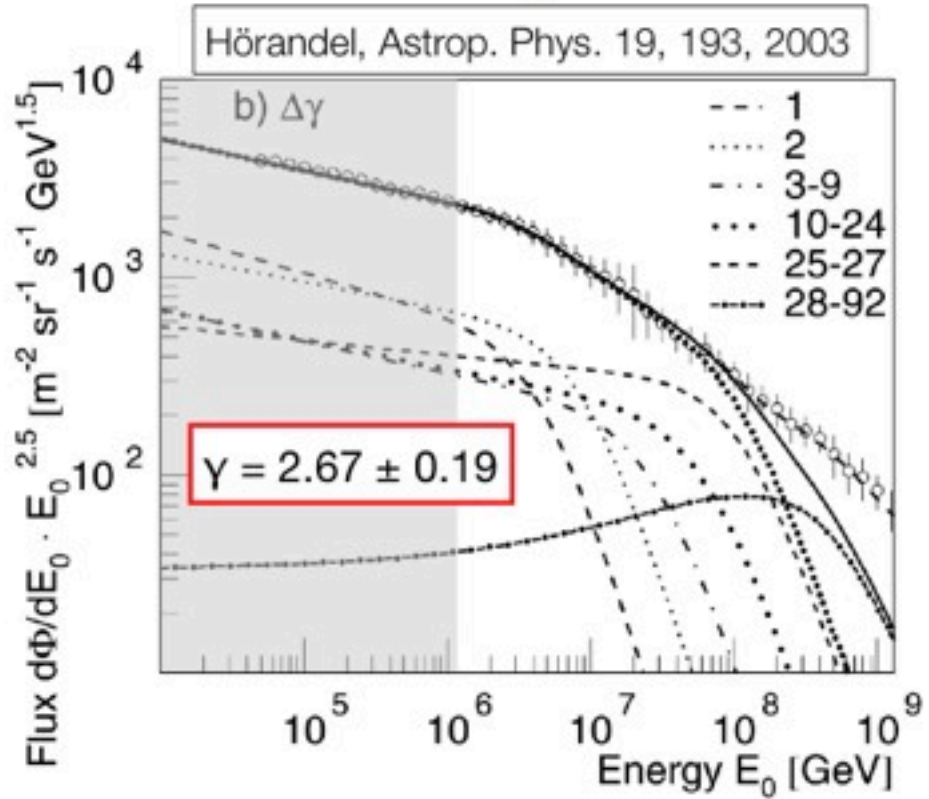
Preliminary



# Earth's motion around the Sun: the Solar dipole



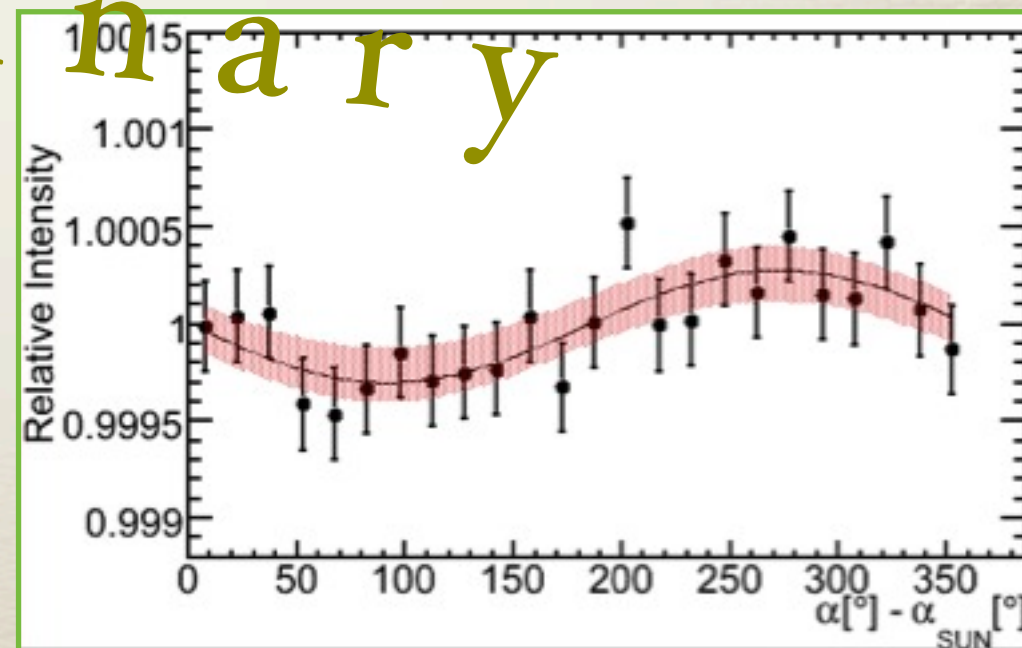
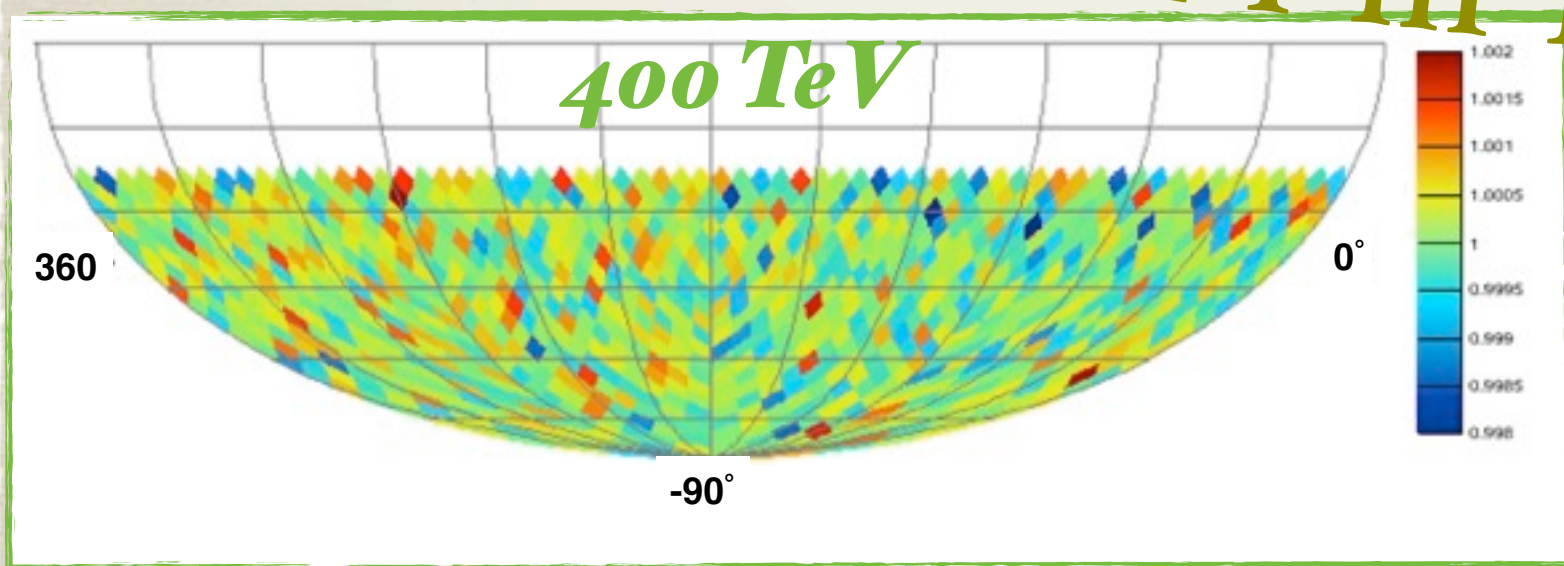
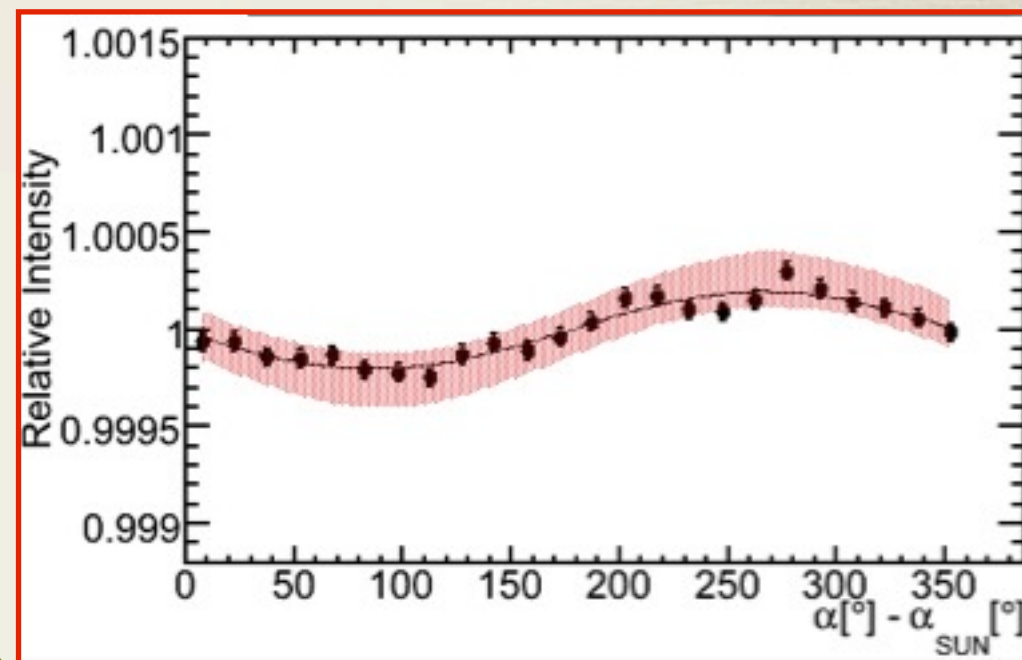
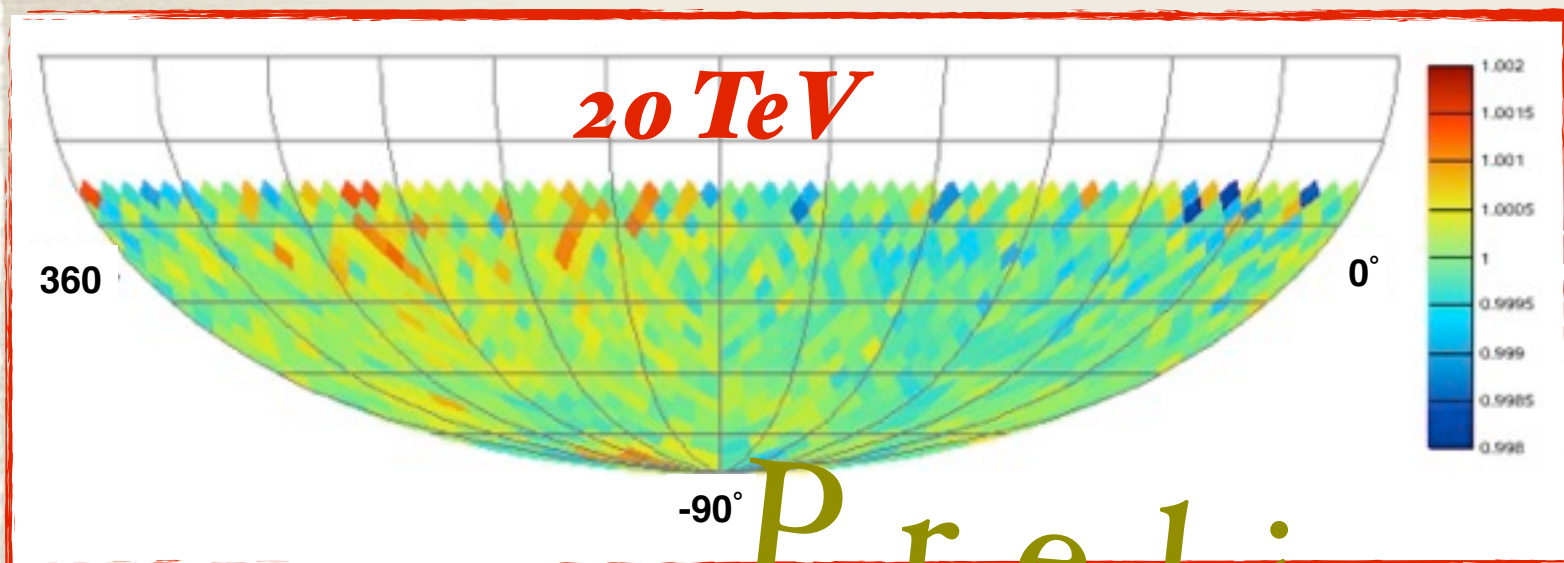
$$\frac{\Delta I}{I} = (\gamma + 2) \frac{v}{c} \cos \theta$$



# Energy dependence of the Solar dipole

- \* IceCube observes the Solar dipole in both energy bins. The observed amplitude is compatible with the expectations within the stat. and sys. uncertainties.
- \* The observation of the solar dipole supports the observation of the sidereal anisotropy in cosmic ray arrival direction.

relative intensity Vs.  $(\alpha[^\circ] - \alpha_{\text{SUN}}[^\circ])$

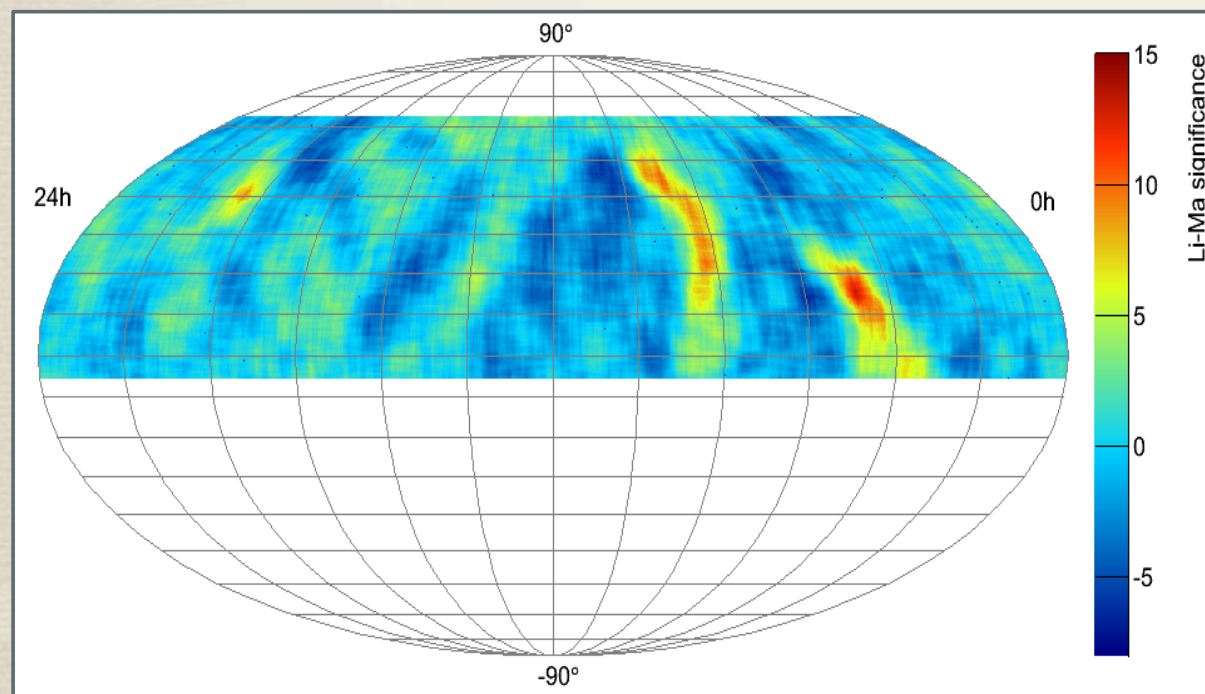


*Preliminary*

# Small scale anisotropy

Several experiments have discovered anisotropies on scales of about  $10^\circ$

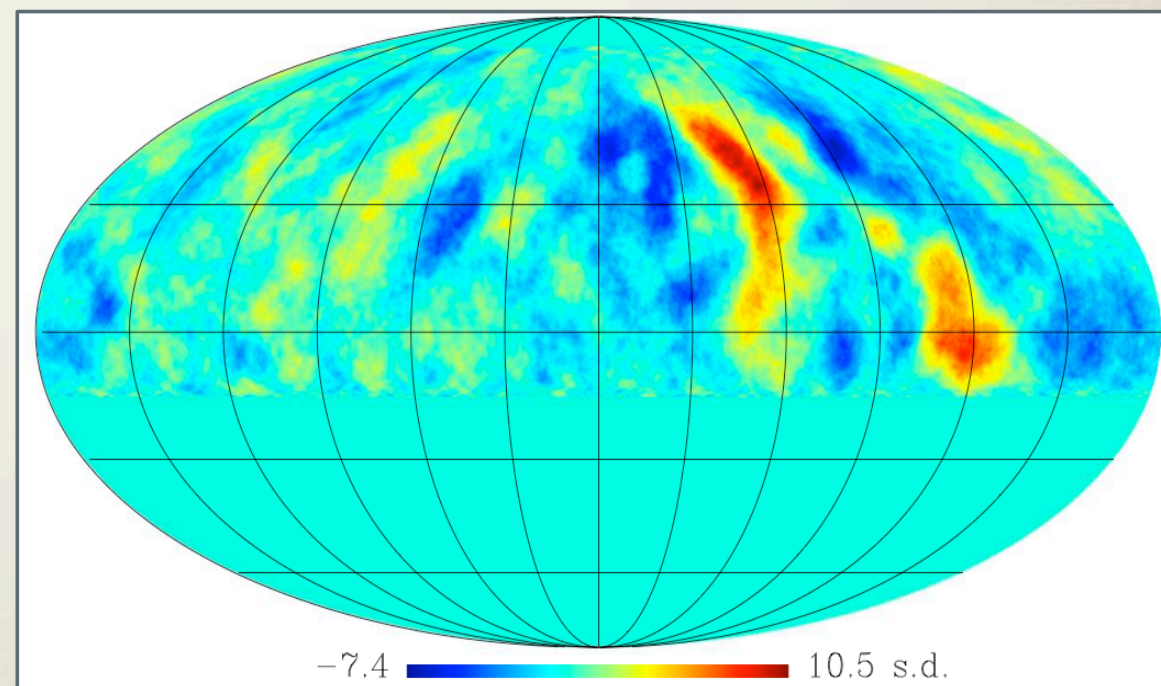
- \* Milagro observes two localized regions with **significance  $> 10\sigma$**  in the total data set of  $2.2 \cdot 10^{11}$  events recorded over 7 years. The “hot” regions have fractional excesses of order several times  $10^{-4}$  relative to the background.
- \* Same structures observed by ARGO-YBJ.



A. Abdo et al., PRL 101 (2008) 221101

**Milagro**

Median Energy: 1 TeV



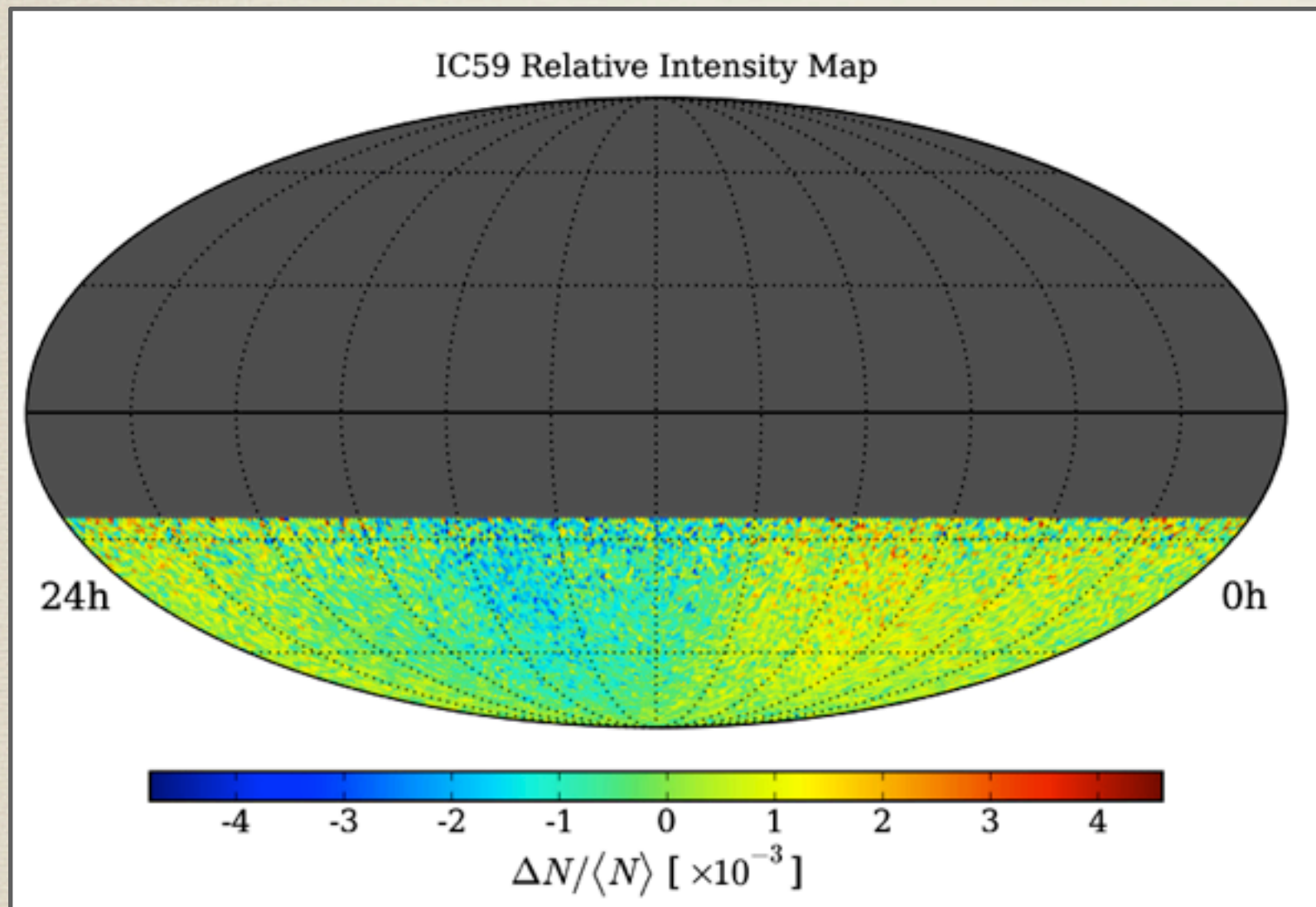
S. Vernetto, Proc. 31st ICRC, 2009

**ARGO-YBJ**

Median Energy: 2 TeV

# Relative Intensity map

*Equatorial sky maps in HEALPix: equal area pixel (size ~ 0.9°)*



**Sky map created using the background estimation technique from real data:**

- $N_i$ : number of data events in the  $i^{th}$  pixel.
- $\langle N_i \rangle$ : expected number of events in an isotropic sky (time scrambling in 24 hr) in the  $i^{th}$  pixel.
- Relative Intensity:

$$\frac{\Delta N_i}{\langle N \rangle_i} = \frac{N_i(\alpha, \delta) - \langle N_i(\alpha, \delta) \rangle}{\langle N_i(\alpha, \delta) \rangle}$$

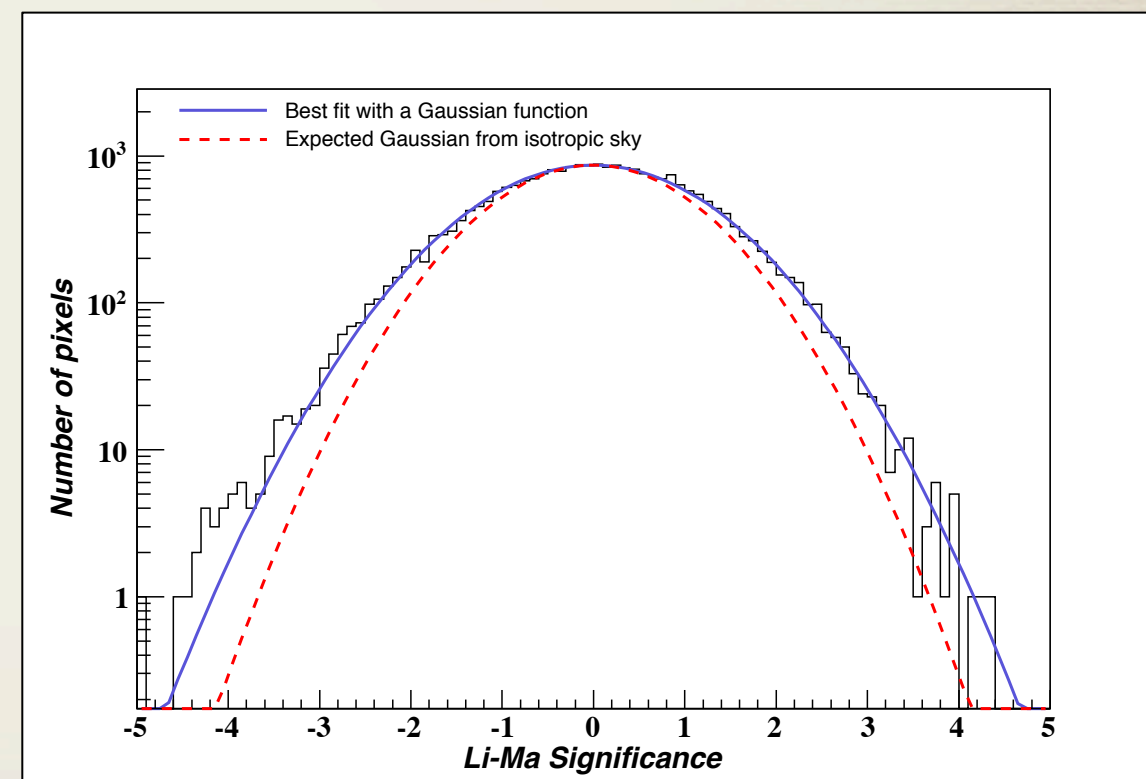
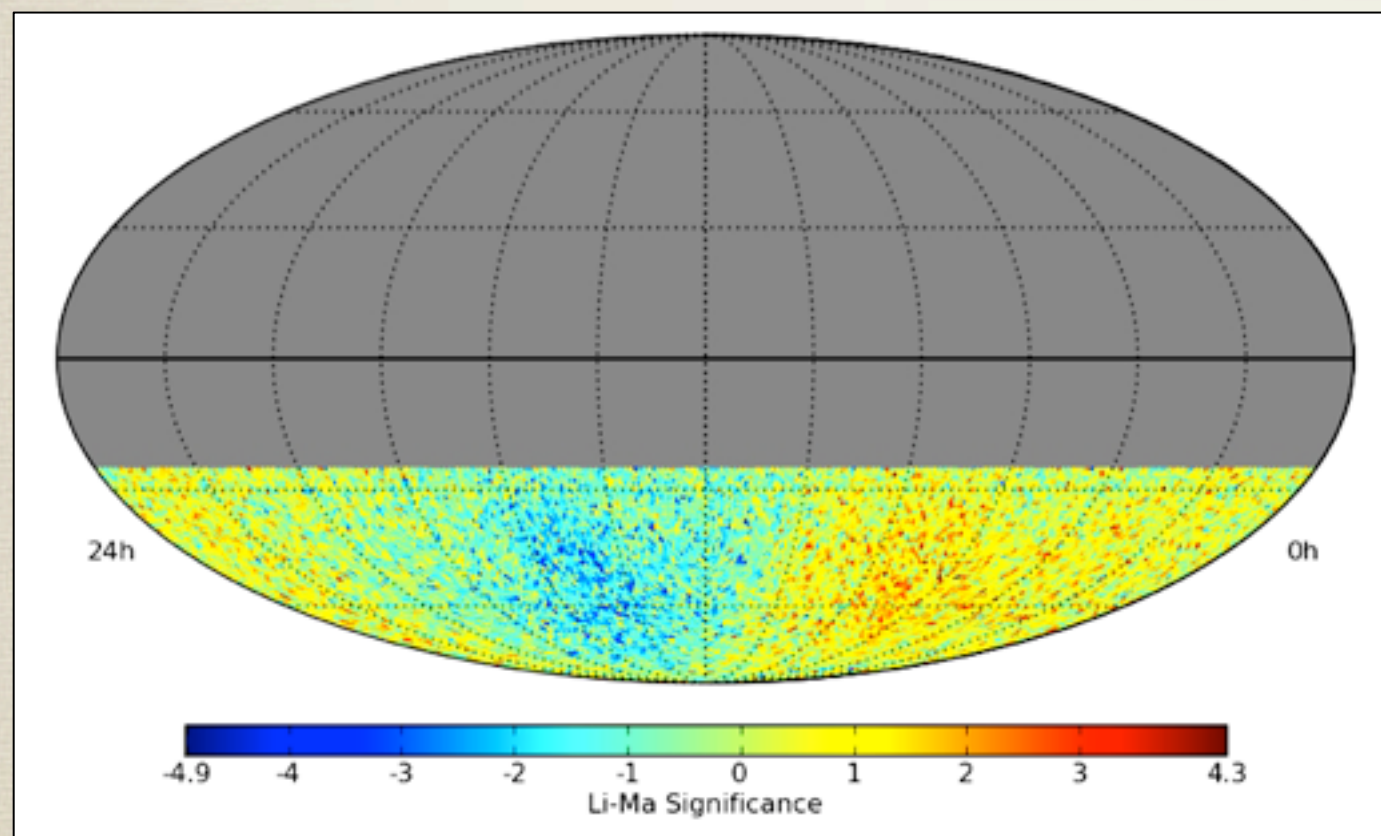
**Relative intensity map is *not isotropic*. In IceCube-59, the *strong large scale structure* already observed in IceCube-22 data is visible in the “raw” data.**

# Significance map

## Significance calculation:

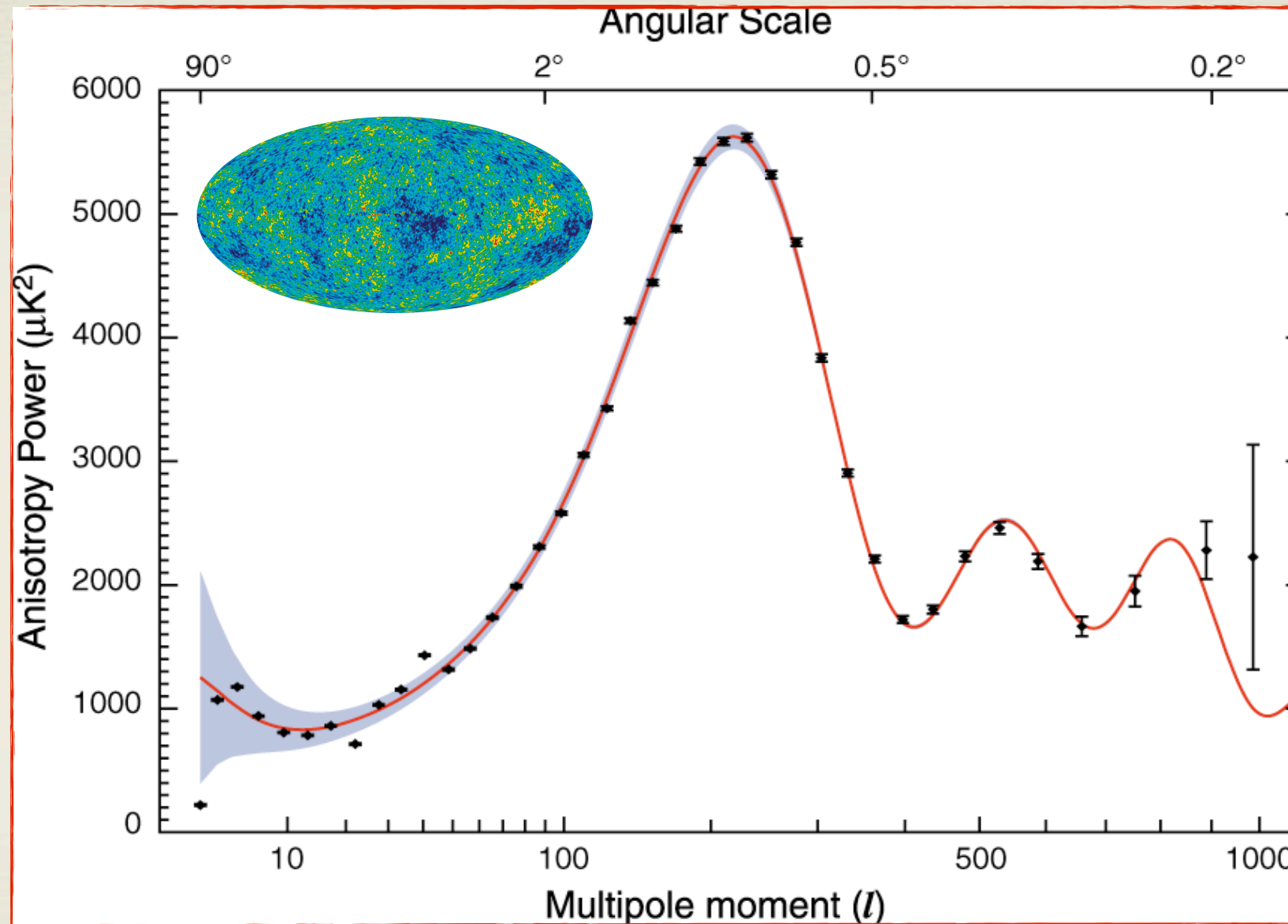
$$s = \sqrt{2} \left\{ N_{\text{on}} \ln \left[ \frac{1 + \alpha}{\alpha} \left( \frac{N_{\text{on}}}{N_{\text{on}} + N_{\text{off}}} \right) \right] + N_{\text{off}} \ln \left[ (1 + \alpha) \left( \frac{N_{\text{off}}}{N_{\text{on}} + N_{\text{off}}} \right) \right] \right\}^{1/2} \quad \alpha = 1/20$$

Li, T., & Ma, Y. 1983, ApJ, 272, 317



# Power spectrum

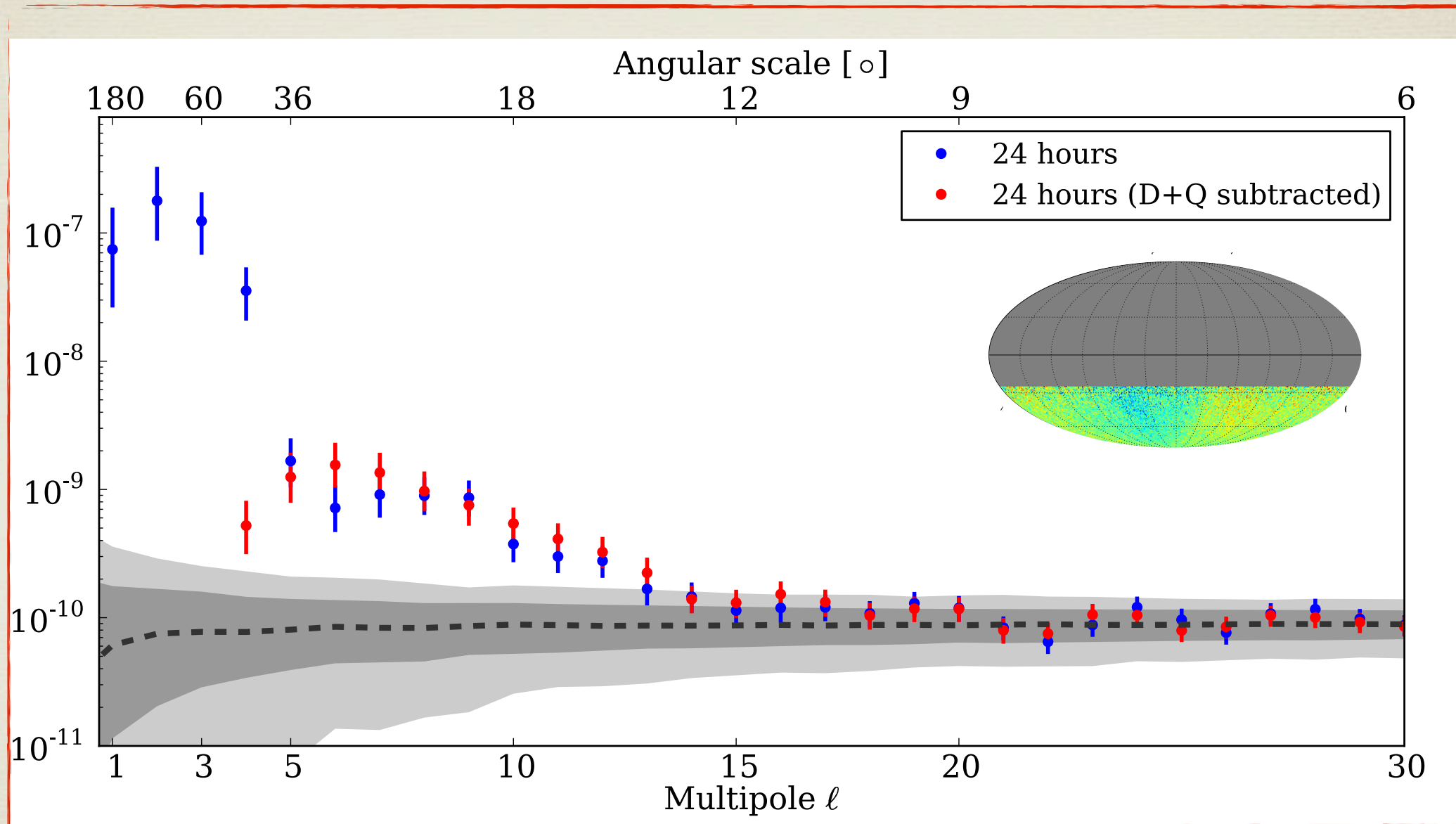
**Angular size**  $\theta \sim \frac{180^\circ}{\ell}$



**Multipole expansion:** 
$$\delta I(\mathbf{u}_i) = \sum_{\ell=1}^{\infty} \sum_{m=-\ell}^{\ell} a_{\ell m} Y_{\ell m}(\mathbf{u}_i) \quad C_{\ell} = \frac{1}{2\ell + 1} \sum_m |a_{\ell m}|^2$$

# Power spectrum

**Angular size**  $\theta \sim \frac{180^\circ}{\ell}$



**Multipole expansion:**

$$\delta I(\mathbf{u}_i) = \sum_{\ell=1}^{\infty} \sum_{m=-\ell}^{\ell} a_{\ell m} Y_{\ell m}(\mathbf{u}_i) \quad C_{\ell} = \frac{1}{2\ell + 1} \sum_m |a_{\ell m}|^2$$

# Dipole and quadrupole fit

$$\delta I(\alpha, \delta) = m_0$$

$$+ p_x \cos \delta \cos \alpha + p_y \cos \delta \sin \alpha + p_z \sin \delta$$

$$+ \frac{1}{2} Q_1 (3 \cos^2 \delta - 1) + Q_2 \sin 2\delta \cos \alpha + Q_3 \sin 2\delta \sin \alpha + Q_4 \cos^2 \delta \cos 2\alpha + Q_5 \cos^2 \delta \sin 2\alpha$$

**monopole**

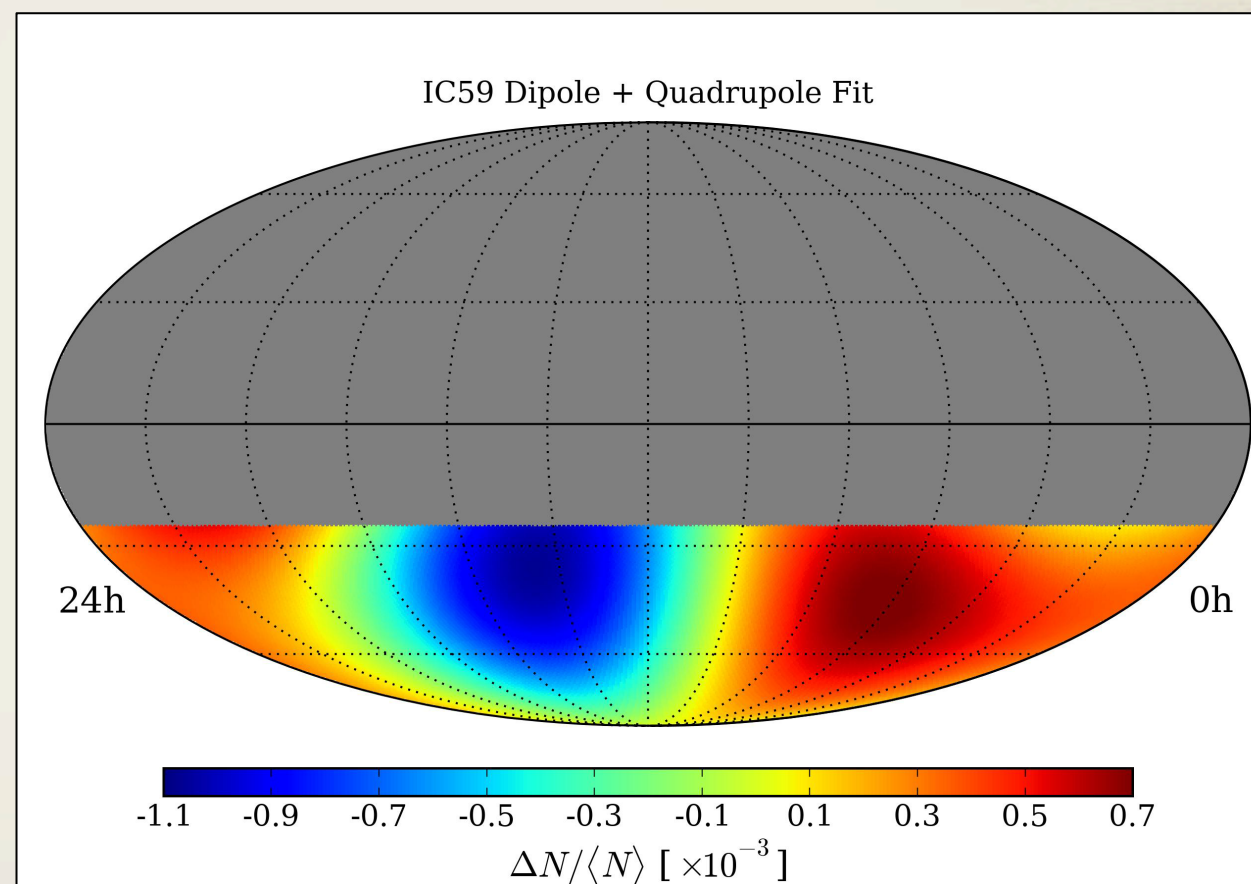
**dipole**

**quadrupole**

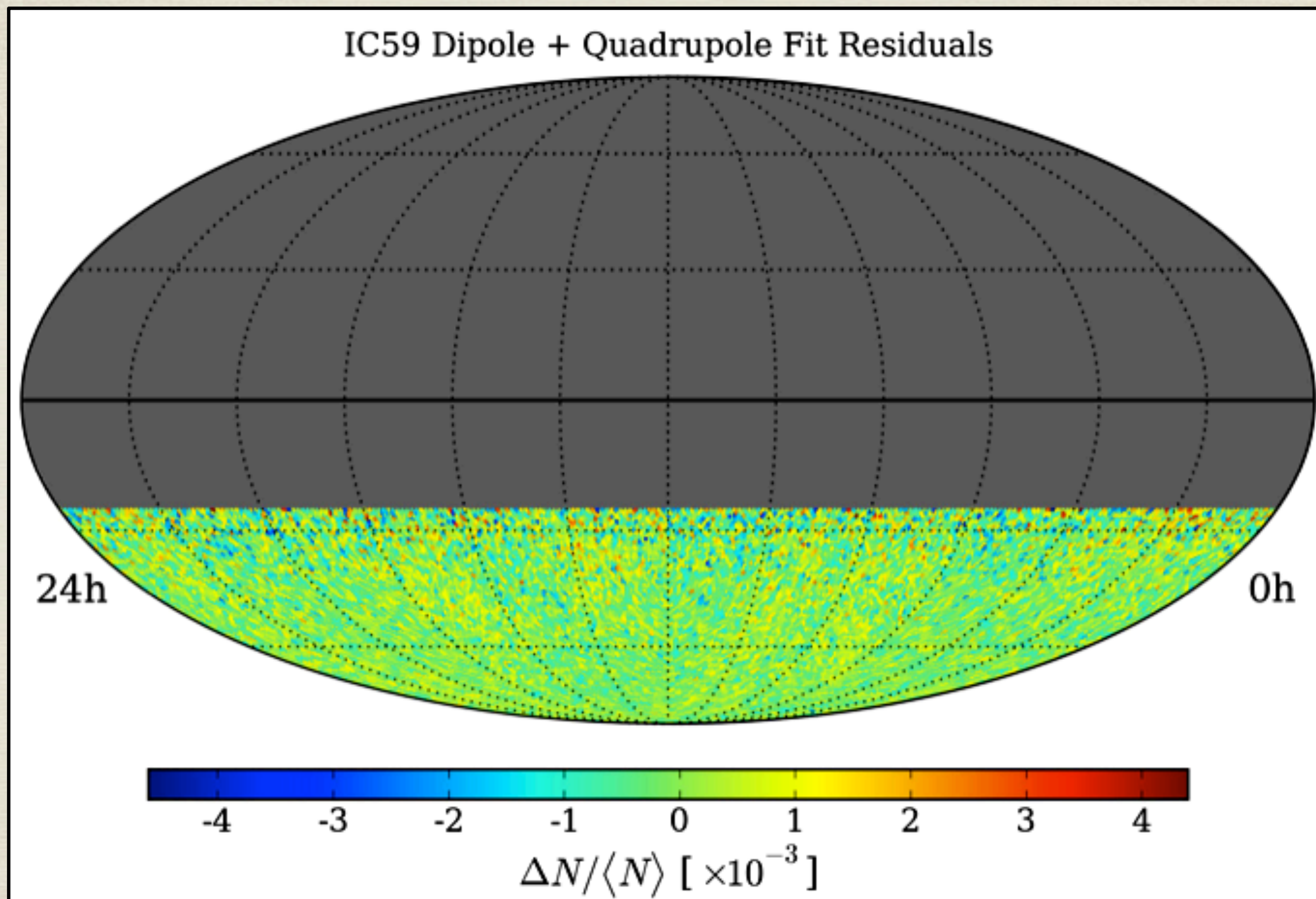
Coefficient	Fit Value
$m_0$	$0.320 \pm 2.264$
$p_x$	$2.435 \pm 0.707$
$p_y$	$-3.856 \pm 0.707$
$p_z$	$0.548 \pm 3.872$
$Q_1$	$0.233 \pm 1.702$
$Q_2$	$-2.949 \pm 0.494$
$Q_3$	$-8.797 \pm 0.494$
$Q_4$	$-2.148 \pm 0.200$
$Q_5$	$-5.268 \pm 0.200$

$$\chi^2/\text{ndf} = 14743.4/14187$$

$$\text{Pr}(\chi^2|\text{ndf}) = 5.5 \times 10^{-4}$$



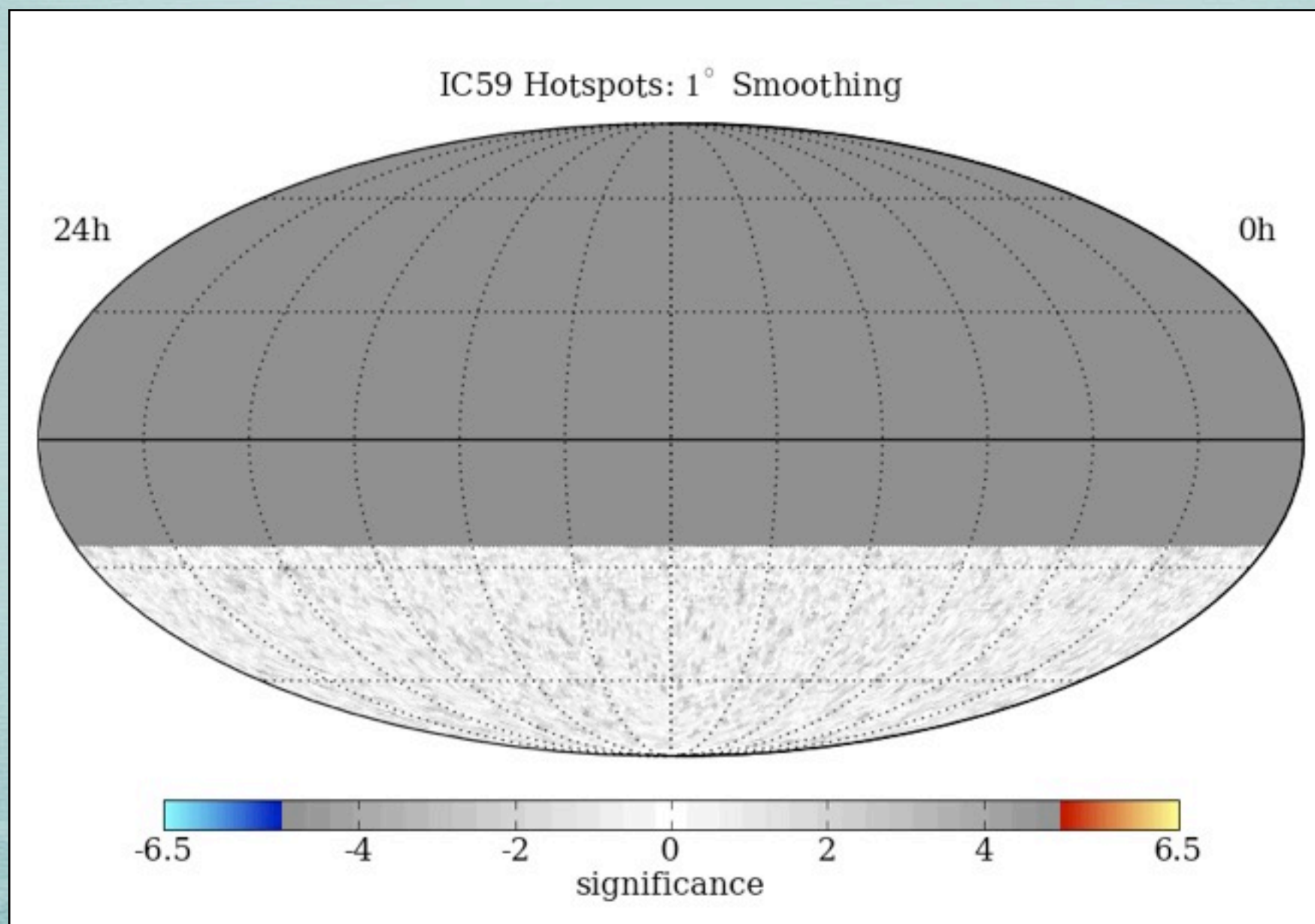
# Residual map



No structures seem to be present: we need to smooth the map.

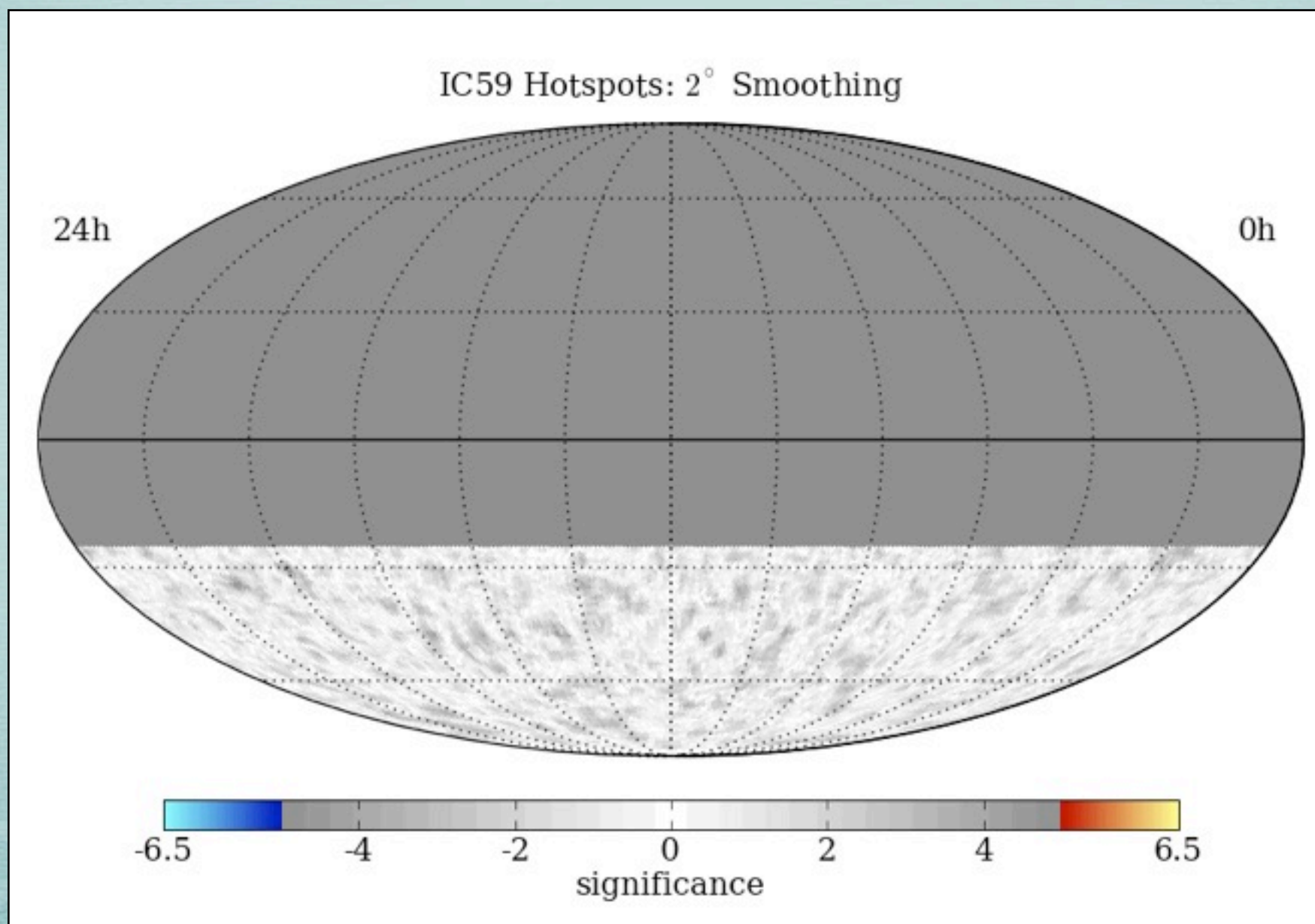
# MAP SMOOTHING SCAN

Scan from 1 - 30° in smoothing  
 Different regions have different optimal angular smoothing  
 Significances are pre-trial



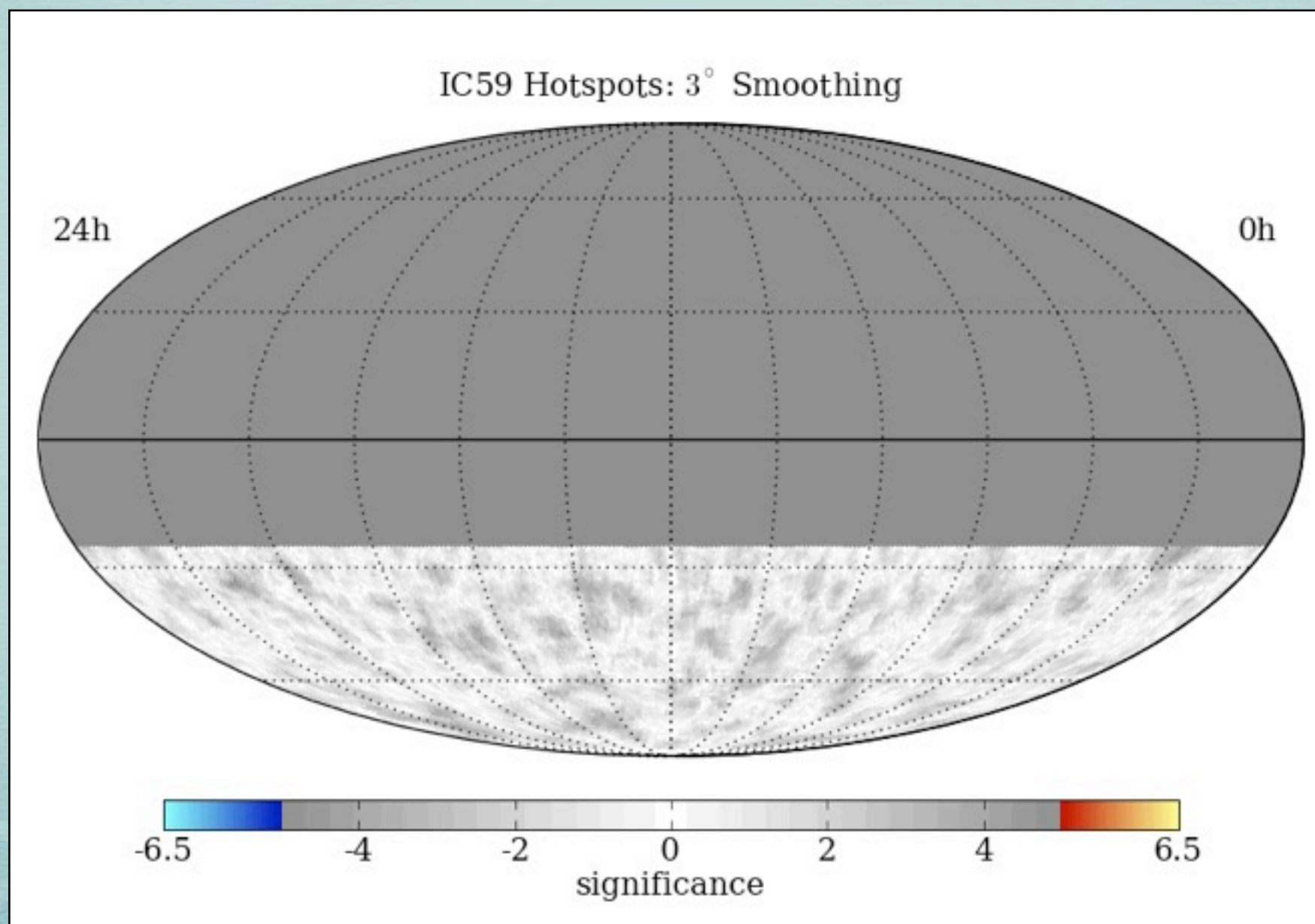
# MAP SMOOTHING SCAN

Scan from 1 - 30° in smoothing  
Different regions have different optimal angular smoothing  
Significances are pre-trial



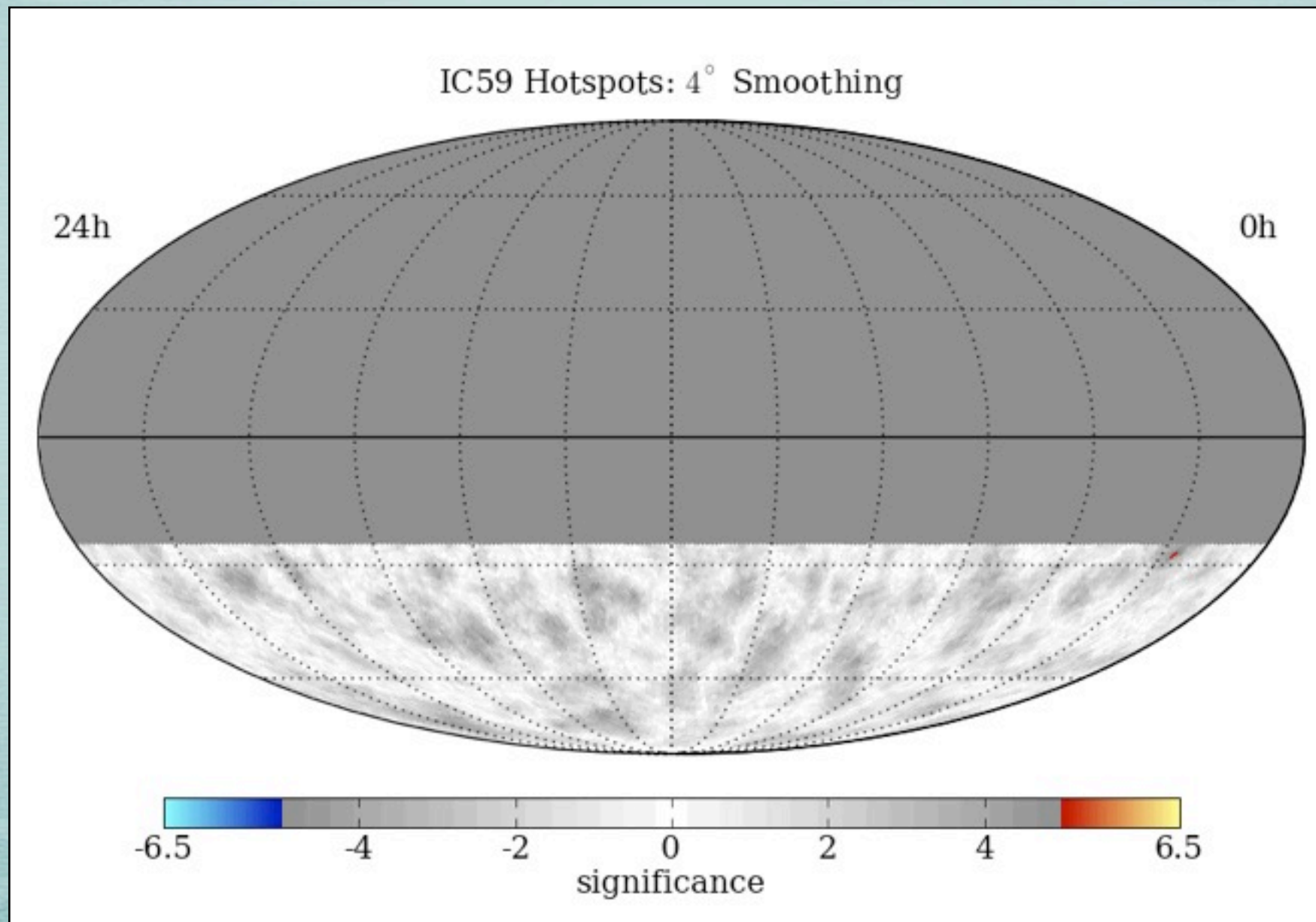
# MAP SMOOTHING SCAN

Scan from 1 - 30° in smoothing  
 Different regions have different optimal angular smoothing  
 Significances are pre-trial



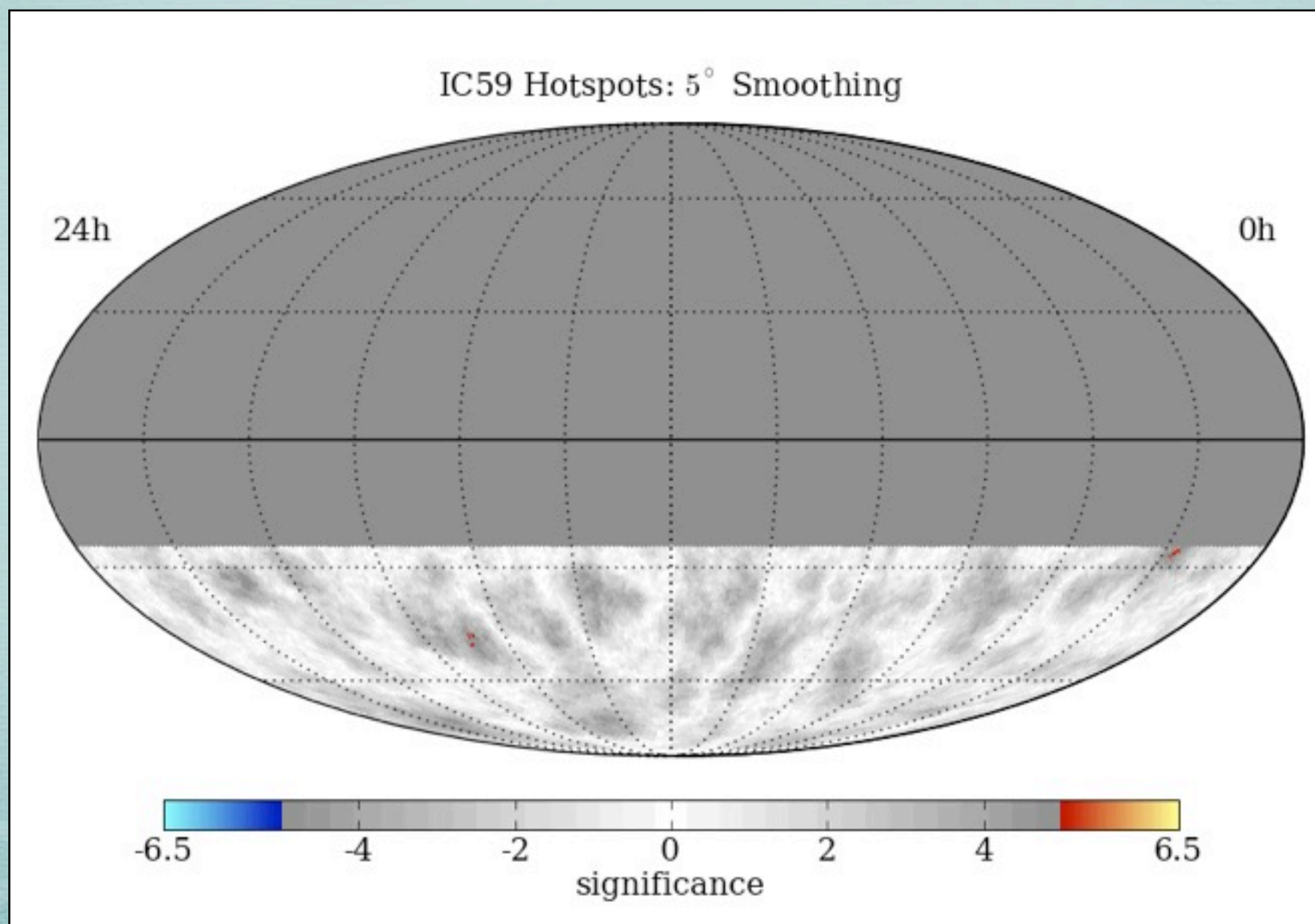
# MAP SMOOTHING SCAN

Scan from 1 - 30° in smoothing  
Different regions have different optimal angular smoothing  
Significances are pre-trial



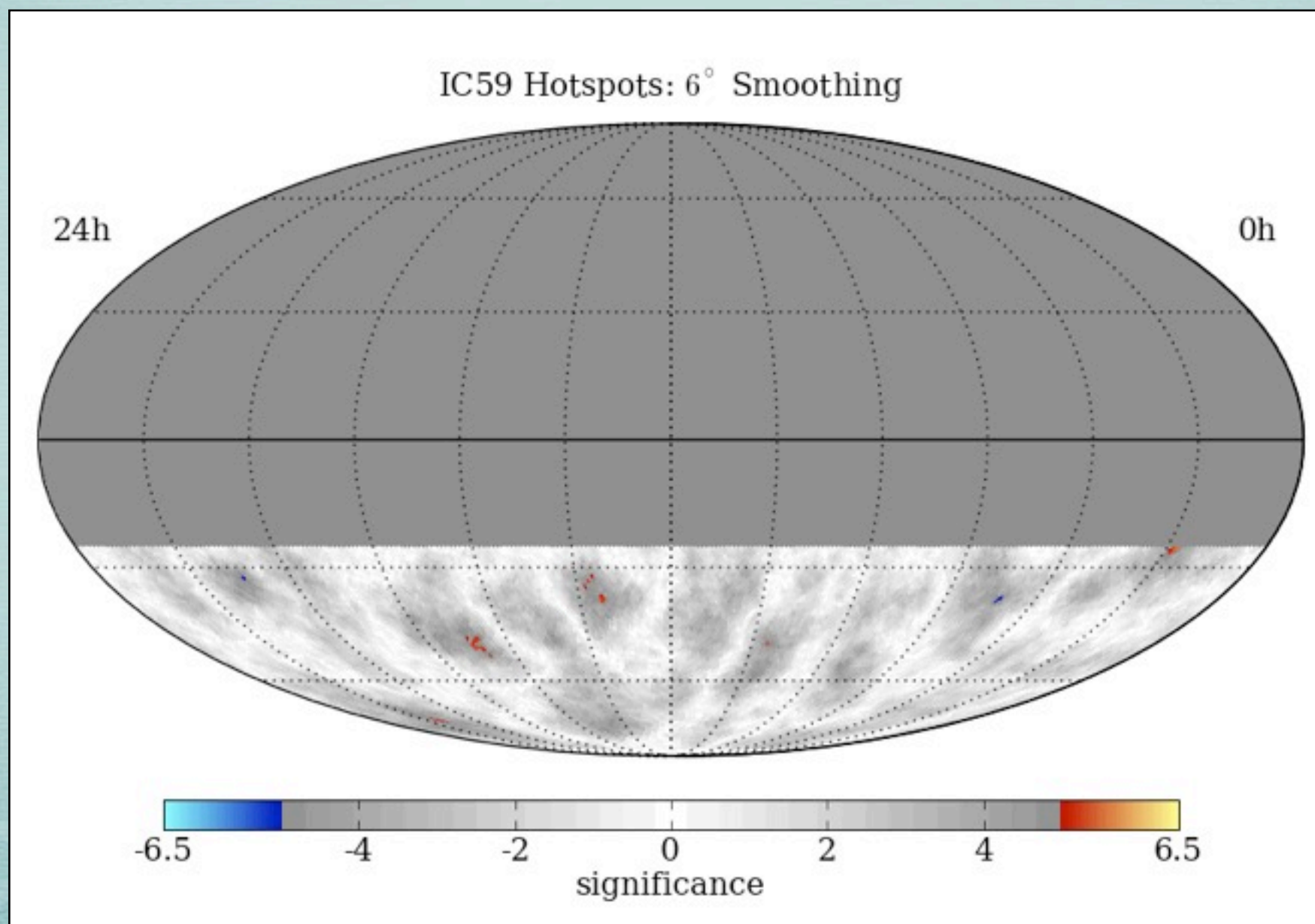
# MAP SMOOTHING SCAN

Scan from 1 - 30° in smoothing  
Different regions have different optimal angular smoothing  
Significances are pre-trial



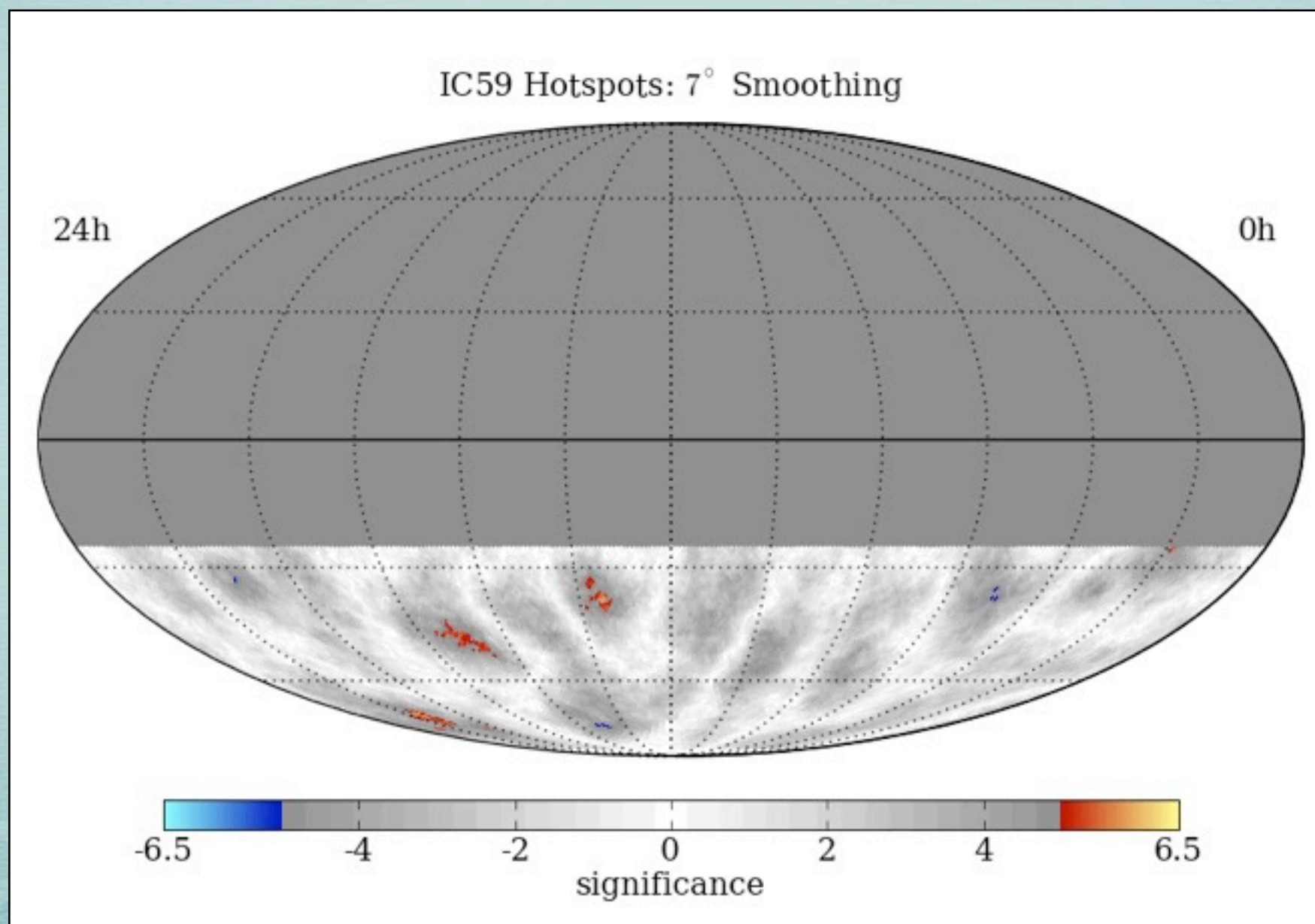
# MAP SMOOTHING SCAN

Scan from 1 - 30° in smoothing  
Different regions have different optimal angular smoothing  
Significances are pre-trial



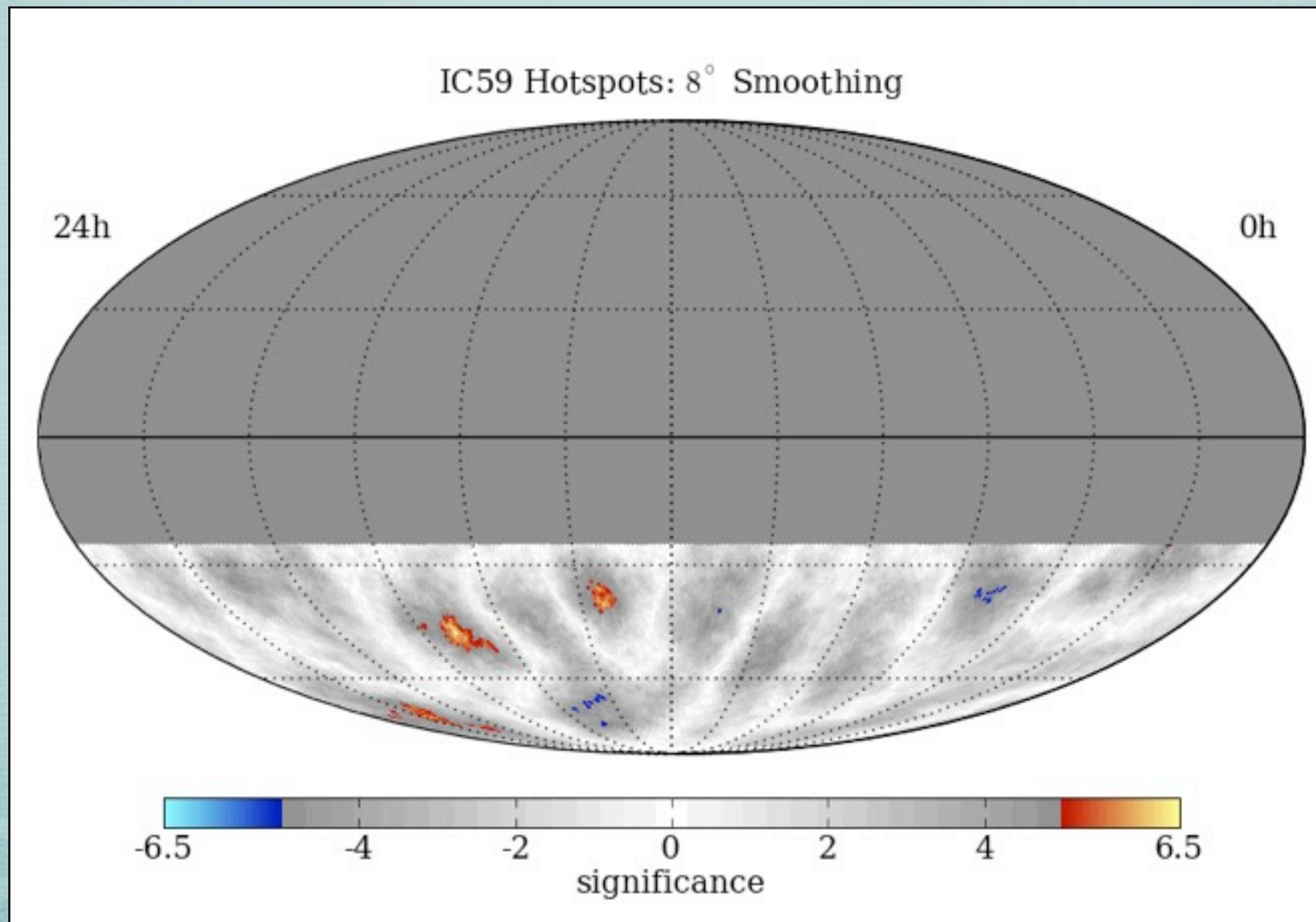
# MAP SMOOTHING SCAN

Scan from 1 - 30° in smoothing  
 Different regions have different optimal angular smoothing  
 Significances are pre-trial



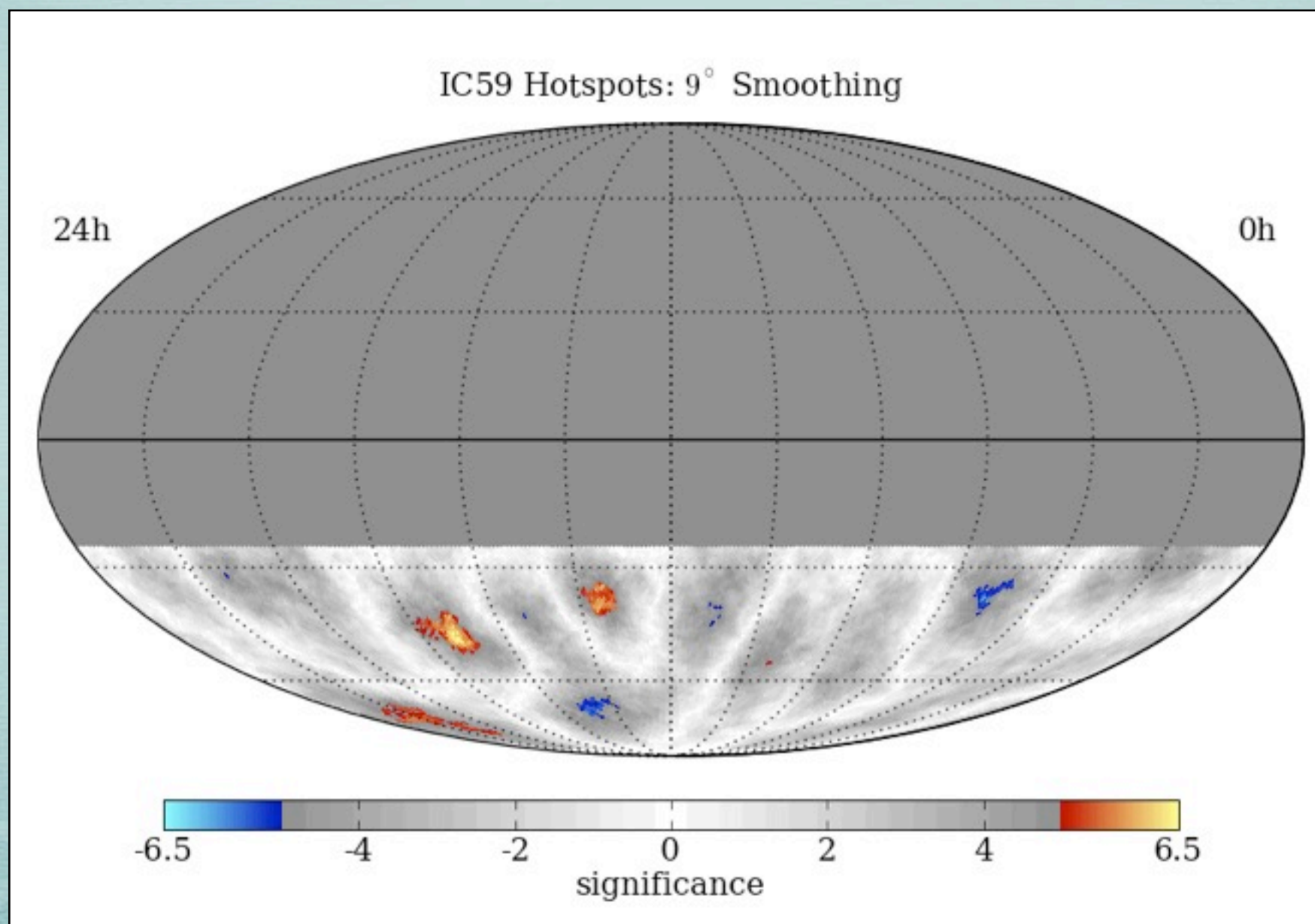
# MAP SMOOTHING SCAN

Scan from 1 - 30° in smoothing  
Different regions have different optimal angular smoothing  
Significances are pre-trial



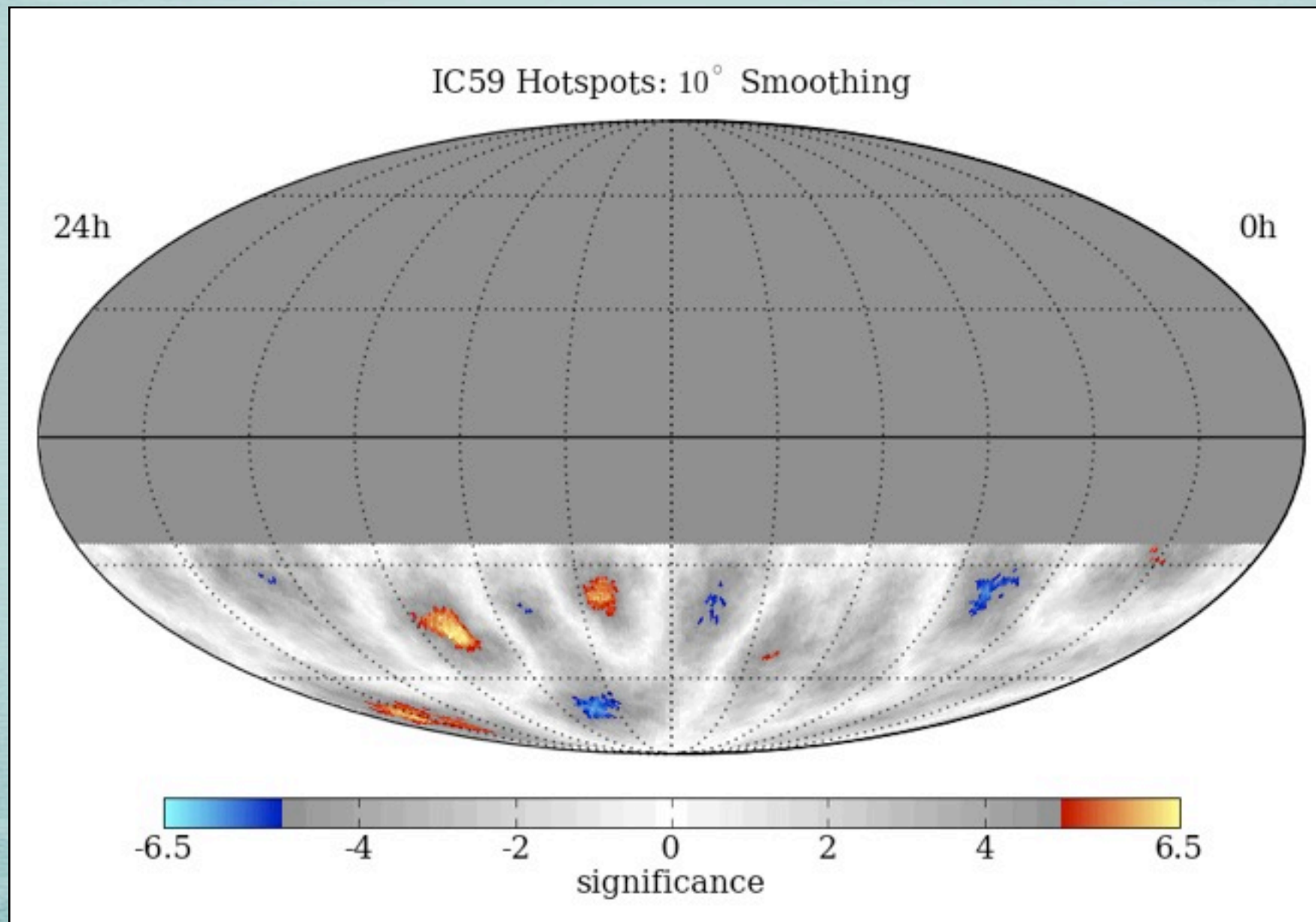
# MAP SMOOTHING SCAN

Scan from 1 - 30° in smoothing  
 Different regions have different optimal angular smoothing  
 Significances are pre-trial



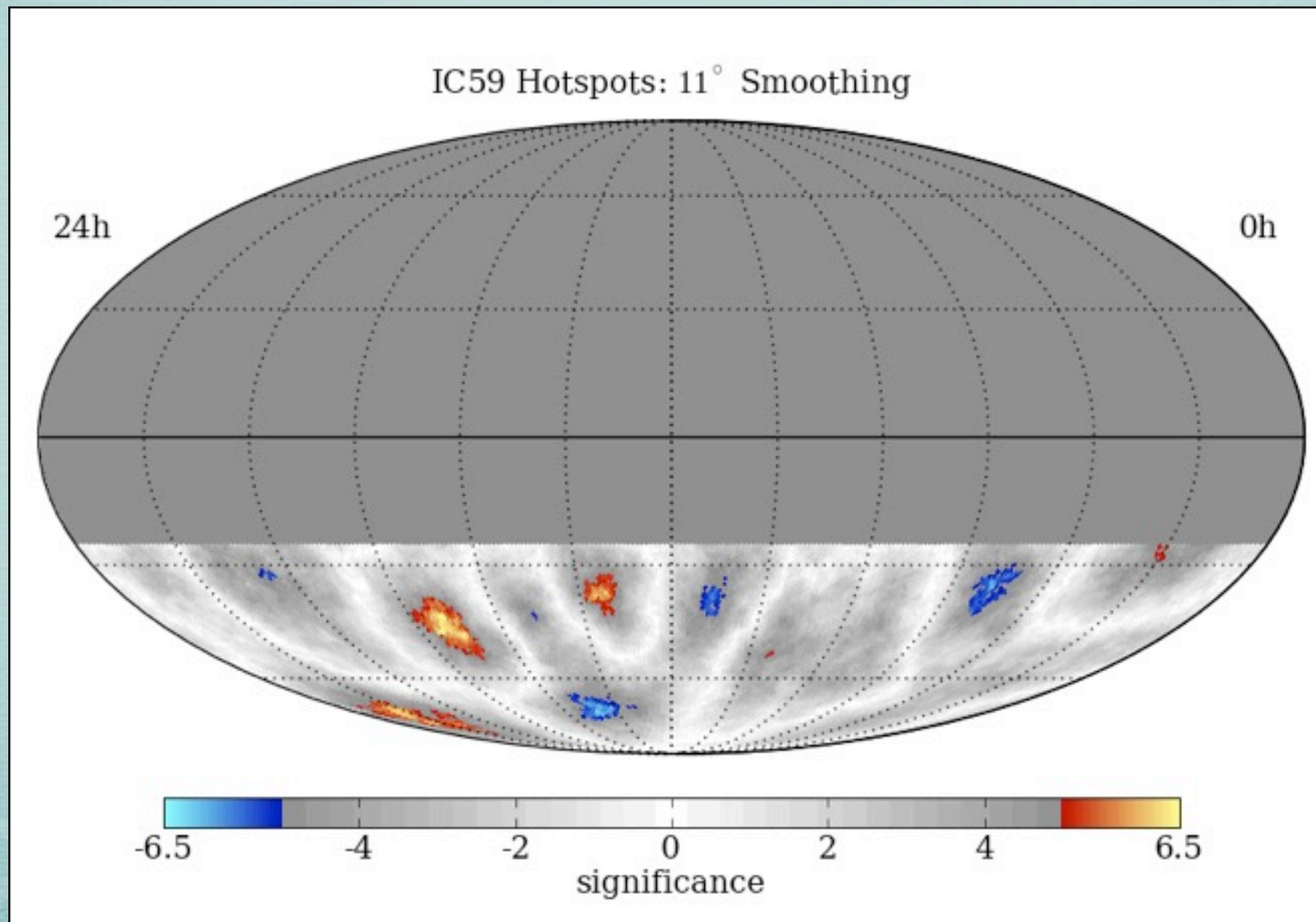
# MAP SMOOTHING SCAN

Scan from 1 - 30° in smoothing  
Different regions have different optimal angular smoothing  
Significances are pre-trial



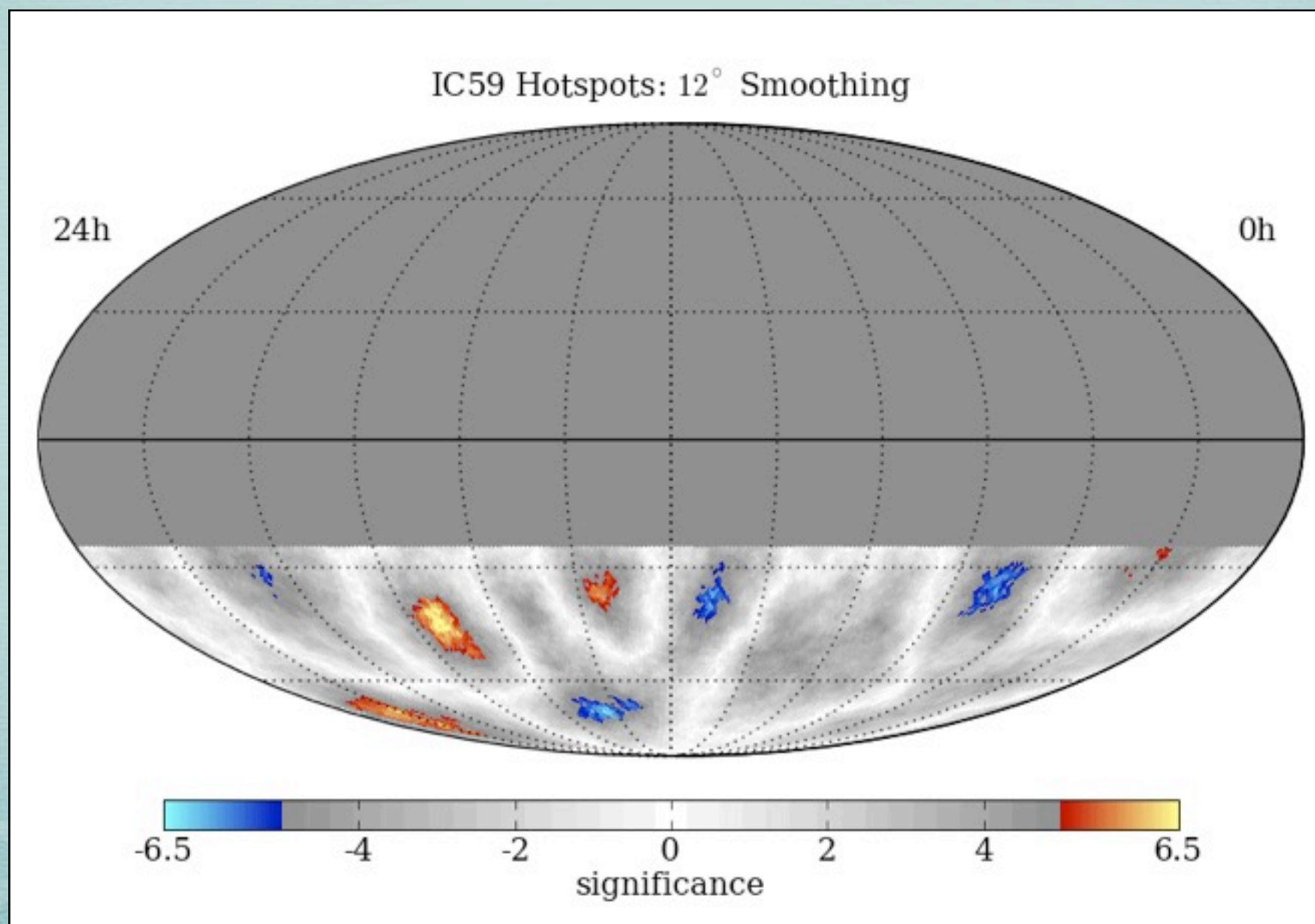
# MAP SMOOTHING SCAN

Scan from 1 - 30° in smoothing  
Different regions have different optimal angular smoothing  
Significances are pre-trial



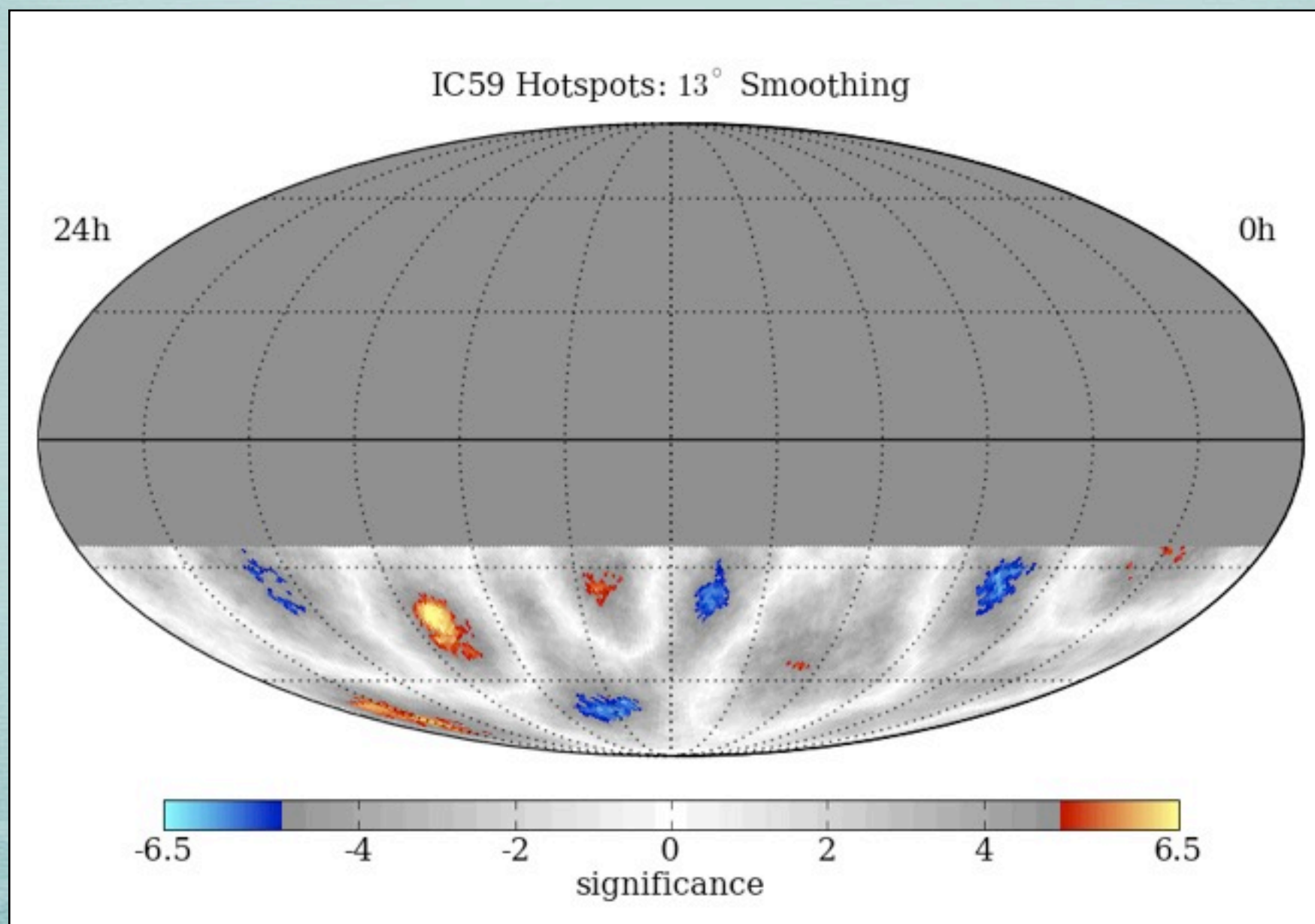
# MAP SMOOTHING SCAN

Scan from 1 - 30° in smoothing  
 Different regions have different optimal angular smoothing  
 Significances are pre-trial



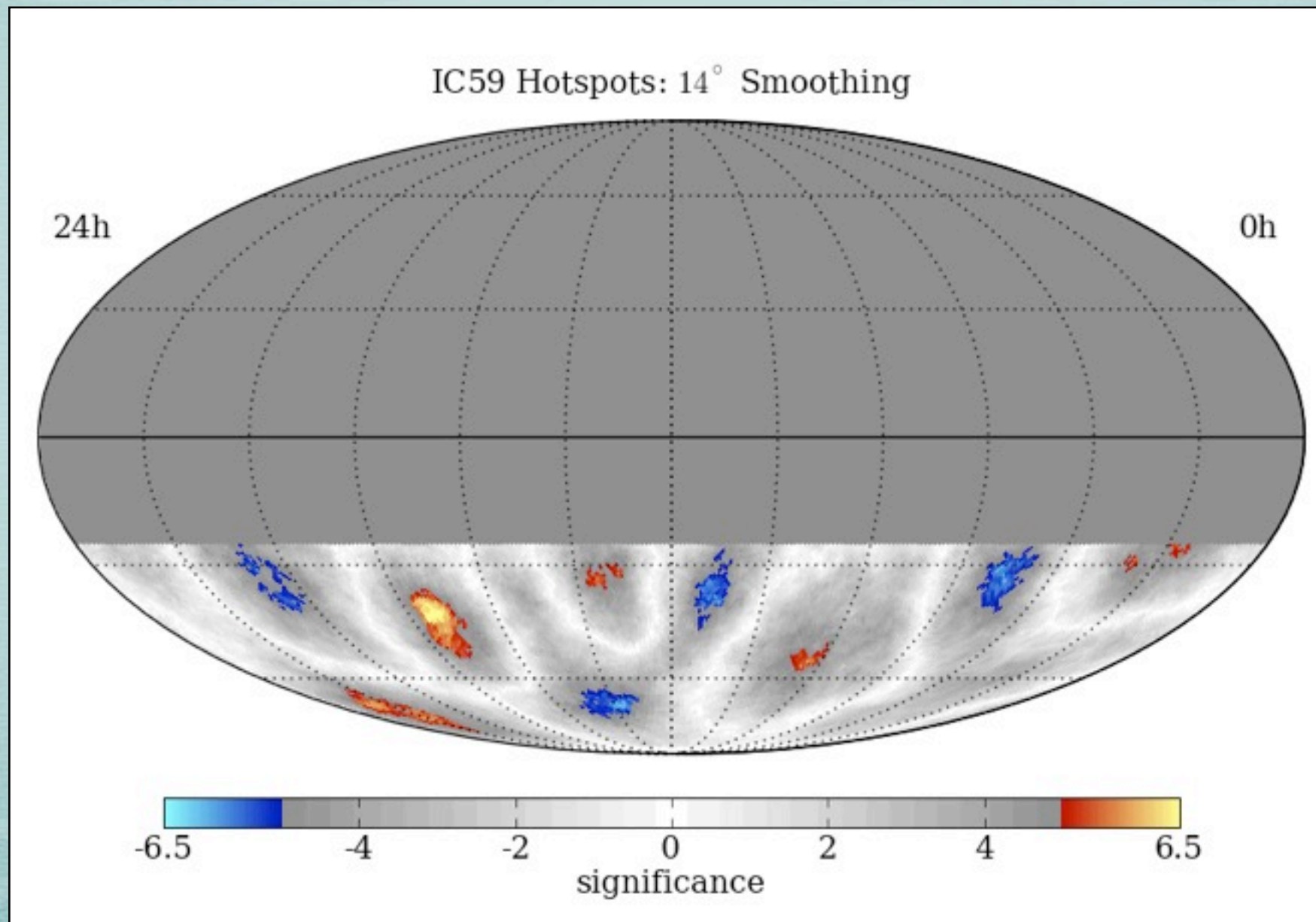
# MAP SMOOTHING SCAN

Scan from 1 - 30° in smoothing  
 Different regions have different optimal angular smoothing  
 Significances are pre-trial



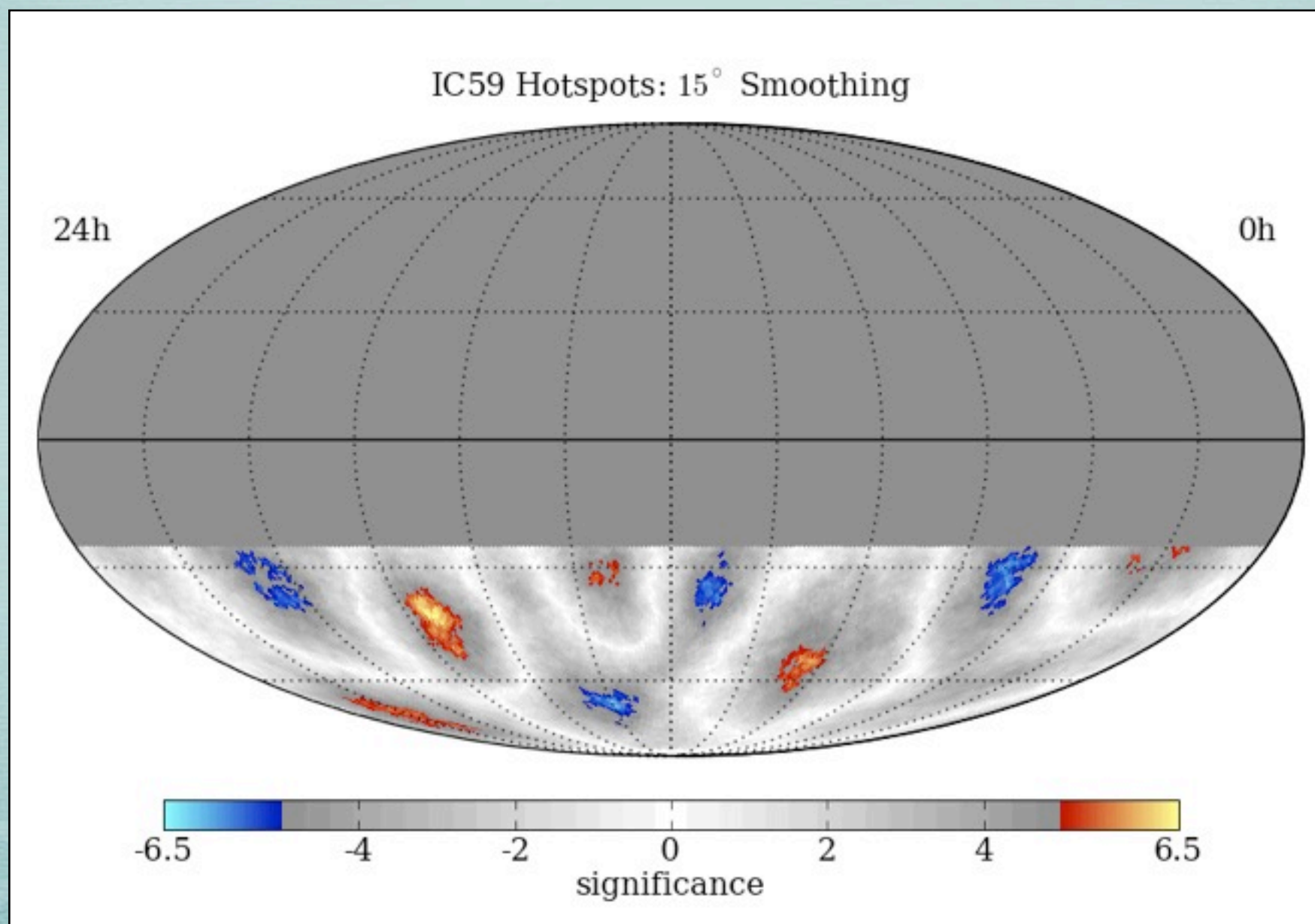
# MAP SMOOTHING SCAN

Scan from 1 - 30° in smoothing  
Different regions have different optimal angular smoothing  
Significances are pre-trial



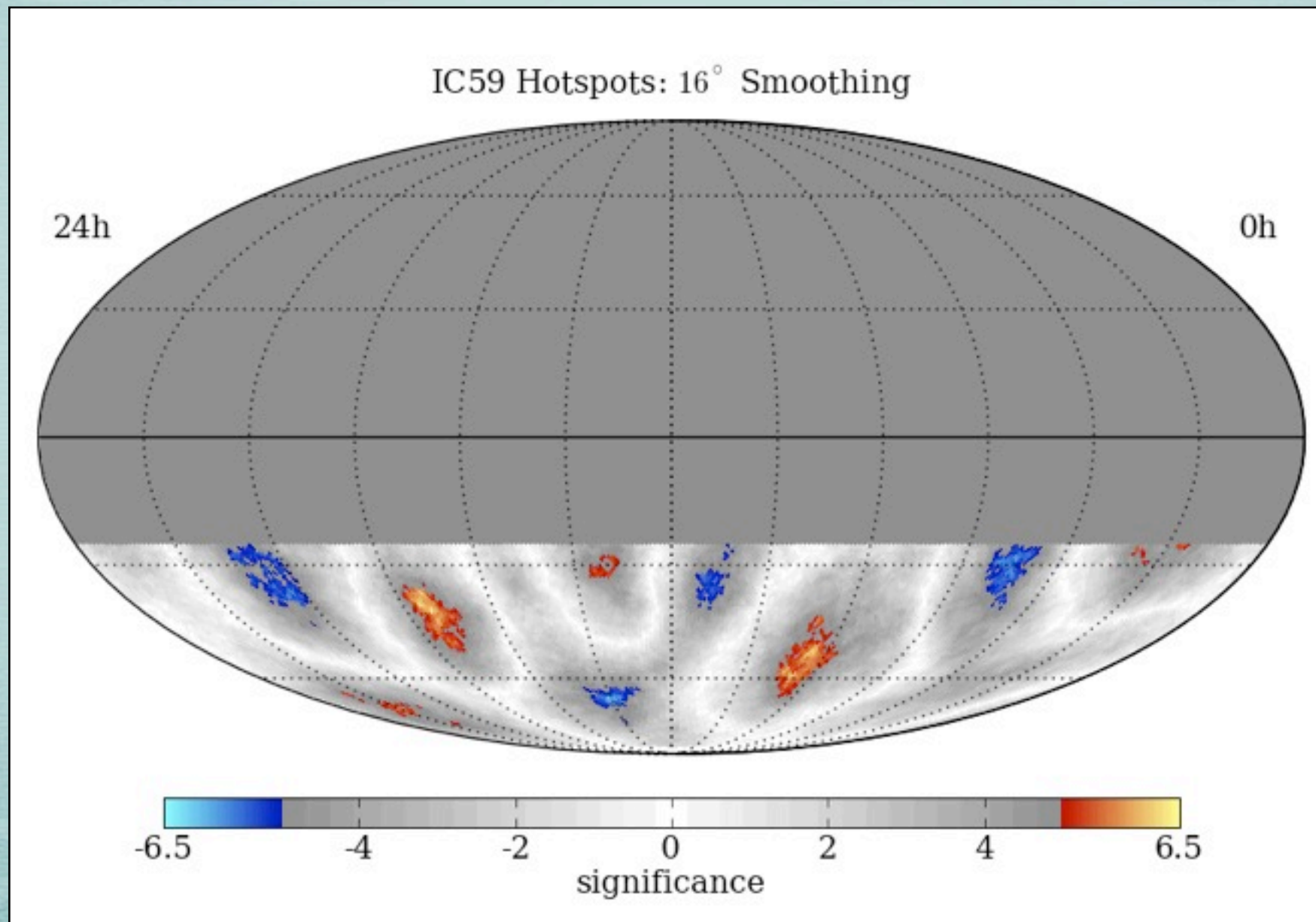
# MAP SMOOTHING SCAN

Scan from 1 - 30° in smoothing  
 Different regions have different optimal angular smoothing  
 Significances are pre-trial



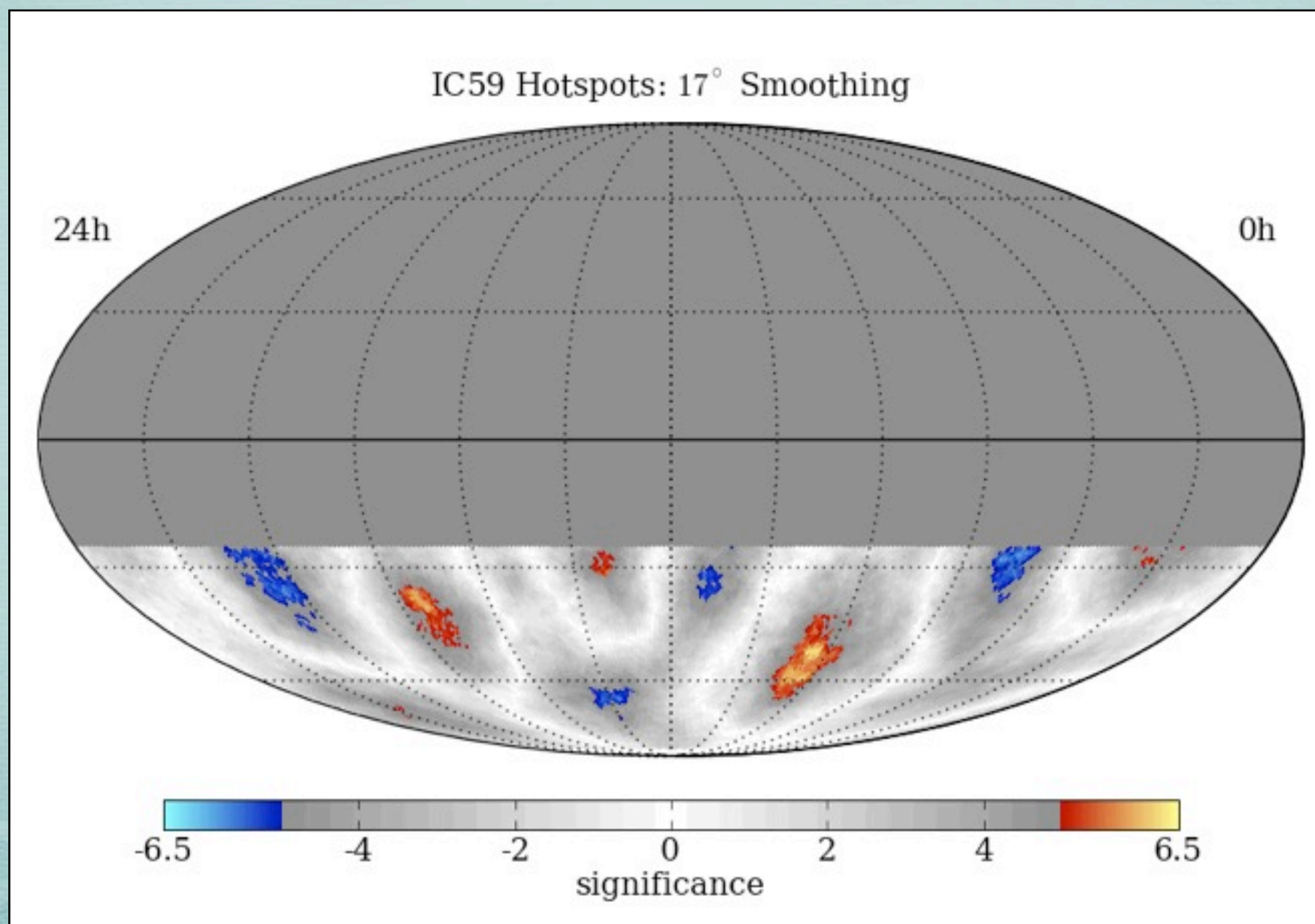
# MAP SMOOTHING SCAN

Scan from 1 - 30° in smoothing  
Different regions have different optimal angular smoothing  
Significances are pre-trial



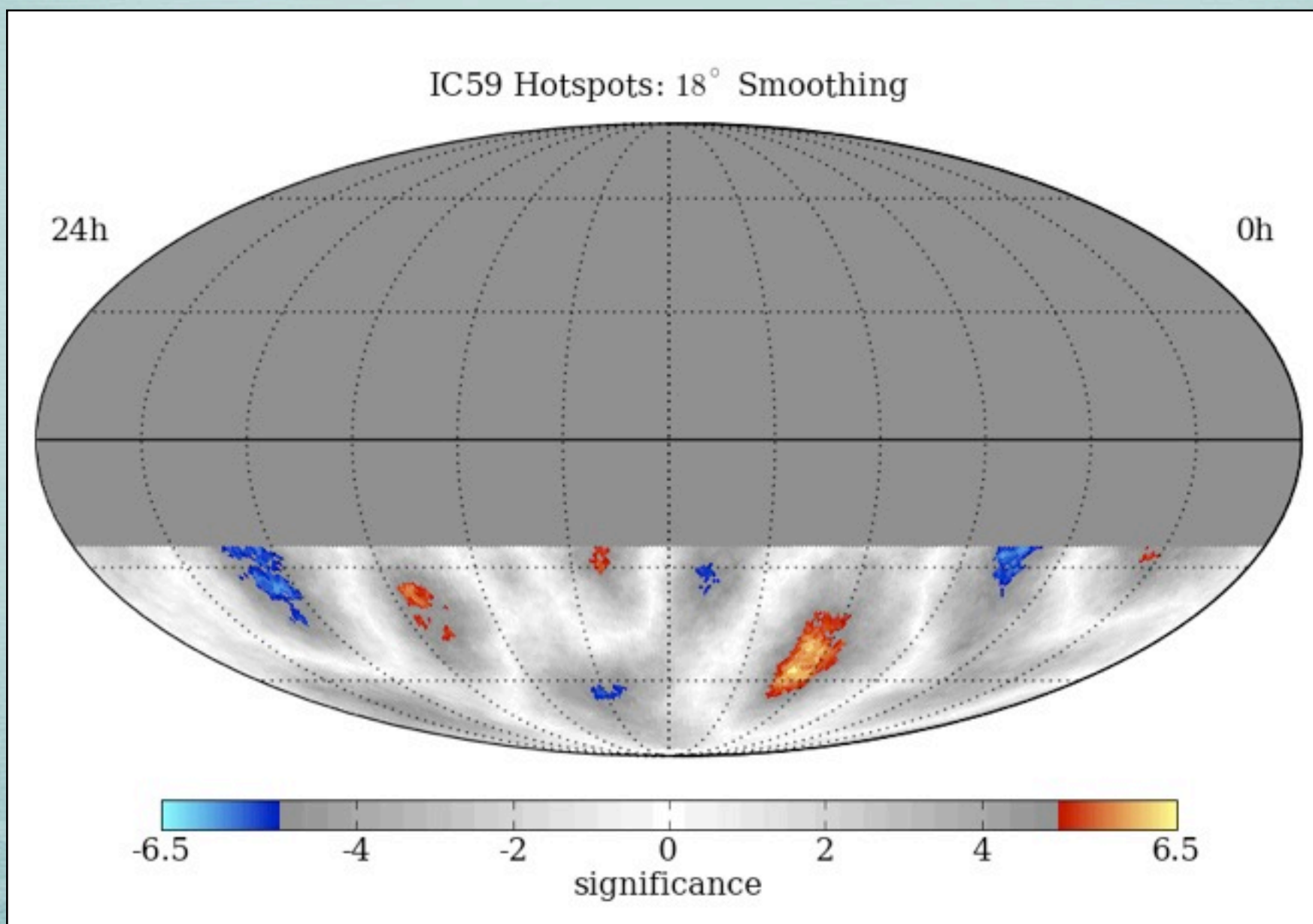
# MAP SMOOTHING SCAN

Scan from 1 - 30° in smoothing  
 Different regions have different optimal angular smoothing  
 Significances are pre-trial



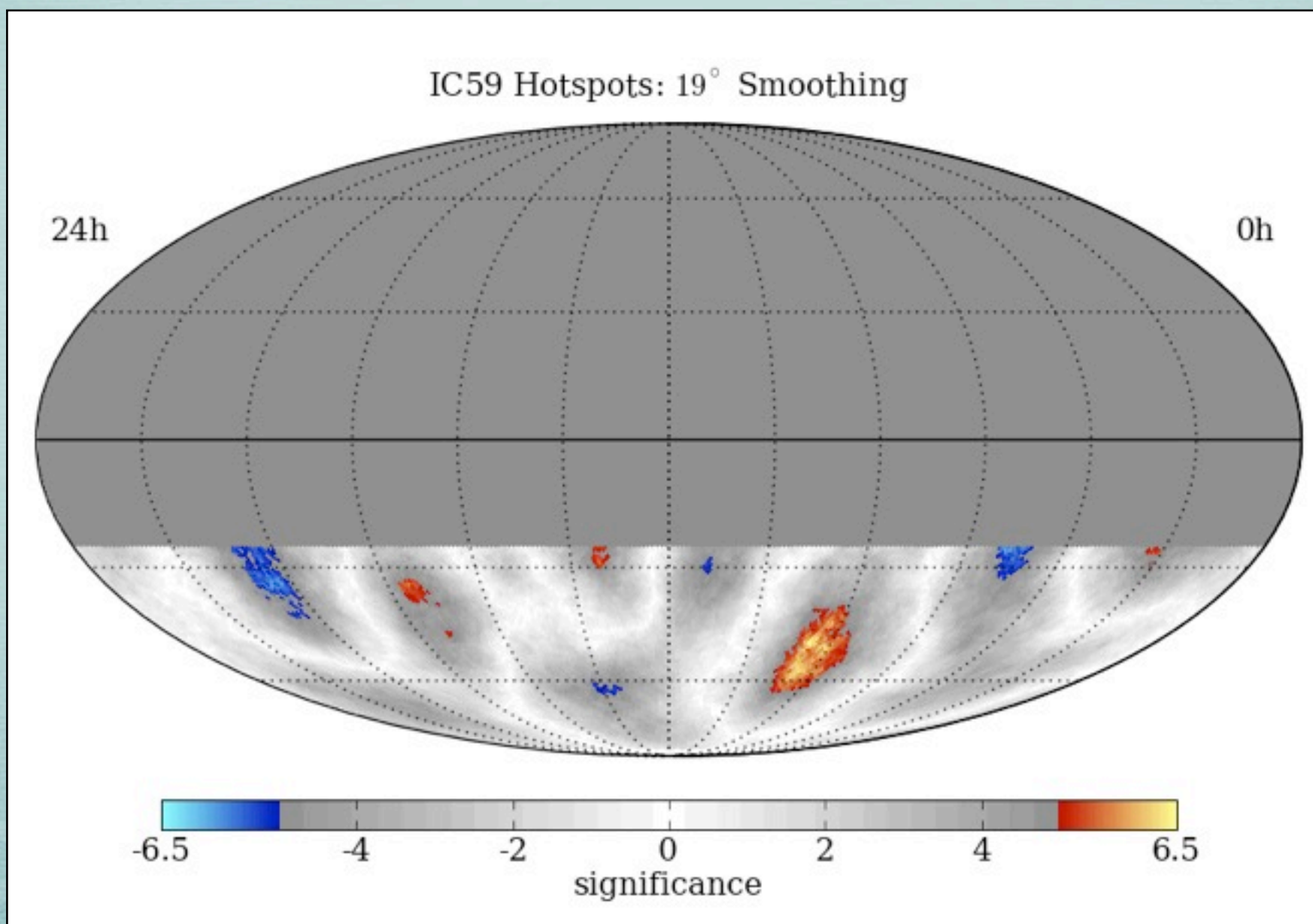
# MAP SMOOTHING SCAN

Scan from 1 - 30° in smoothing  
 Different regions have different optimal angular smoothing  
 Significances are pre-trial



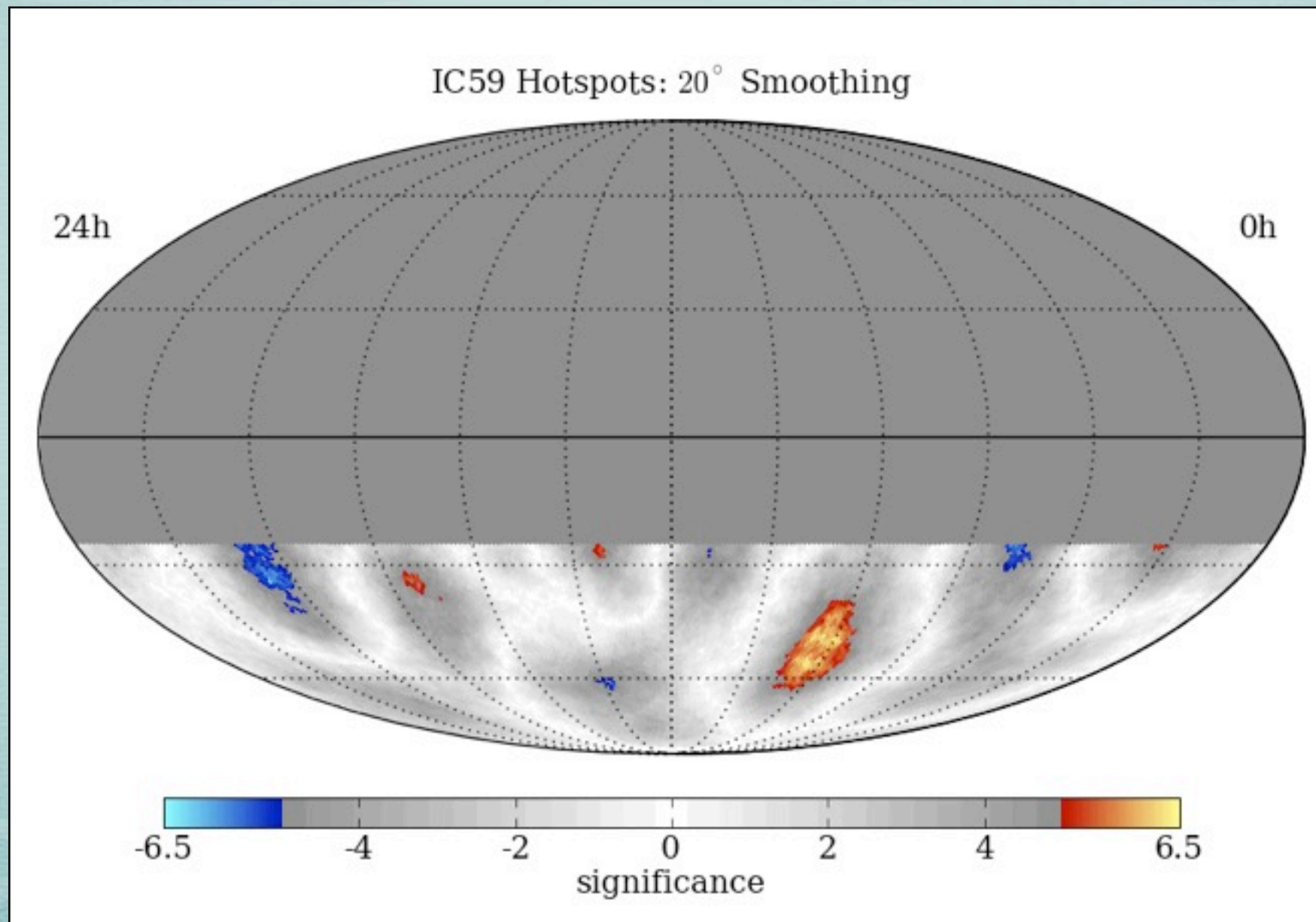
# MAP SMOOTHING SCAN

Scan from 1 - 30° in smoothing  
 Different regions have different optimal angular smoothing  
 Significances are pre-trial



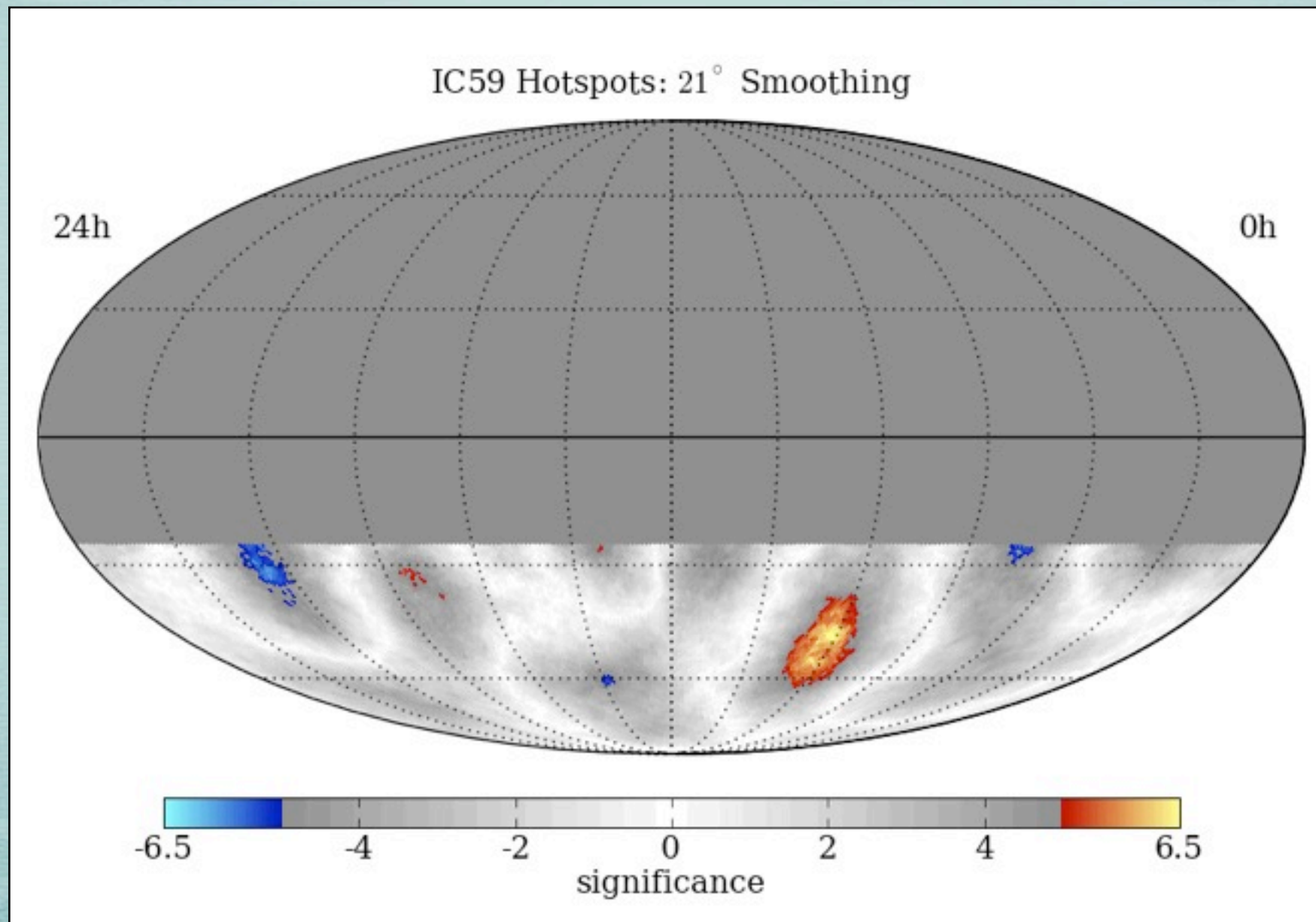
# MAP SMOOTHING SCAN

Scan from 1 - 30° in smoothing  
Different regions have different optimal angular smoothing  
Significances are pre-trial



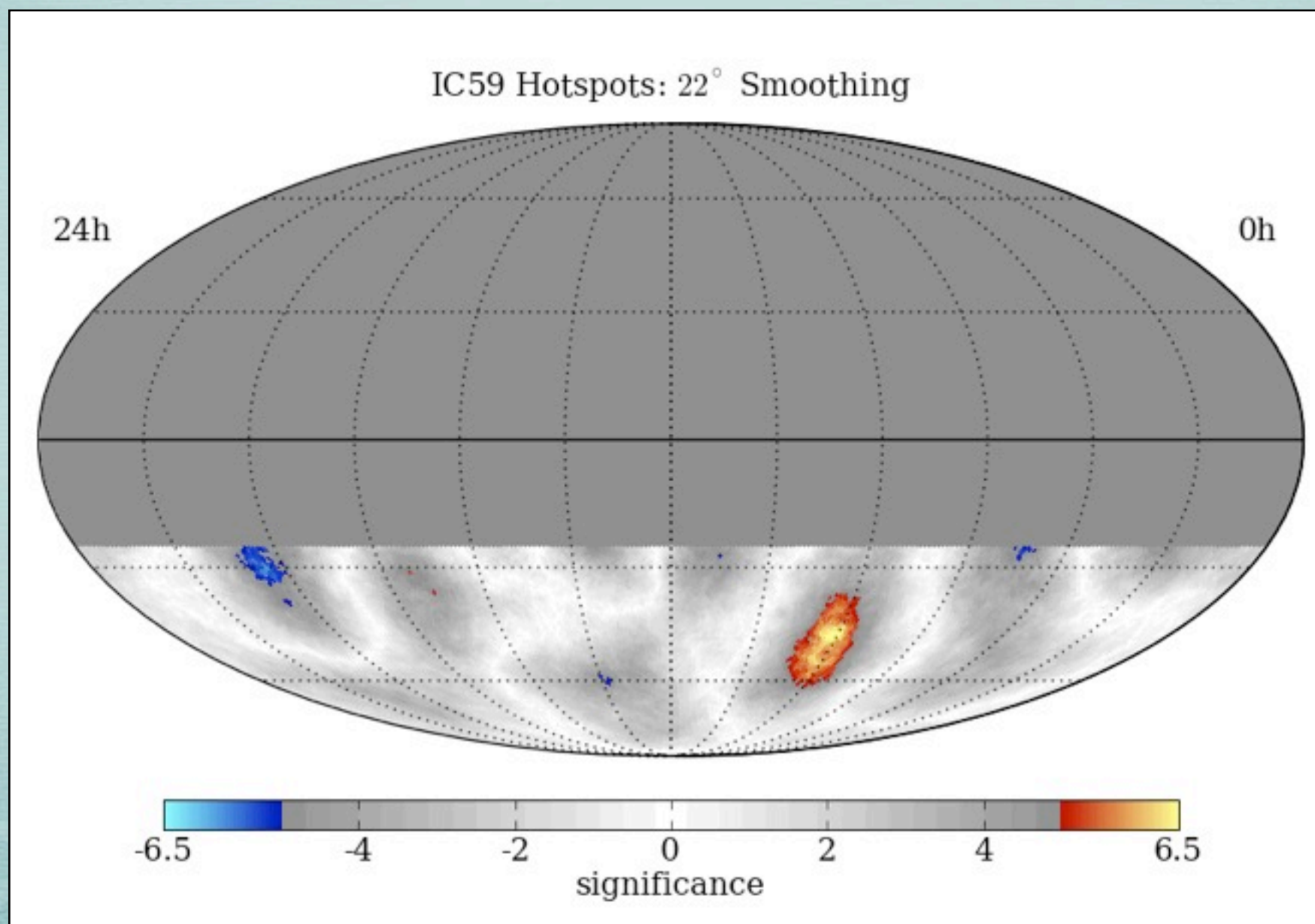
# MAP SMOOTHING SCAN

Scan from 1 - 30° in smoothing  
Different regions have different optimal angular smoothing  
Significances are pre-trial



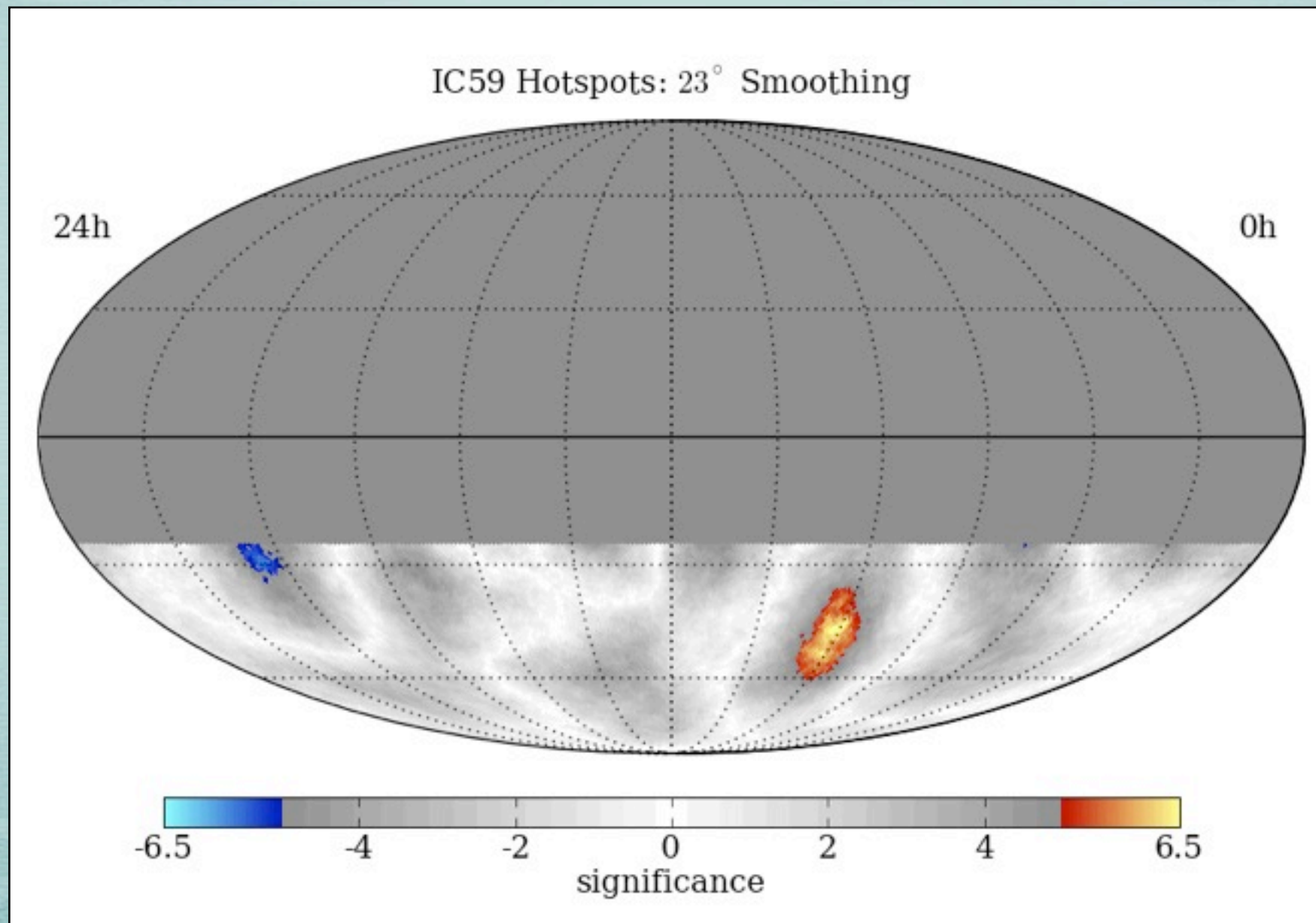
# MAP SMOOTHING SCAN

Scan from 1 - 30° in smoothing  
Different regions have different optimal angular smoothing  
Significances are pre-trial



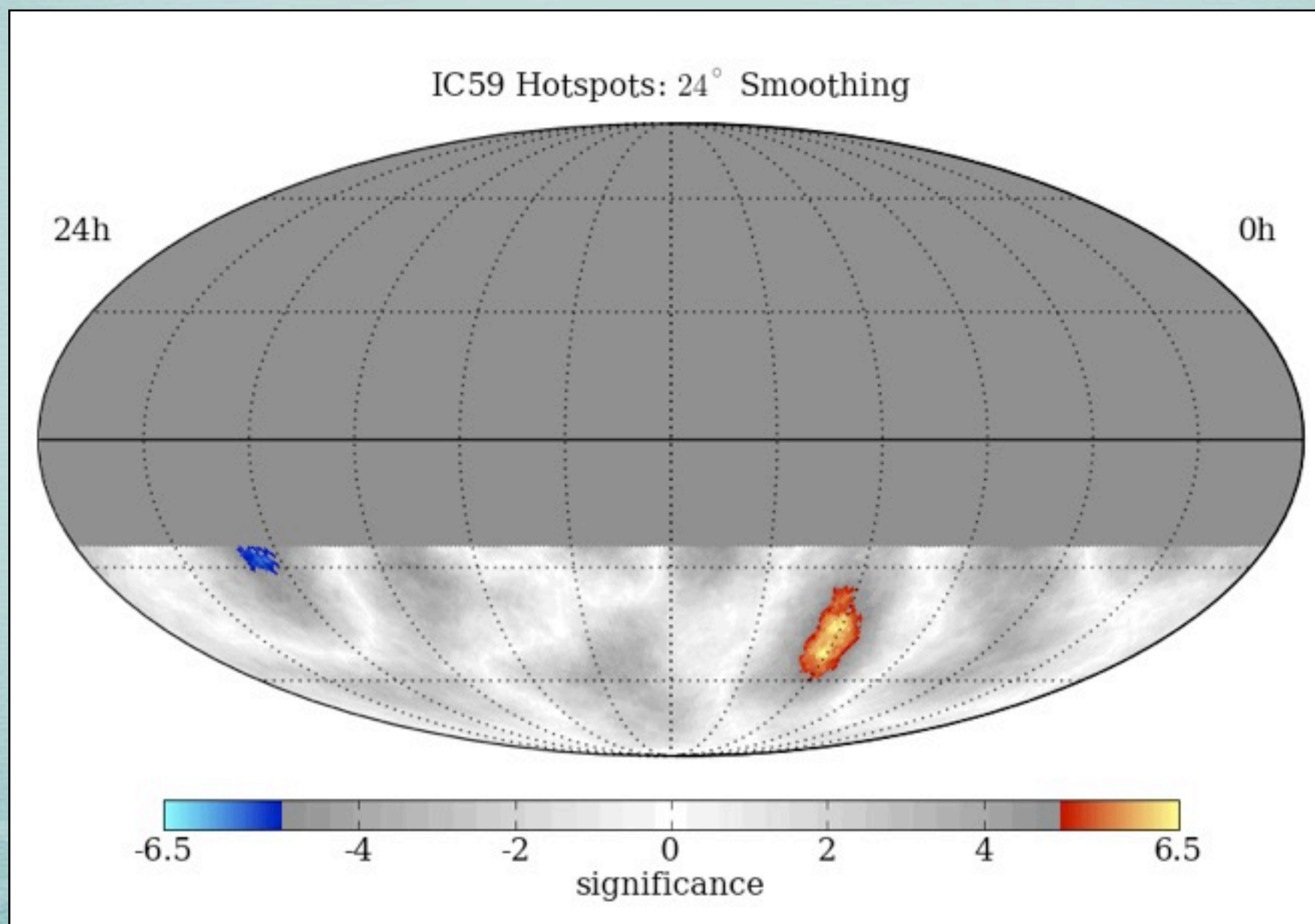
# MAP SMOOTHING SCAN

Scan from 1 - 30° in smoothing  
 Different regions have different optimal angular smoothing  
 Significances are pre-trial



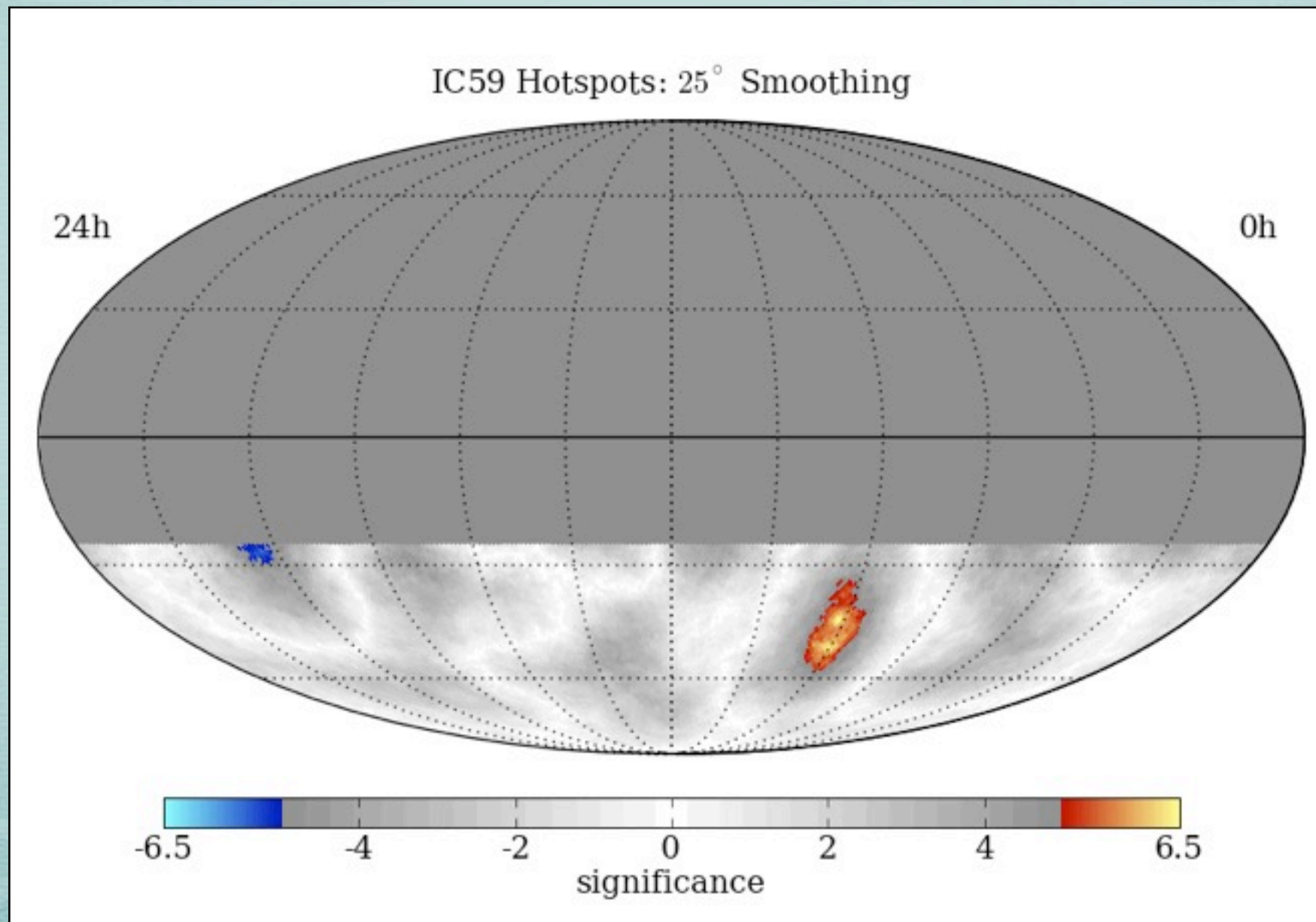
# MAP SMOOTHING SCAN

Scan from 1 - 30° in smoothing  
 Different regions have different optimal angular smoothing  
 Significances are pre-trial



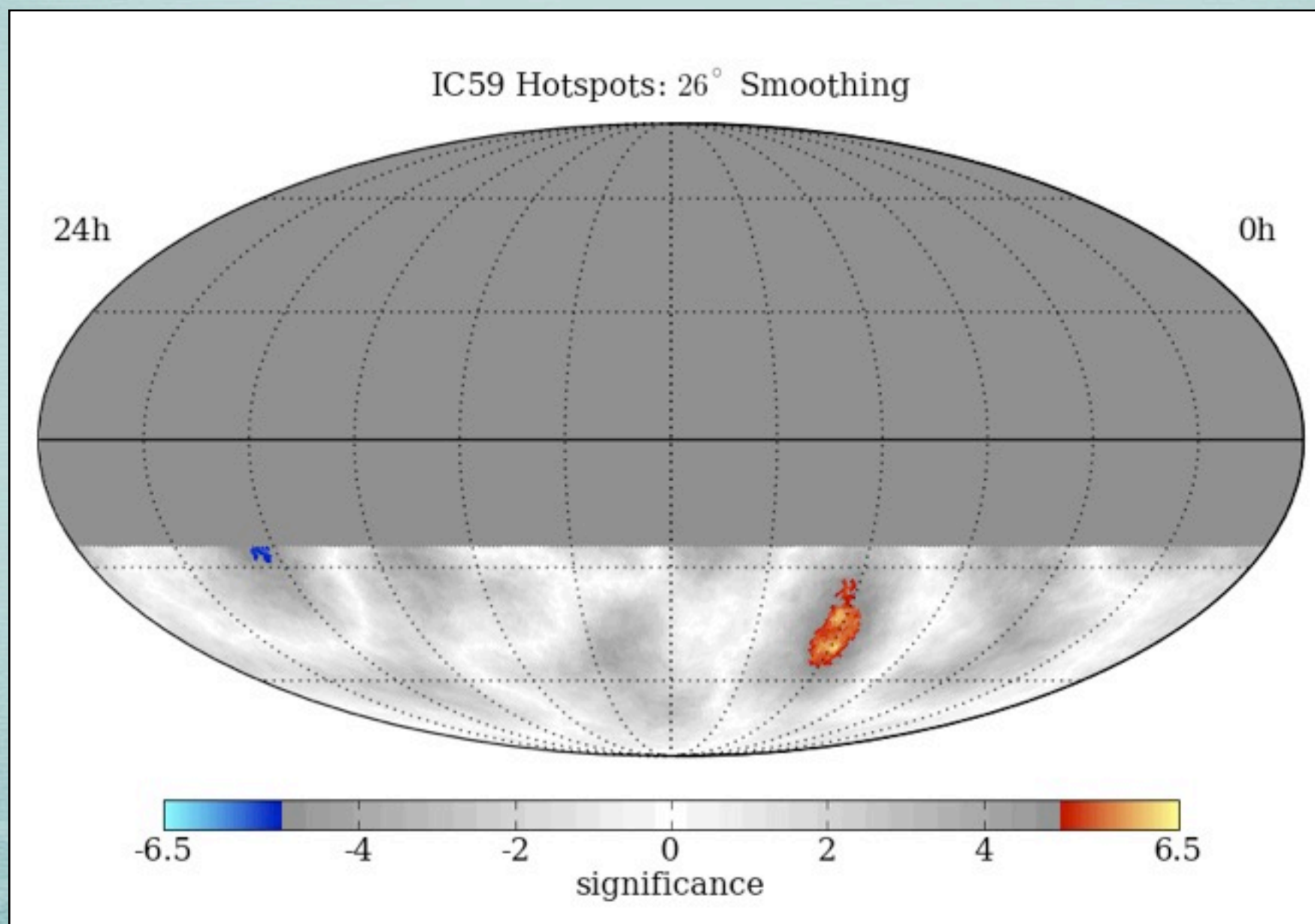
# MAP SMOOTHING SCAN

Scan from 1 - 30° in smoothing  
Different regions have different optimal angular smoothing  
Significances are pre-trial



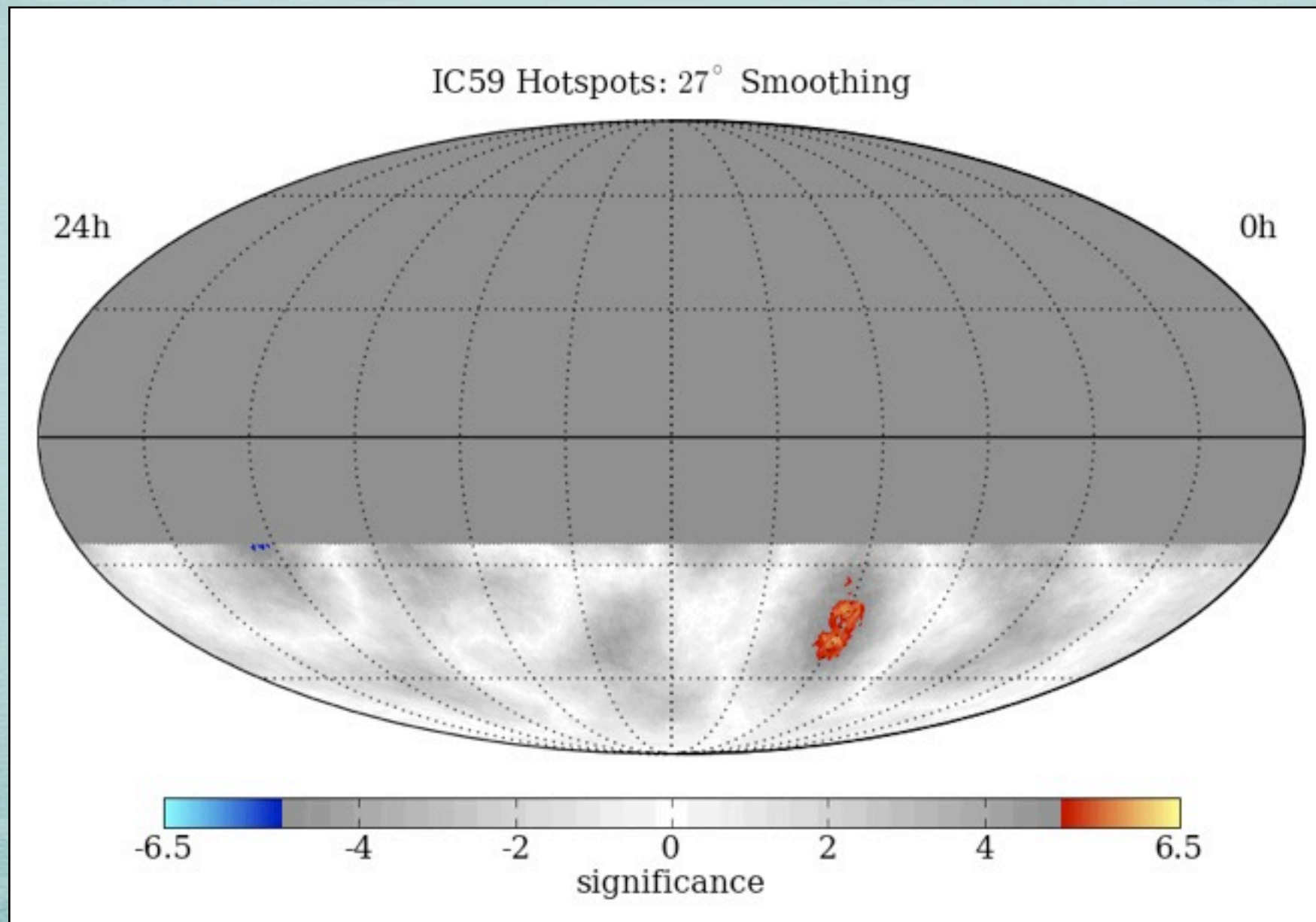
# MAP SMOOTHING SCAN

Scan from 1 - 30° in smoothing  
 Different regions have different optimal angular smoothing  
 Significances are pre-trial



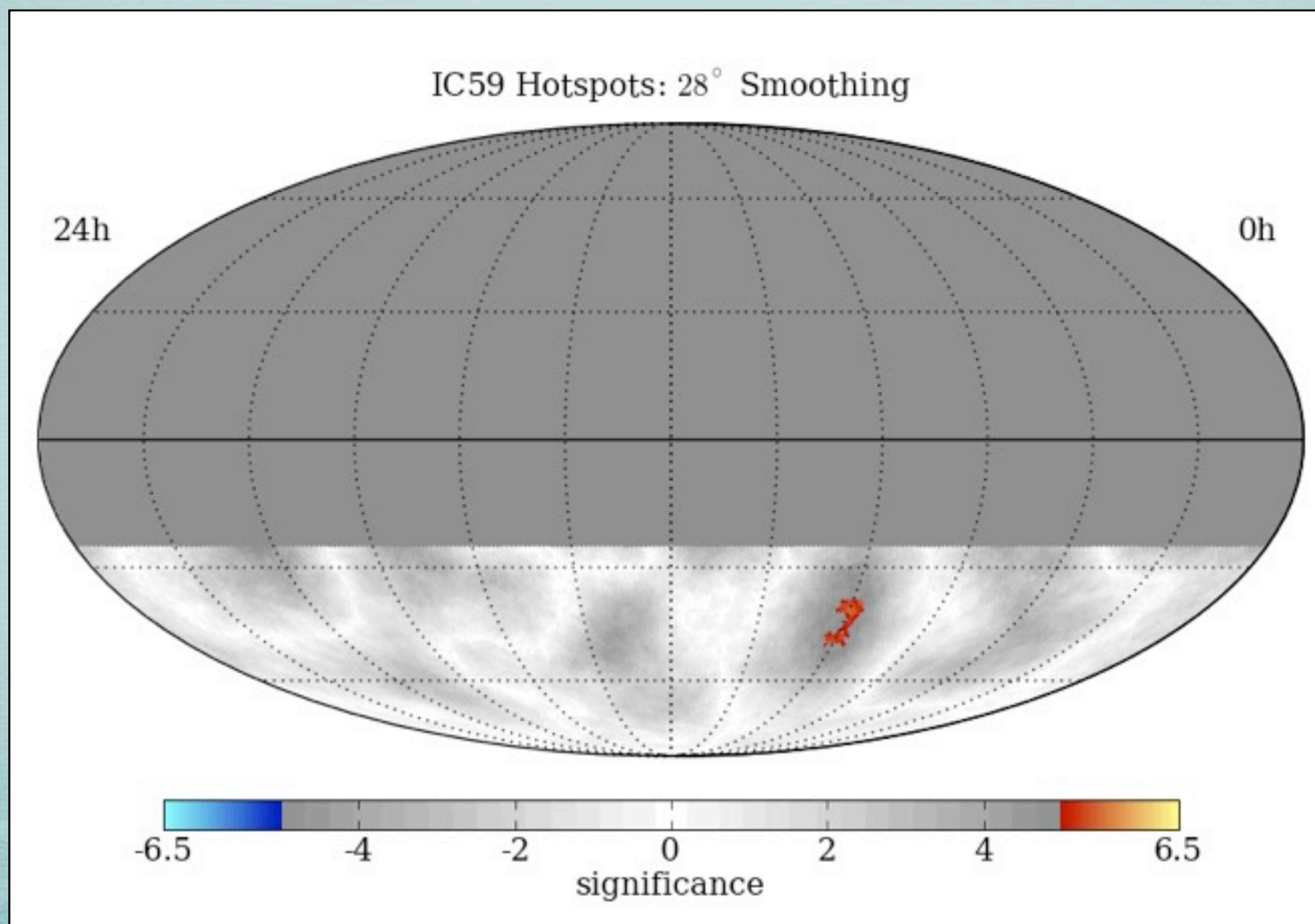
# MAP SMOOTHING SCAN

Scan from 1 - 30° in smoothing  
Different regions have different optimal angular smoothing  
Significances are pre-trial



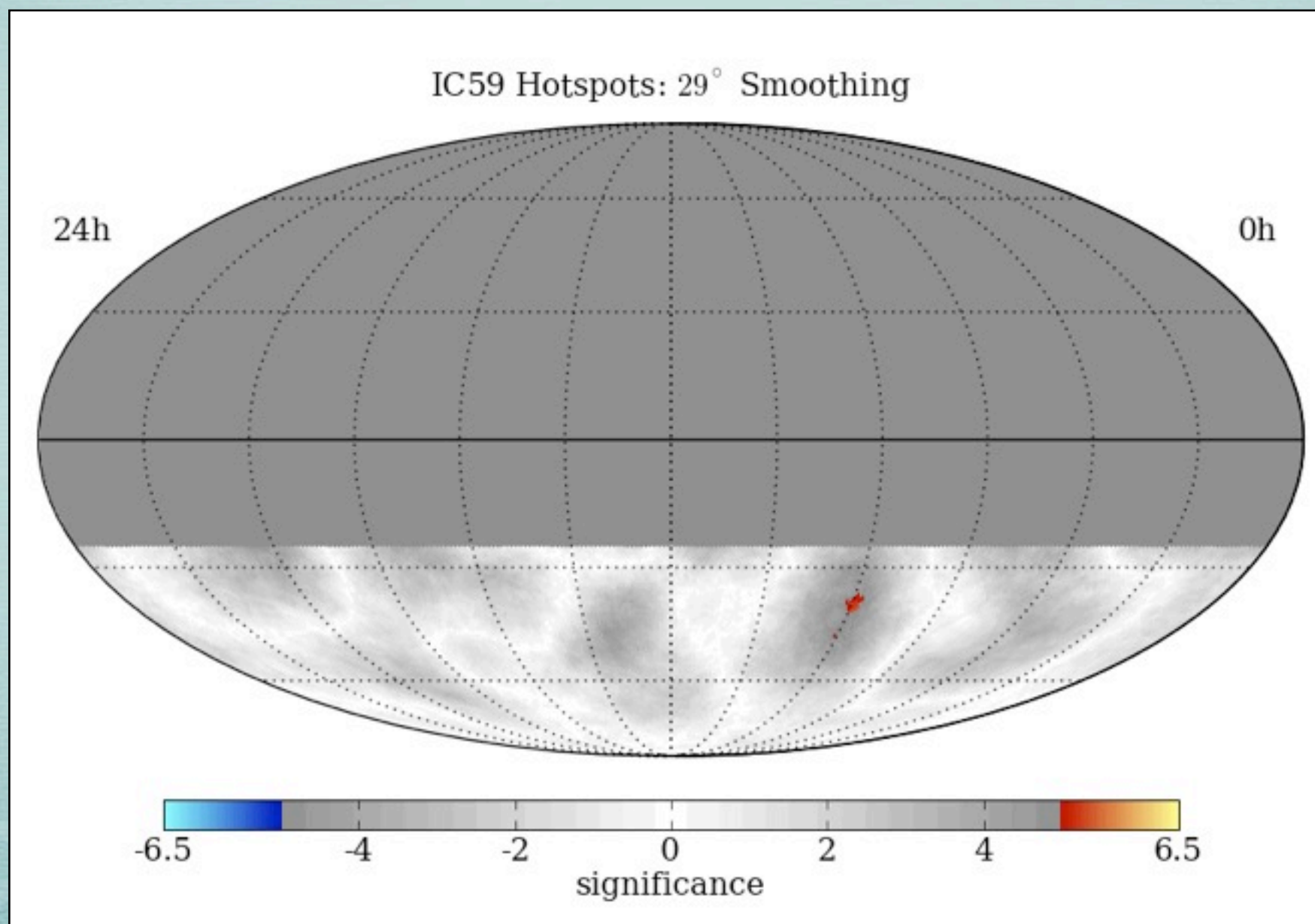
# MAP SMOOTHING SCAN

Scan from 1 - 30° in smoothing  
 Different regions have different optimal angular smoothing  
 Significances are pre-trial



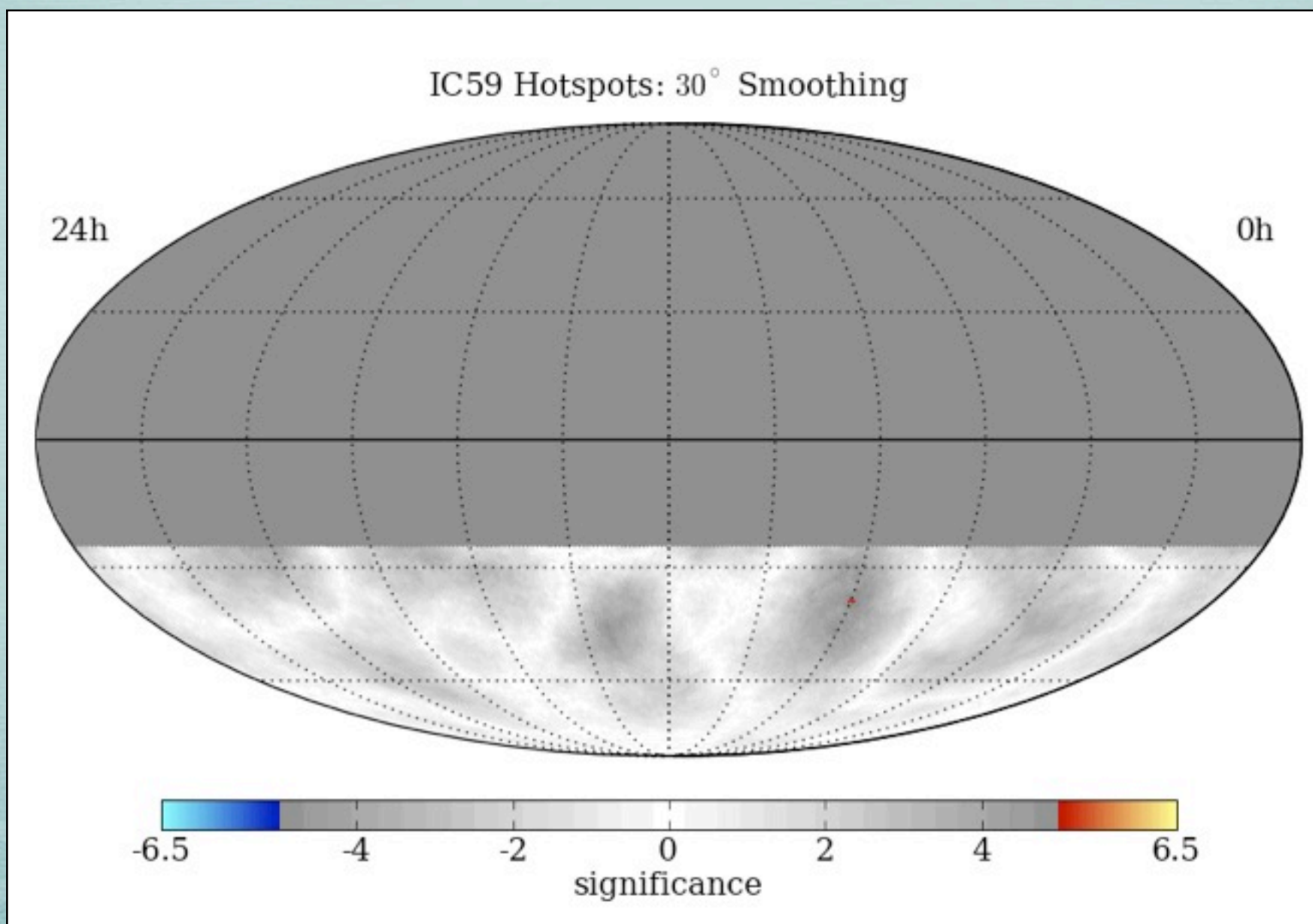
# MAP SMOOTHING SCAN

Scan from 1 - 30° in smoothing  
 Different regions have different optimal angular smoothing  
 Significances are pre-trial



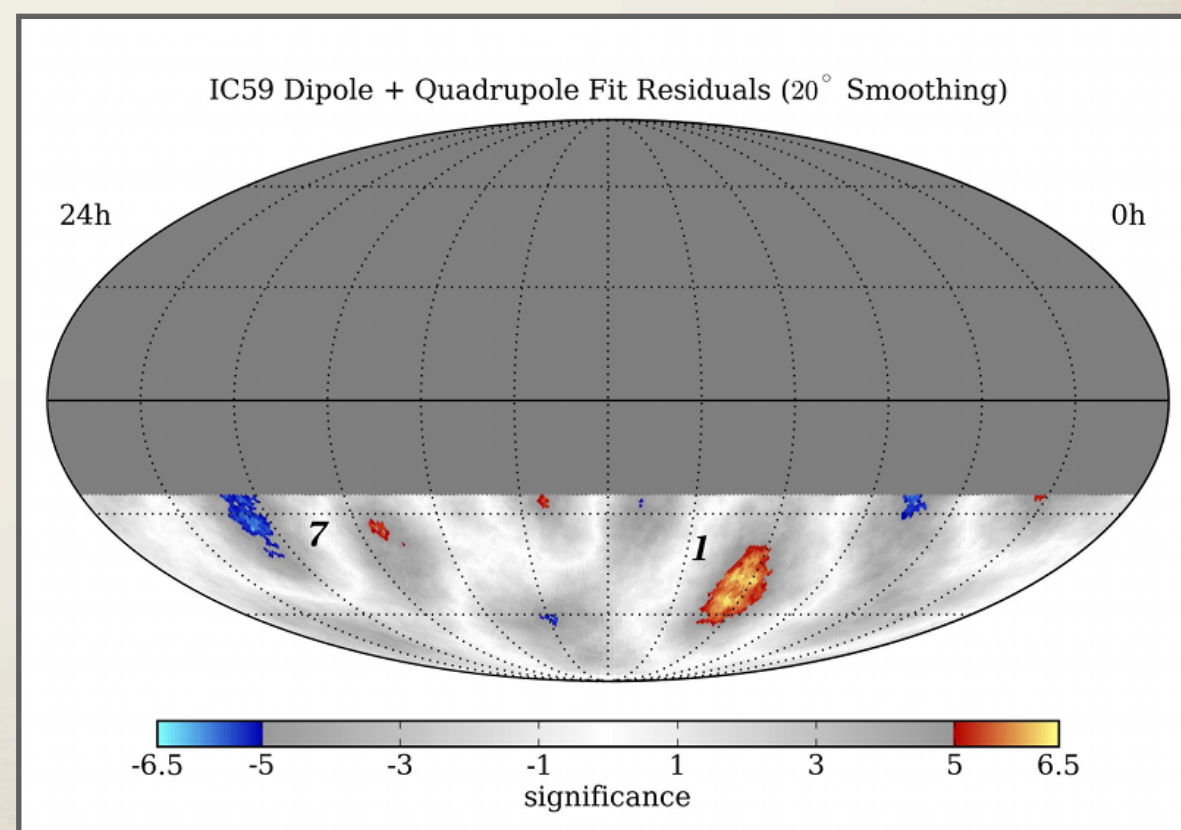
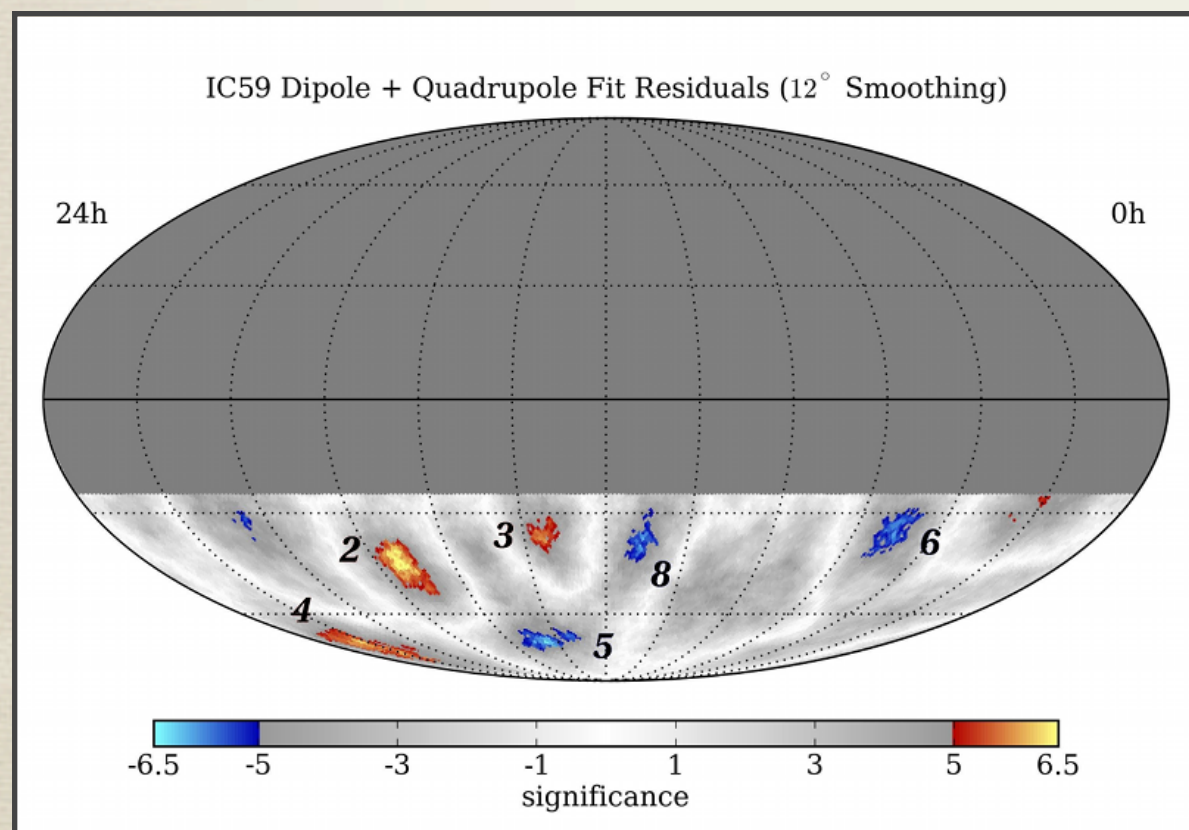
# MAP SMOOTHING SCAN

Scan from 1 - 30° in smoothing  
 Different regions have different optimal angular smoothing  
 Significances are pre-trial



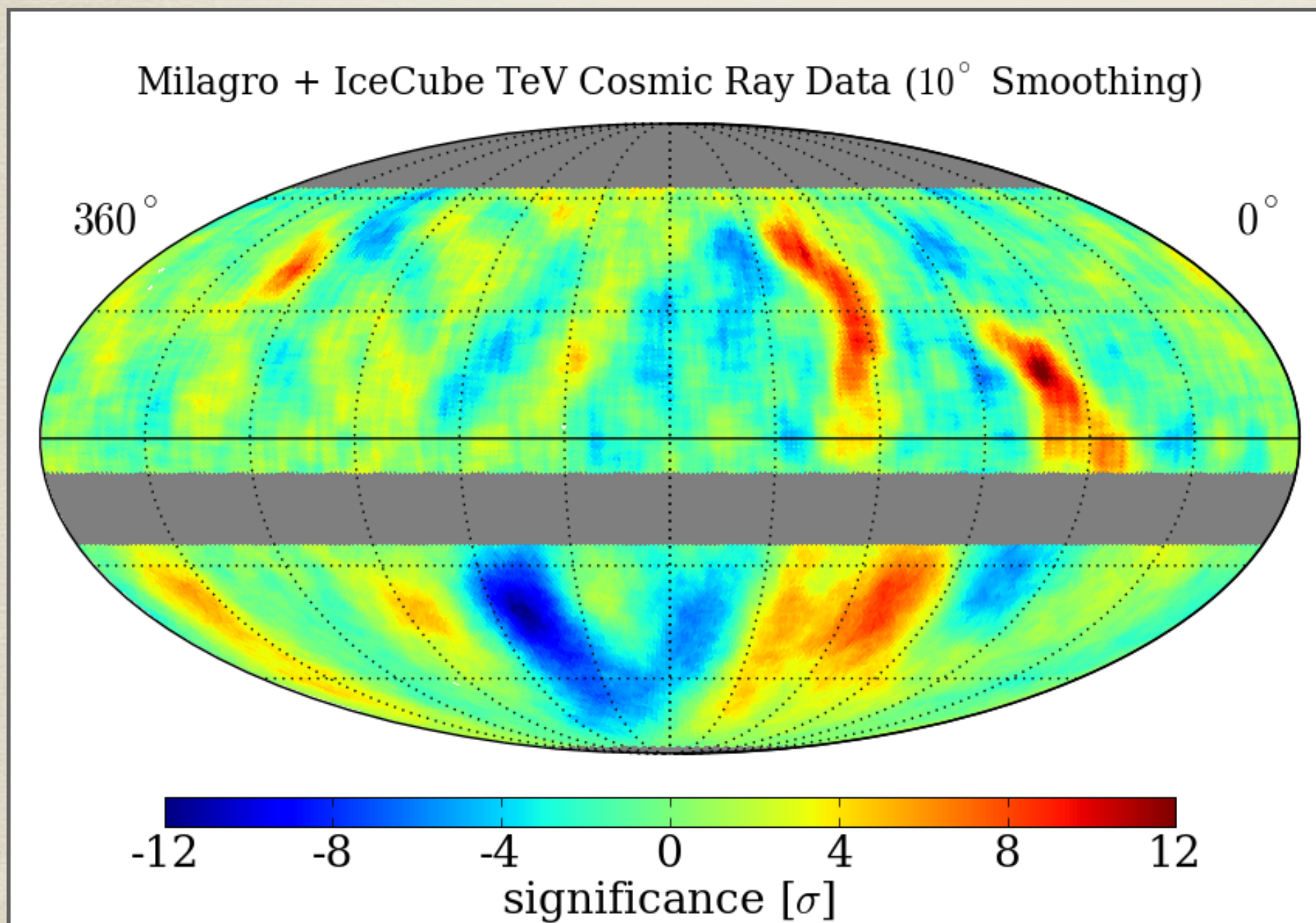
# Identification of significant structures

region	right ascension	declination	optimal scale	peak significance	post-trials
1	$(122.4^{+4.1}_{-4.7})^\circ$	$(-47.4^{+7.5}_{-3.2})^\circ$	$22^\circ$	$7.0\sigma$	<b><math>5.3\sigma</math></b>
2	$(263.0^{+3.7}_{-3.8})^\circ$	$(-44.1^{+5.3}_{-5.1})^\circ$	$13^\circ$	$6.7\sigma$	$4.9\sigma$
3	$(201.6^{+6.0}_{-1.1})^\circ$	$(-37.0^{+2.2}_{-1.9})^\circ$	$11^\circ$	$6.3\sigma$	$4.4\sigma$
4	$(332.4^{+9.5}_{-7.1})^\circ$	$(-70.0^{+4.2}_{-7.6})^\circ$	$12^\circ$	$6.2\sigma$	$4.2\sigma$
5	$(217.7^{+10.2}_{-7.8})^\circ$	$(-70.0^{+3.6}_{-2.3})^\circ$	$12^\circ$	$-6.4\sigma$	$-4.5\sigma$
6	$(77.6^{+3.9}_{-8.4})^\circ$	$(-31.9^{+3.2}_{-8.6})^\circ$	$13^\circ$	$-6.1\sigma$	$-4.1\sigma$
7	$(308.2^{+4.8}_{-7.7})^\circ$	$(-34.5^{+9.6}_{-6.9})^\circ$	$20^\circ$	$-6.1\sigma$	$-4.1\sigma$
8	$(166.5^{+4.5}_{-5.7})^\circ$	$(-37.2^{+5.0}_{-5.7})^\circ$	$12^\circ$	$-6.0\sigma$	$-4.0\sigma$



# Milagro + IceCube combined map

IceCube map contains all data from IC22, IC40 and IC59 data sets



## Milagro map:

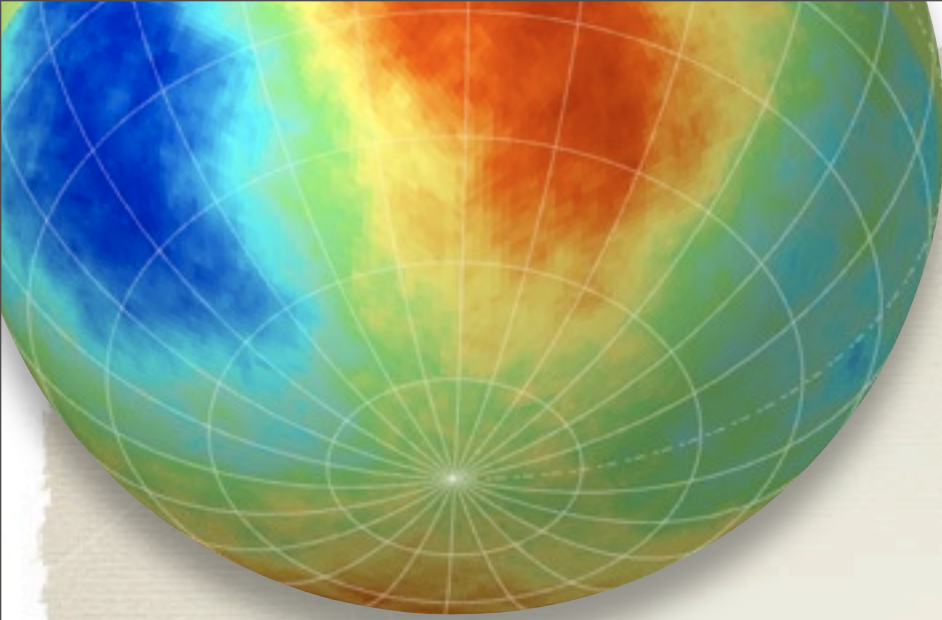
[Abdo, A. A., et al. 2008, Phys. Rev. Lett., 101, 221101]

- $2.2 \times 10^{11}$  events
- direct integration (2 hr)
- $10^\circ$  smoothing
- median energy **1 TeV**

## IceCube map:

- $5.6 \times 10^{10}$  events
- time scrambling (4 hr)
- $10^\circ$  smoothing
- median energy **20 TeV**

# Conclusions

- 
- \* **IceCube** detector was **completed in December 2010** and is now taking data in its final configuration (86 strings).
  - \* **Large scale anisotropy:**
    - ▶ Sidereal anisotropy at 20 TeV confirms previous observation.
    - ▶ First observation of sidereal anisotropy @ 400 TeV in southern hemisphere.
    - ▶ Indication of a persistence of anisotropy @ 400 TeV: evidence of a “dip”.
  - \* **Small and medium scale** structures:
    - ▶ Southern sky in TeV cosmic rays shows significant anisotropy across a wide range of angular scales (10-180 degrees).
  - \* **The origin of the anisotropy is still unknown.**

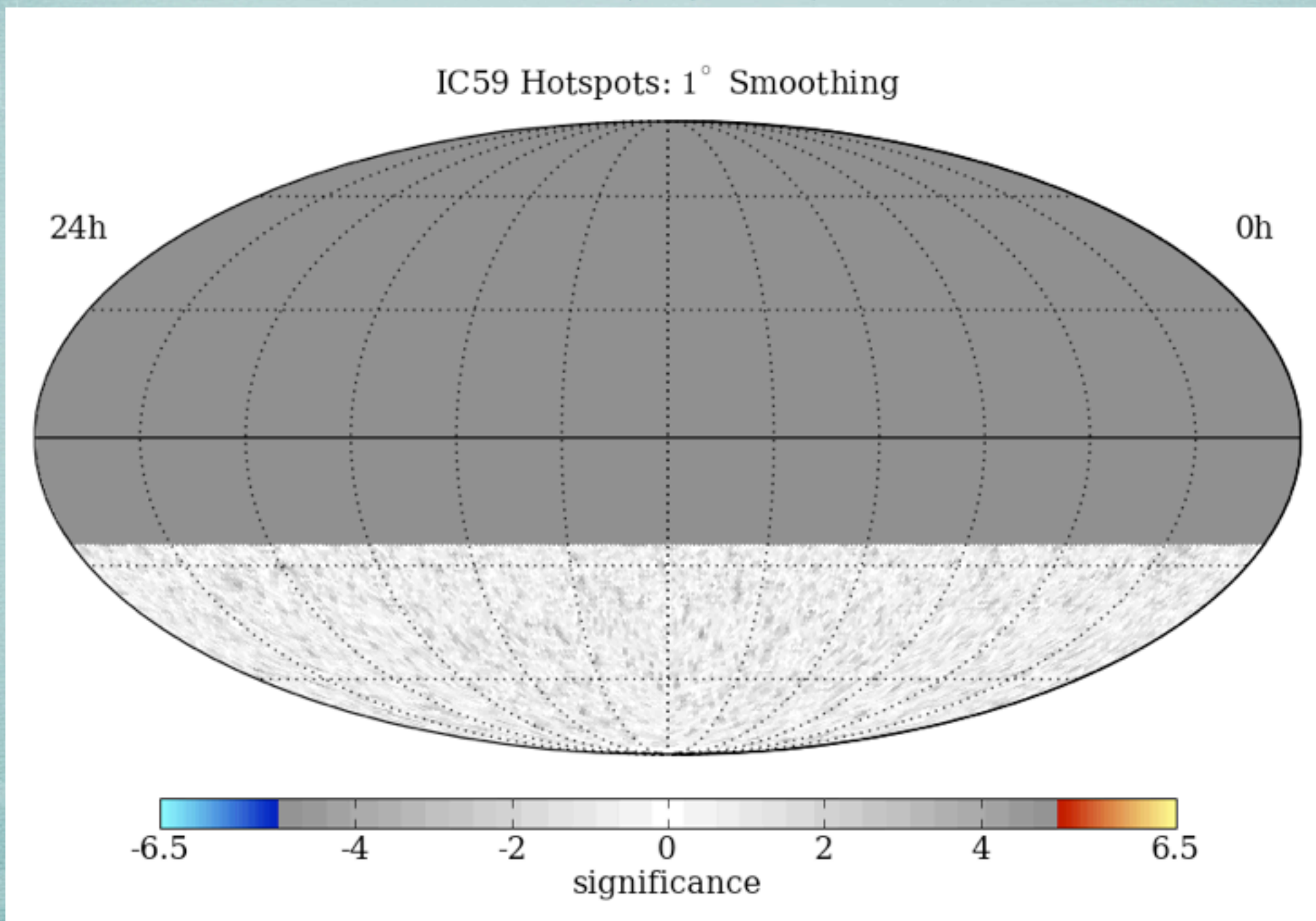
# BACKUP SLIDES

# MAP SMOOTHING SCAN

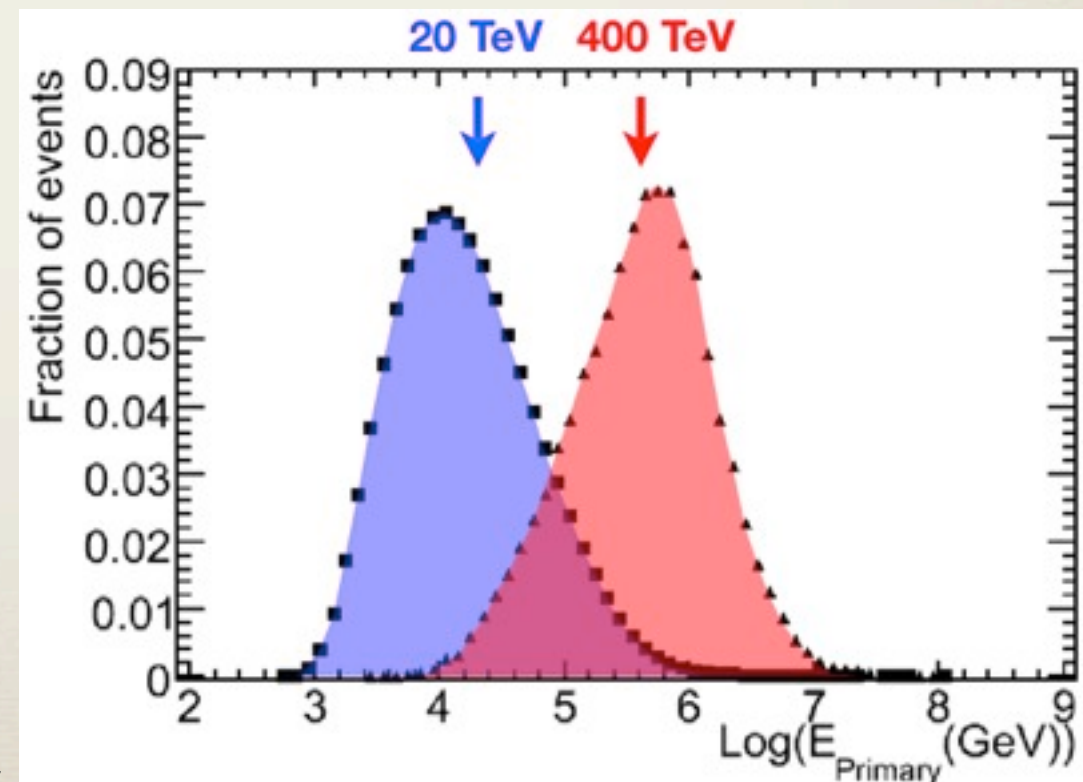
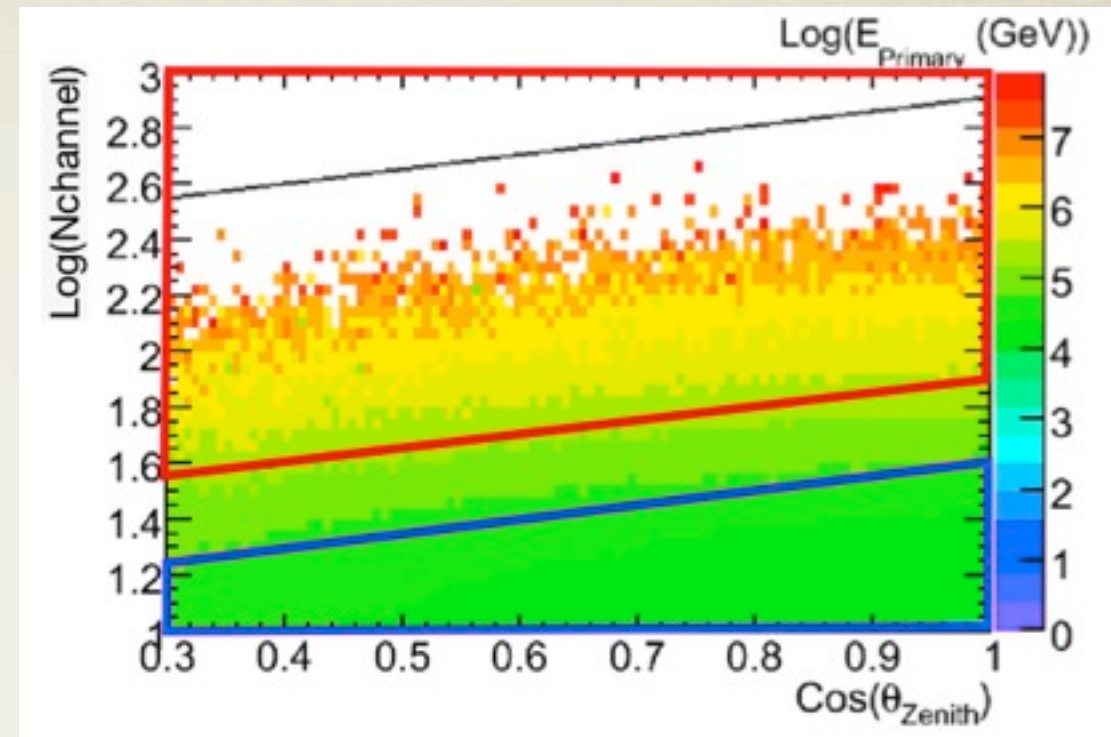
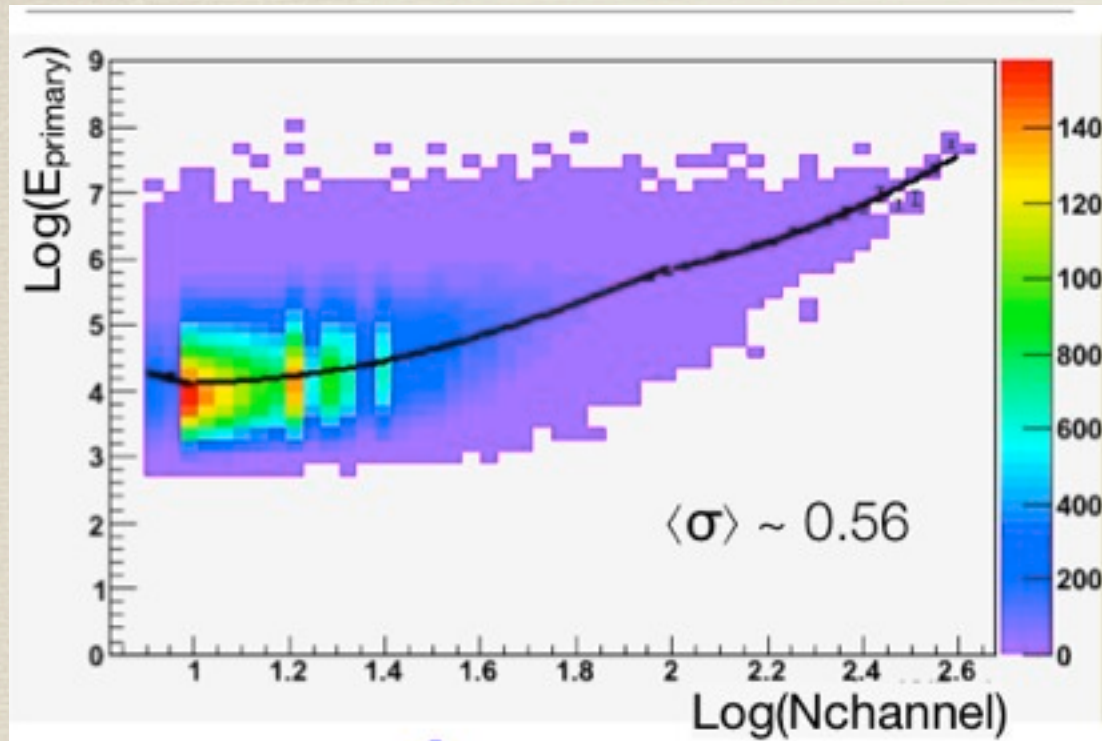
**Scan from 1 - 30° in smoothing**  
**Different regions have different optimal angular smoothing**  
**Significances are pre-trial**

# MAP SMOOTHING SCAN

Scan from 1 - 30° in smoothing  
Different regions have different optimal angular smoothing  
Significances are pre-trial

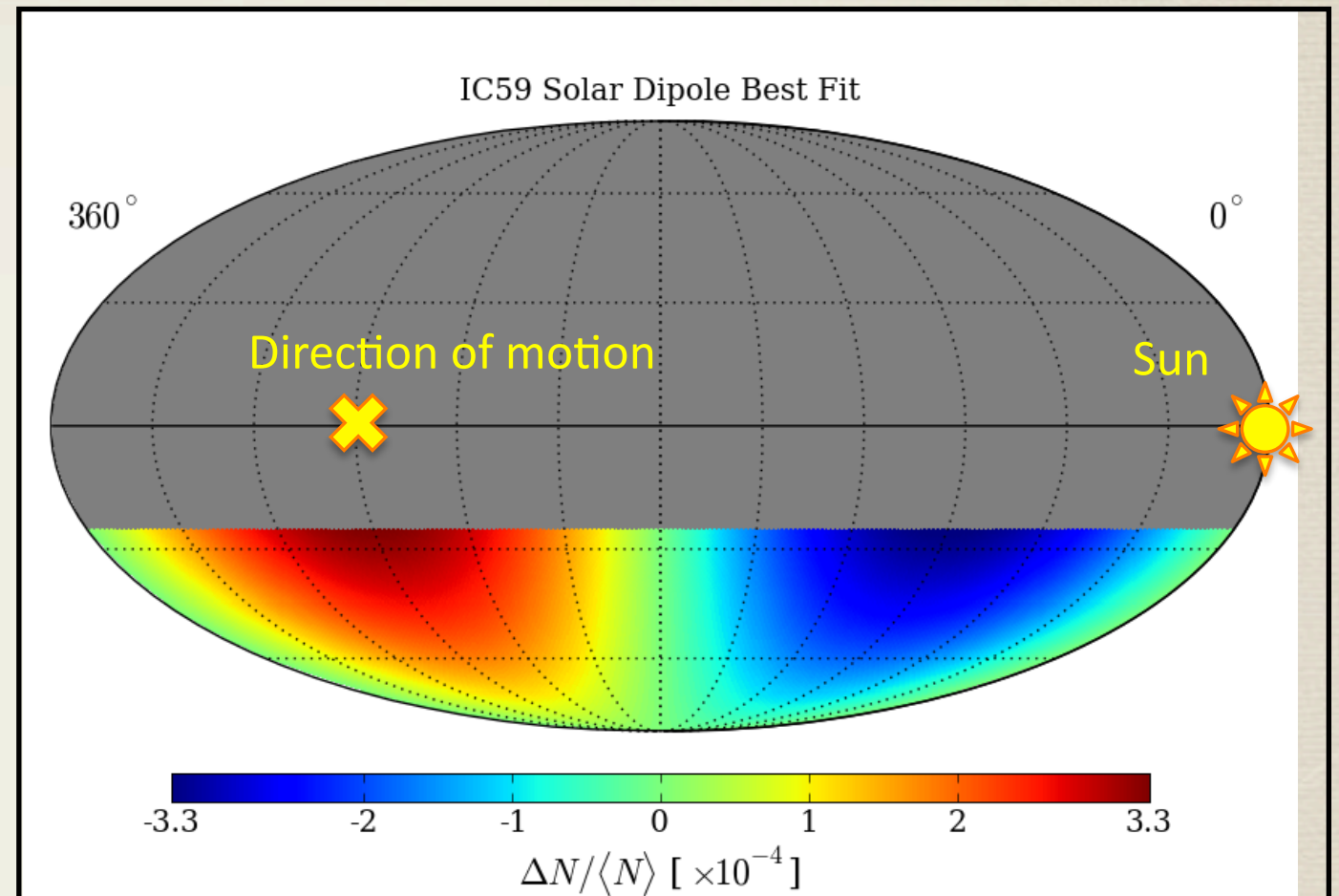
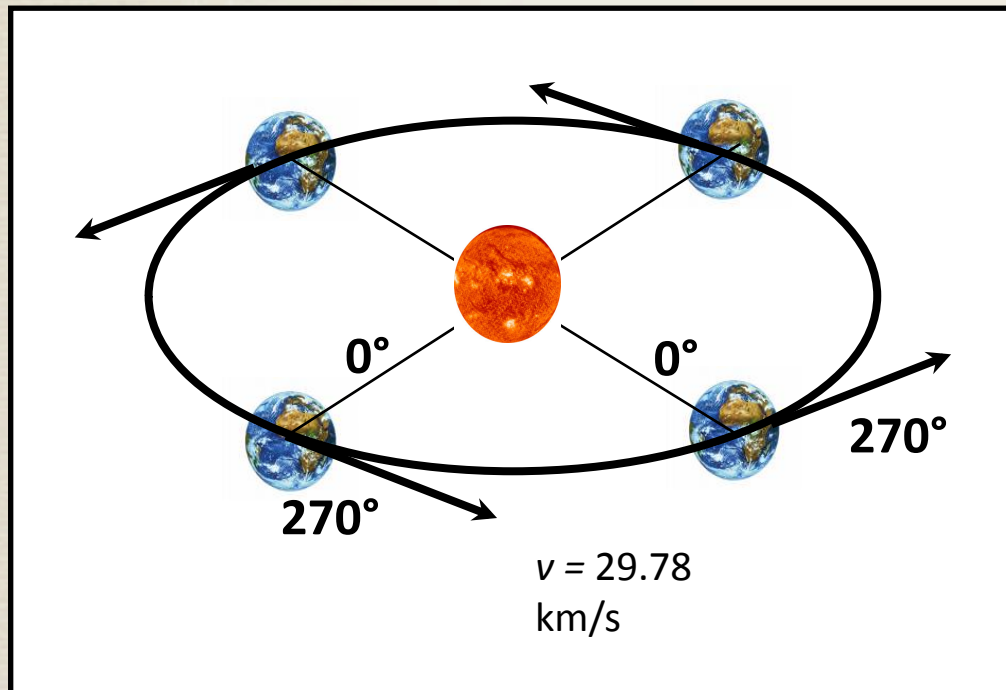


# Energy estimation



# Systematics: Solar Dipole

We are sensitive to the motion of the Earth around the Sun ( $10^{-4}$  effect is expected): visible when UT is used in local-celestial coord. transformation.

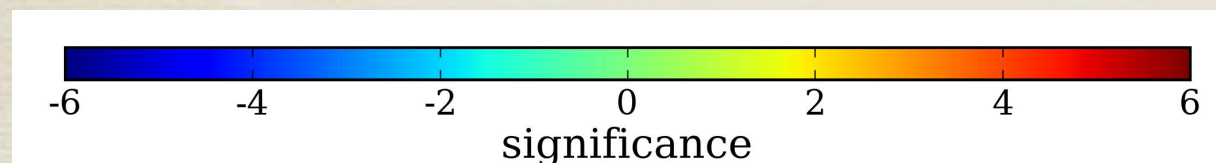


Coefficient	Fit Value ( $\times 10^{-4}$ )
$m_0$	$-0.029 \pm 0.058$
$p_x$	$0.017 \pm 0.142$
$p_y$	$-3.661 \pm 0.142$
$p_z$	$-0.027 \pm 0.072$

$$\chi^2 / \text{ndf} = 14206.8 / 14192$$

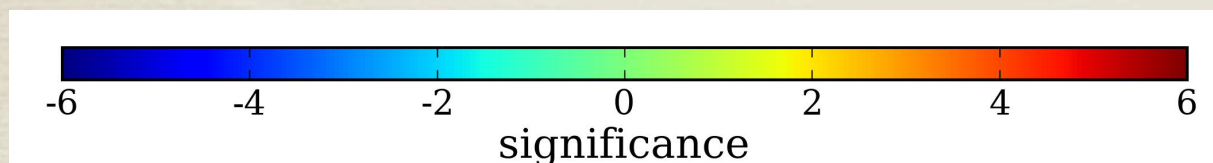
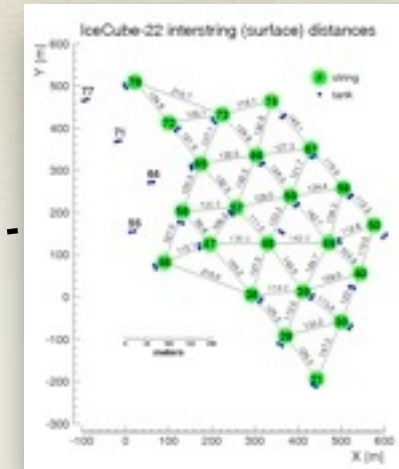
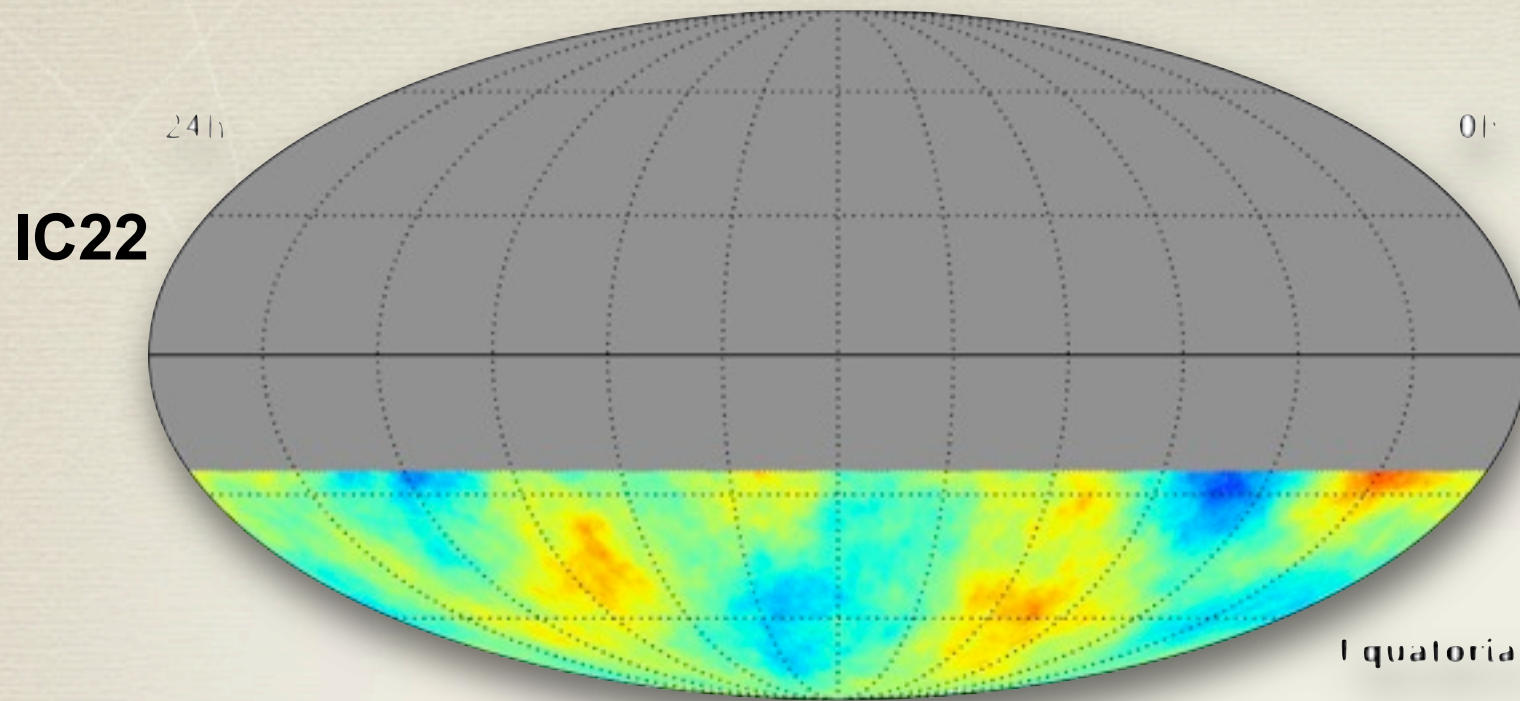
$$\text{Pr}(\chi^2 | \text{ndf}) = 0.416$$

# Systematics: previous data sets



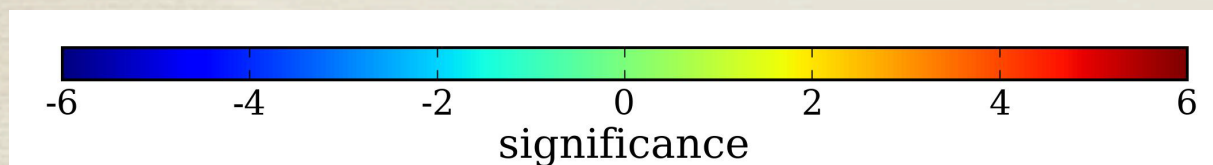
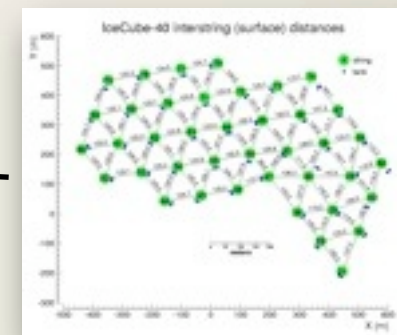
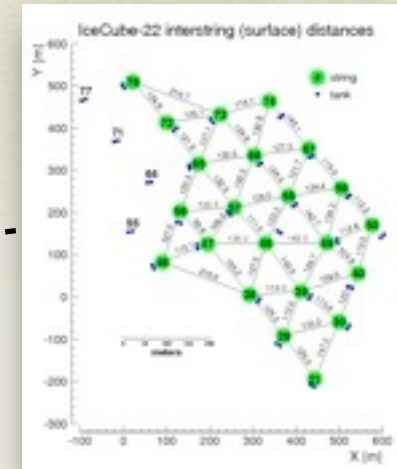
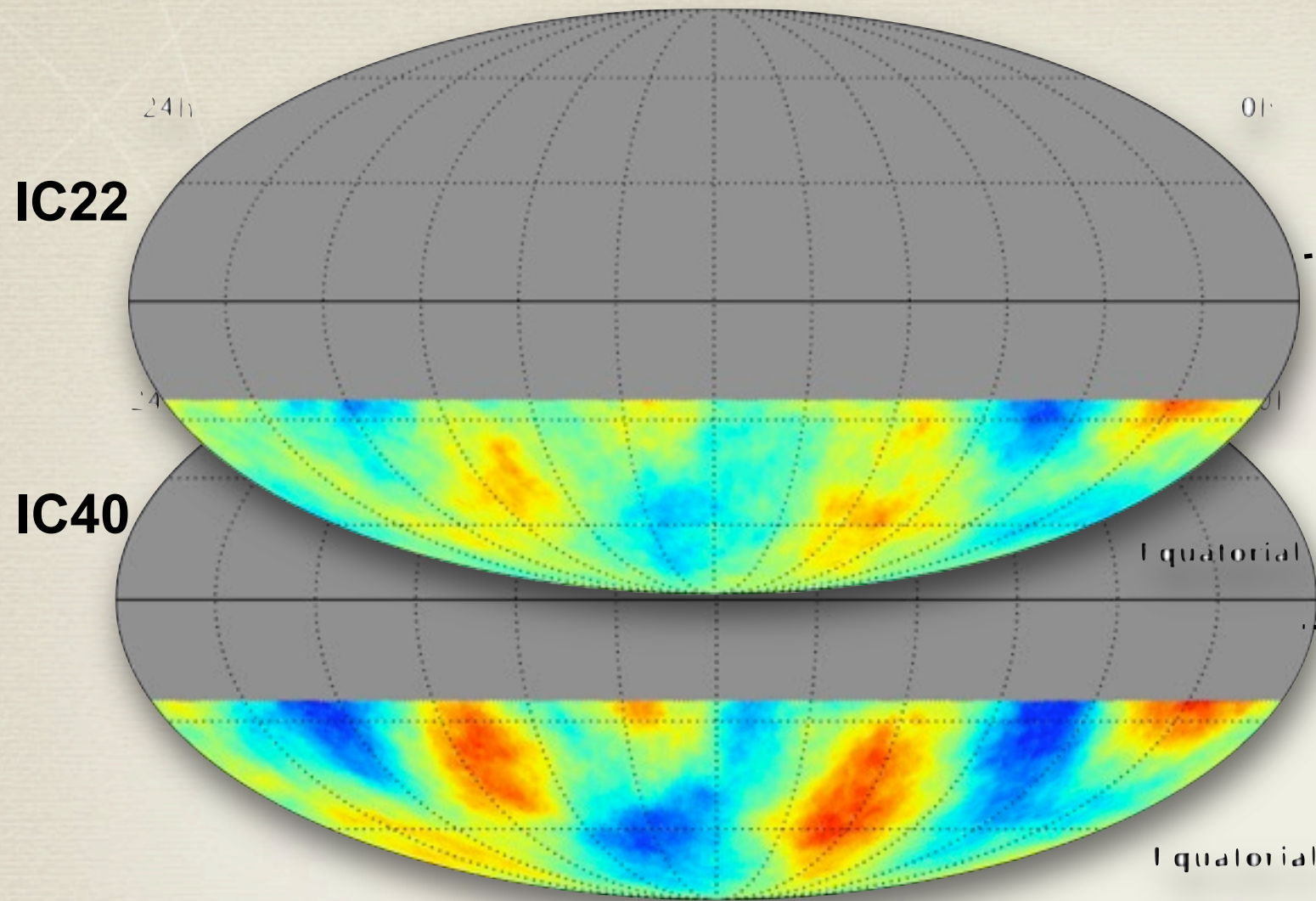
**Different geometries, same structure**  
**Signal grows with statistics**

# Systematics: previous data sets



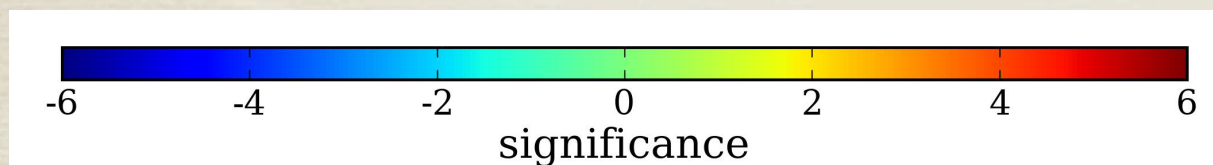
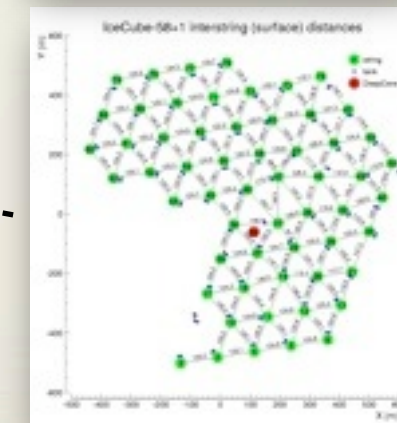
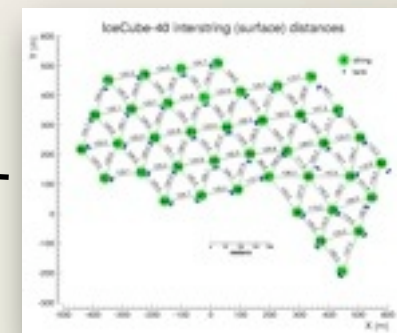
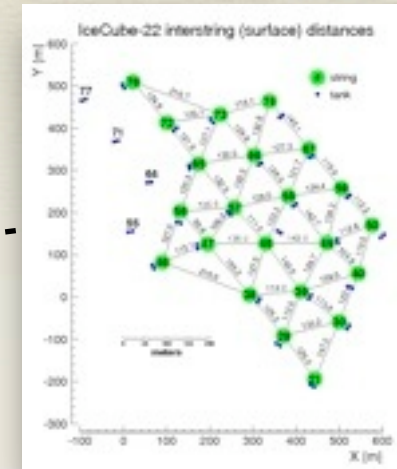
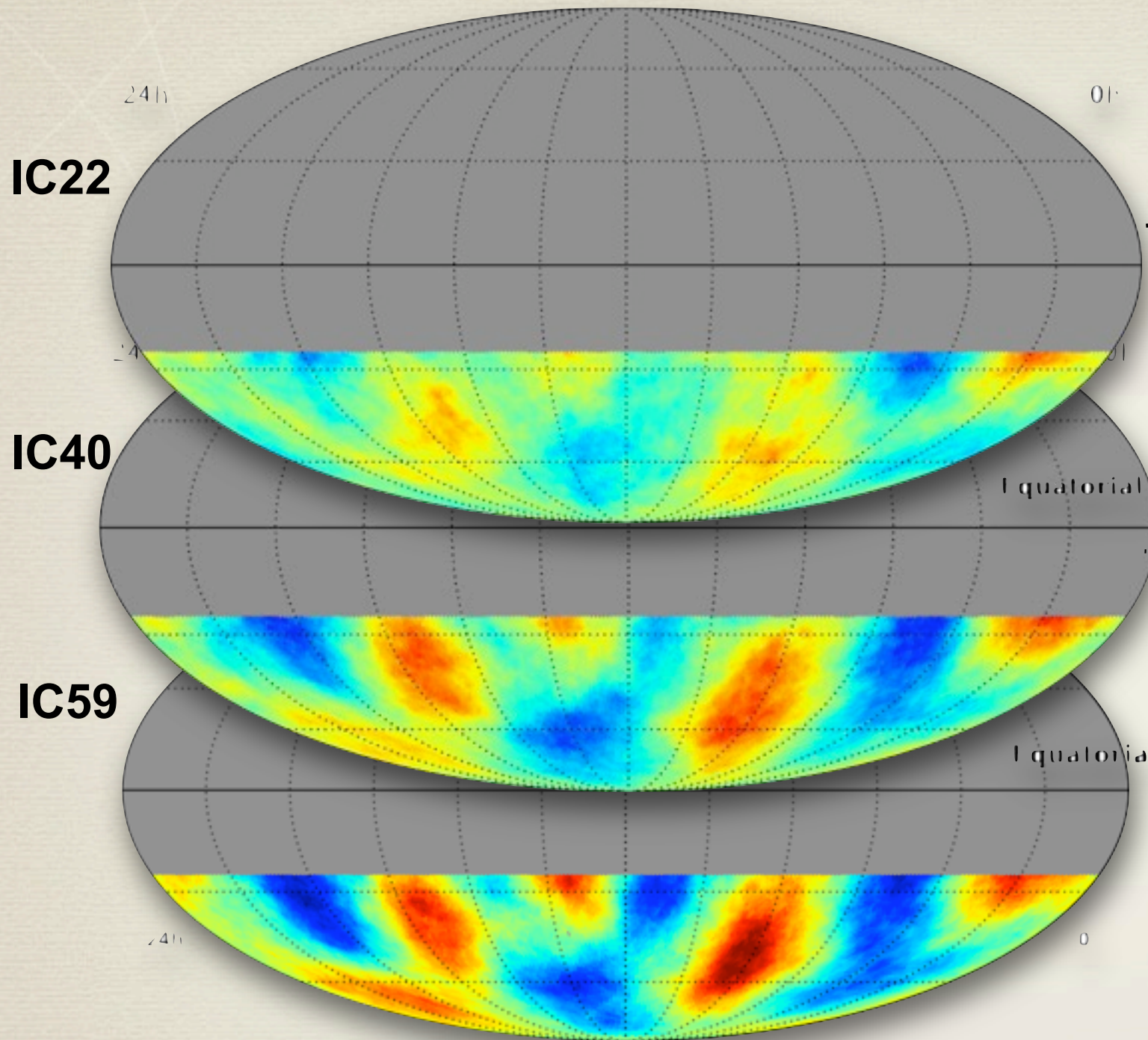
**Different geometries, same structure**  
**Signal grows with statistics**

# Systematics: previous data sets



**Different geometries, same structure**  
**Signal grows with statistics**

# Systematics: previous data sets

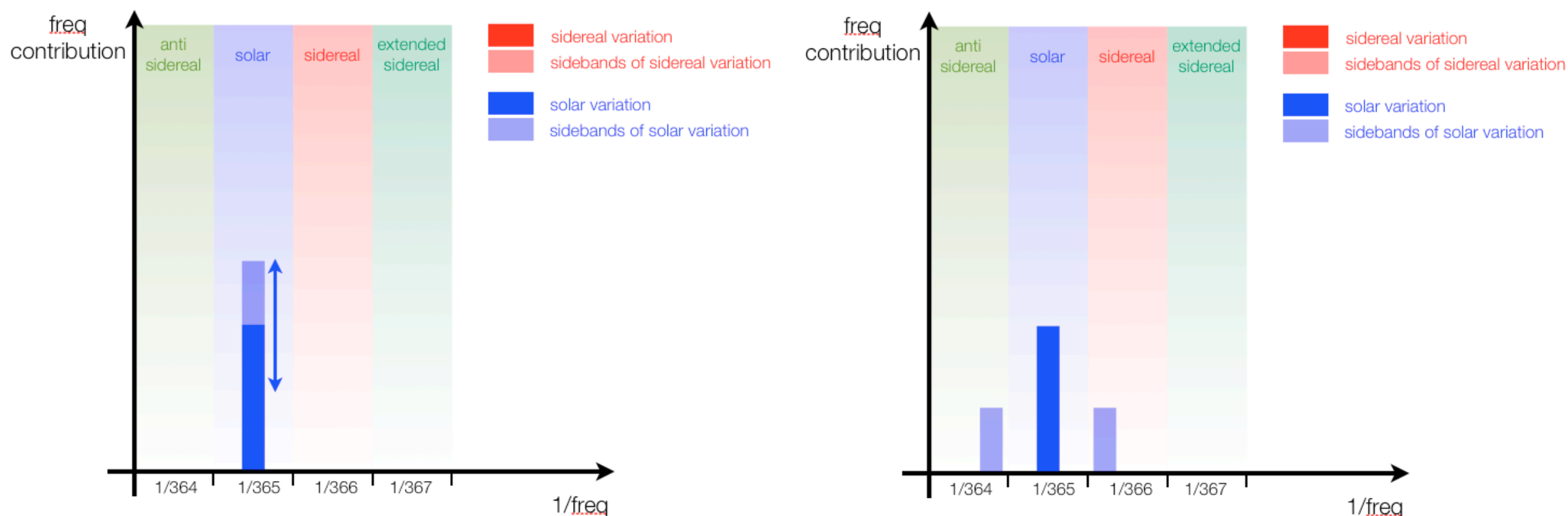


**Different geometries, same structure**  
**Signal grows with statistics**

# anti- / extended-sidereal reference frames

A static distribution in **solar** (sidereal) reference frame averages to zero in **sidereal** (solar) frame after one year

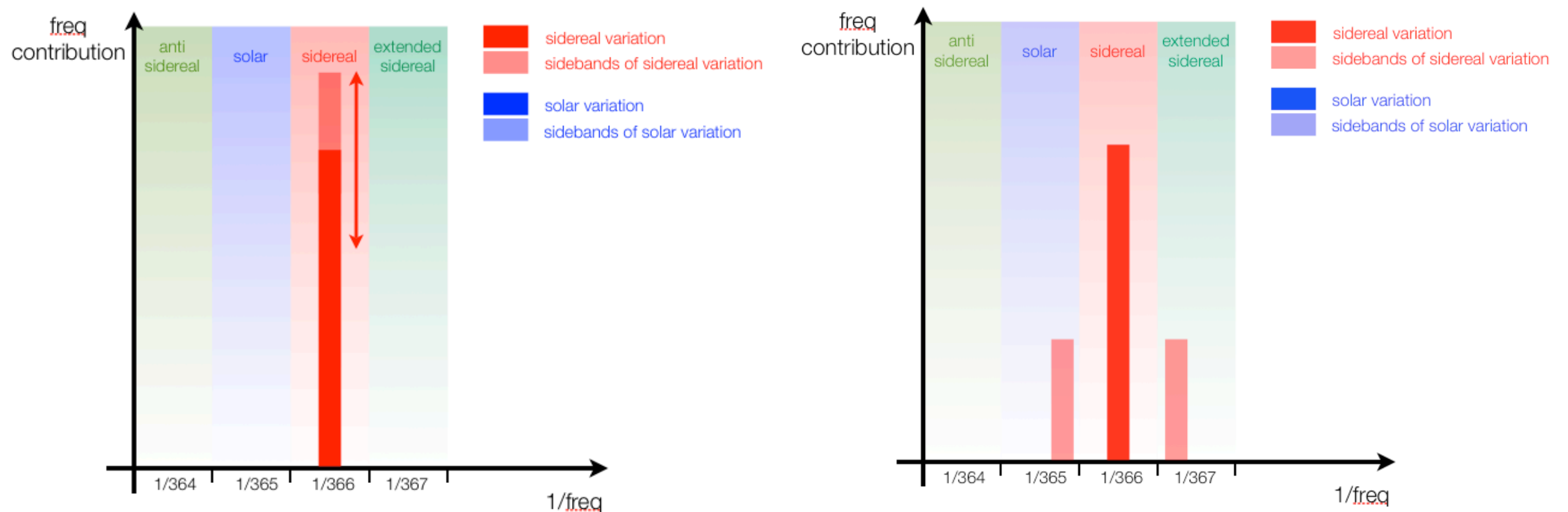
An annual modulation of the **solar** (sidereal) distribution does not compensate and produces distortions on the **sidereal** (solar) anisotropies



# anti- / extended-sidereal reference frames

A static distribution in solar (**sidereal**) reference frame averages to zero in sidereal (solar) frame after one year

An annual modulation of the solar (**sidereal**) distribution does not compensate and produces distortions on the sidereal (**solar**) anisotropies



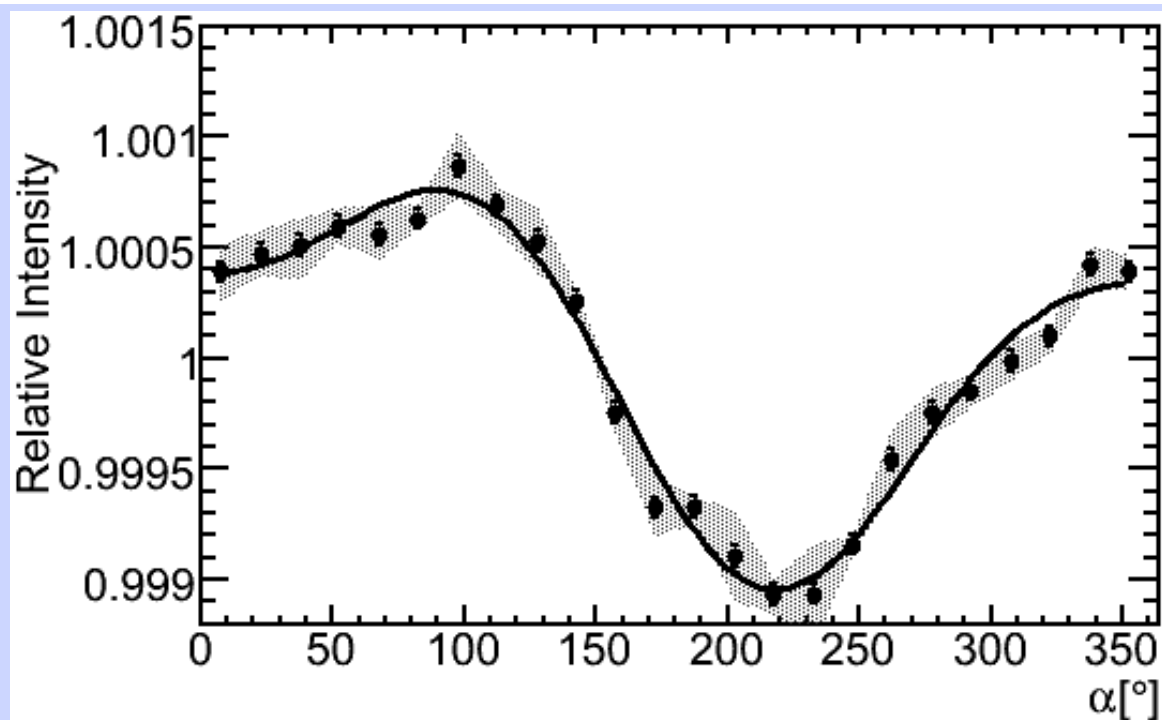
# Summary of measurements for IC59

$$\sum_{j=1}^{n=2} A_j \cos[i(\alpha - \phi_j)] + B$$

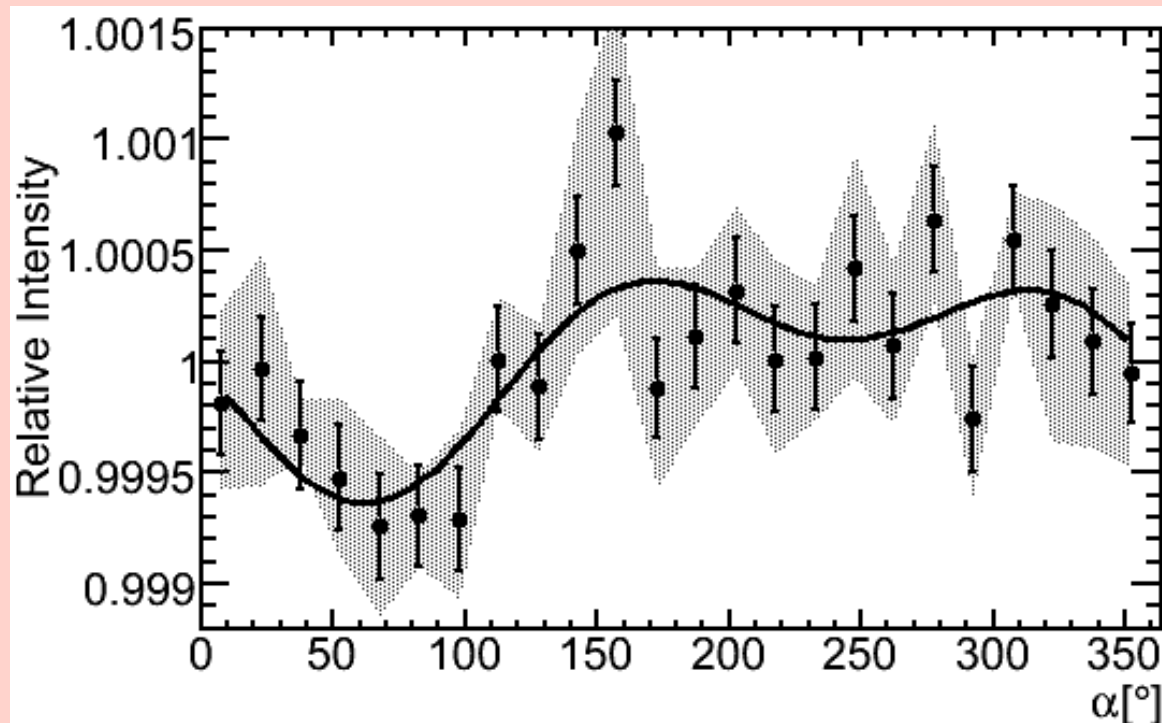
	$E_{\text{primary}}$ (TeV)	events ( $10^9$ )	$A_1$ ( $10^{-4}$ )	$\varphi_1$ ( $^\circ$ )	$A_2$ ( $10^{-4}$ )	$\varphi_2$ ( $^\circ$ )	$\chi^2/\text{ndf}$
sidereal	20	17.9	$7.9 \pm 0.1 \pm 0.4$	$50^\circ.5 \pm 1^\circ.0 \pm 1^\circ.1$	$2.9 \pm 0.1 \pm 0.4$	$299^\circ.5 \pm 1^\circ.3 \pm 1^\circ.5$	95/19
	400	0.5	$3.7 \pm 0.7 \pm 0.7$	$239^\circ.2 \pm 10^\circ.6 \pm 10^\circ.8$	$2.7 \pm 0.7 \pm 0.6$	$152^\circ.7 \pm 7^\circ.0 \pm 4^\circ.2$	34.19
solar	20		$1.9 \pm 0.1 \pm 0.6$	$267^\circ.1 \pm 3^\circ.8 \pm 7^\circ.5$			23/21
	400		$2.9 \pm 0.7 \pm 1.0$	$272^\circ.1 \pm 13^\circ.3 \pm 5^\circ.0$			12/21
anti-sidereal	20		$0.4 \pm 0.1$	$1^\circ.5 \pm 18^\circ.5$			29/21
	400		$0.5 \pm 0.7$	$324^\circ.6 \pm 75^\circ.4$			17/21
extended-sidereal	20		$0.7 \pm 0.1$	$165^\circ.7 \pm 10^\circ.3$			29/21
	400		$0.7 \pm 0.7$	$212^\circ.9 \pm 54^\circ.5$			23/21

# Systematic uncertainties IceCube-59

statistical stability tests + anti-sidereal effect



20 TeV

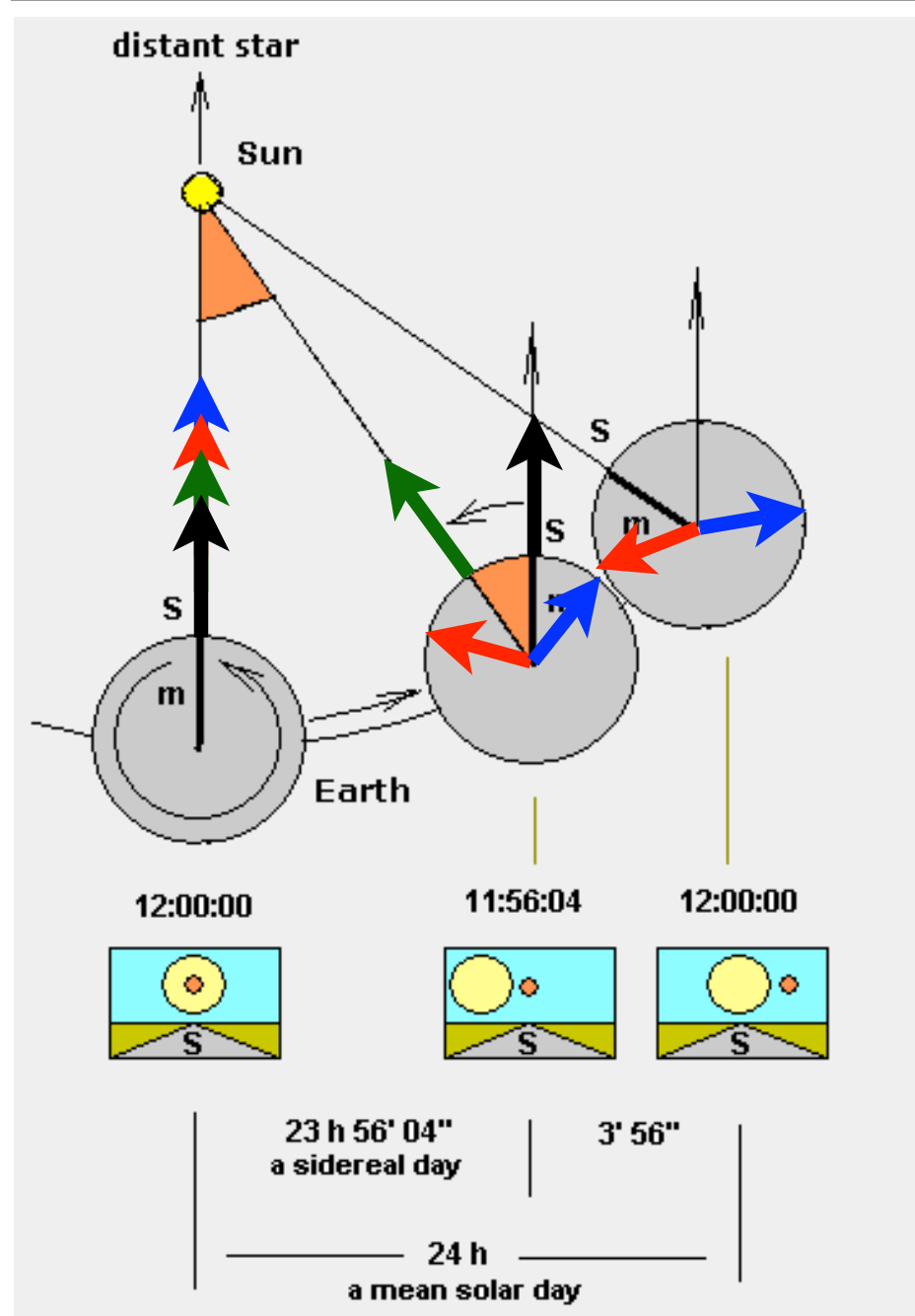


400 TeV

statistical stability tests:

- ▶ summer/winter season datasets
- ▶ rate  $\cong$  median daily rate
- ▶ even/odd sub-runs (2 mins data)
- ▶ random sub-run selection
- ▶ use  $\sim$ 20hr full days (214/324 d)

# anti- / extended-sidereal reference frames



The anti- / extended-sidereal reference frames are unphysical and no anisotropy is expected

An anisotropy in anti-sidereal (extended-sidereal) frame is to be associated to the corresponding distortion of the sidereal (solar) arrival distributions

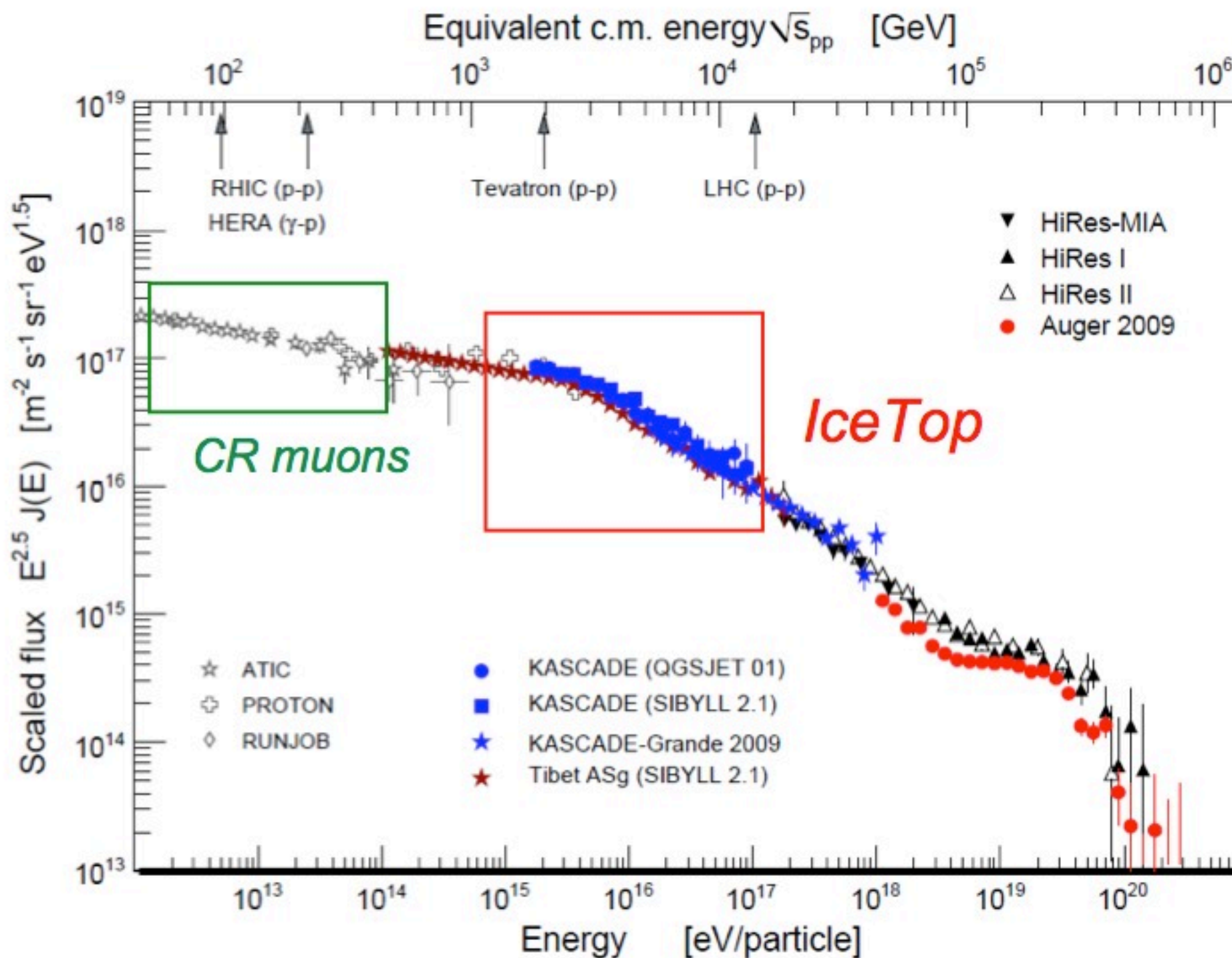
**solar time**

**sidereal time**

**anti-sidereal time**

**extended-sidereal time**

# Cosmic Ray Energy Spectrum



- Data taken between [May 20, 2009](#) and [May 30, 2010](#). Integrated livetime 335.5 days.
- $3.4 \times 10^{10}$  events stored in a special format suitable for high data rate.
- Simulations: median energy and angular resolution depend on zenith angle.
- Zenith angle cut: accept events  $< 65^\circ$ .

